

Hydrothermal Reactions of Algae Model Compounds

by

Shujauddin M. Changi

**A dissertation submitted in partial fulfillment
of the requirements for the degree of
Doctor of Philosophy
(Chemical Engineering)
in The University of Michigan
2012**

Doctoral Committee:

**Professor Phillip E. Savage, Chair
Professor Adam J. Matzger
Assistant Professor Charles W. Monroe
Adjunct Professor Shawn E. Hunter**

© Shujauddin M. Changi

2012

To my parents, Munira and Mohsin
and my wife, Nazneen

Acknowledgments

I thank my advisor Professor Phillip E. Savage who has always been there whenever needed throughout the course of my PHD. His clarity of thought, recommendations, suggestions, and criticisms have greatly added to my personal and professional development. His mentorship has gone a long way in helping me successfully write this dissertation.

I also acknowledge my other committee members, Professor Adam J. Matzger, Assistant Professor Charles W. Monroe, and Adjunct Professor Shawn E. Hunter for their valuable advice and suggestions during the course of this PHD. Discussions with them have helped shape this dissertation the way it is.

I am grateful to former group members, Tanawan Pinnarat, Tylisha Brown, and Minghan Zhu, who have also co-authored with me on different manuscripts. I learned a lot from each of them by working on different projects. I would also like to thank current group members Robert Levine and Peter Valdez for help in training to use GC-FID and Jacob Dickinson for useful discussions in MATLAB coding. I also thank Apurva Lingnuarkar, my mentee, whose experiments helped me finish my work smoothly and quickly.

I acknowledge other former Savage group members, Peigao Duan, Natalie Rebacz, Jie Fu, Qingqing Guan, Dongil Kang and current group members including Zheng Li, Chad Huelsman, Thomas Yeh, Allison Franck, Tiffany Mo, Julia Faeth, and Yang Guo for their help, advice and suggestion at some point or the other.

I would like to thank Susan Hamlin for taking care of all the administrative matters and paperwork. I acknowledge Claire O'Connor, Shelly Fellers, Michael Africa, Laurel Neff, and Connie Raymond for taking care of all the departmental issues.

I acknowledge the NSF Grant – EFRI 0937992 for financial support in carrying out this research.

I thank my distant family members living in Ann Arbor, my friends: Priyanka Pande, Nasim Balou, Lilian Hsiao, Priska Poan, Elizabeth Stewart, Andiappan Marimuthu, Ines Pons, Nick Stuckert, Matthew Morabito, Khamir Mehta, Mohammad Sichani, Adam Patterson, Muhammad Murshed Khadija, and my Northwood Community Apartment neighbors, all of whom have made my life enjoyable throughout my PHD. I am grateful to my friend Amey Bandekar for being with me through the ups and downs in this journey.

I am indebted to all my professors throughout my Bachelor's degree at Institute of Chemical Technology (formerly U.D.C.T.) (especially Prof. G. D. Yadav and V. C. Malshe), my Master's degree at Massachusetts Institute of Technology and my PHD degree at University of Michigan for teaching me different subjects and helping me develop the foundations in chemical engineering.

I am very grateful to my mentors Winnie Torres-Ordoñez, Craig Colling, and Ramachandra Surve, who have helped me constantly be motivated and achieve success in life. I thank all my relatives back in India for their love and support throughout. I am grateful to my in-laws (Fakhera, Khozema, and Hussain Glttham) whose care and support have gone a long way in my PHD. I thank my wife Nazneen for being by my side and being my strength through thick and thin. Finally, I owe everything to my parents (Munira and Mohsin Changi) whose love, emotional support, encouragement, sacrifice and advice have helped me travel and complete the journey of obtaining a PHD.

Table of Contents

Dedication.....	ii
Acknowledgements.....	iii
List of Figures.....	viii
List of Tables.....	xi
List of Appendices.....	xiii
Abstract.....	xiv
Chapter	
1. Introduction.....	1
1.1 Motivation.....	1
1.2 Relevance to Sustainability.....	3
1.3 Composition of Algae.....	4
1.4 Selection of Model Compounds.....	8
2. Literature Review.....	17
2.1 Ethyl Oleate.....	17
2.2 Phenylalanine.....	21
2.3 Phytol.....	24
2.4 DOPC.....	25
2.5 Binary Mixtures.....	27
2.6 Summary of Gaps in Literature.....	29

3. Experimental Setup.....	38
3.1 Materials.....	38
3.2 General Experimental Setup.....	39
3.3 Individual Model Compound Experimental Setup....	40
4. Behavior of Ethyl Oleate in HTW.....	52
4.1 Control Experiment.....	52
4.2 Effect of Reaction Conditions.....	53
4.3 Phenomenological Autocatalytic Kinetics.....	57
4.4 Mechanistic Autocatalytic Kinetics.....	66
4.5 Conclusions.....	80
5. Behavior of Phenylalanine in HTW.....	84
5.1 Control Experiment.....	84
5.2 Effect of Reaction Conditions.....	84
5.3 Kinetics of Phenylalanine Disappearance.....	88
5.4 Reaction Pathways.....	89
5.5 Kinetic Model.....	93
5.6 Conclusions.....	96
6. Behavior of Phytol in HTW.....	100
6.1 Control Experiment.....	100
6.2 Effect of Reaction Conditions.....	101
6.3 Kinetics of Phytol Disappearance.....	107
6.4 Reaction Pathways.....	108
6.5 Kinetic Model.....	114
6.6 Conclusions.....	119
7. Behavior of DOPC in HTW.....	124
7.1 Control Experiment.....	124
7.2 Effect of Reaction Conditions.....	124
7.3 Reaction Pathways.....	130
7.4 Phenomenological Autocatalytic Kinetics.....	135
7.5 Kinetic Model.....	138
7.6 Conclusions.....	143

8. Behavior of Binary Mixtures in HTW.....	146
8.1 Control Experiment.....	146
8.2 Binary Mixtures of Inorganics and Phenylalanine...	147
8.3 Binary Mixture of Ethyl Oleate and Phenylalanine..	149
8.4 Conclusions.....	165
9. Implications, Conclusions, and Future Work.....	169
Appendices.....	176

List of Figures

Figure

1.1	Properties of pure water at 250 bar as a function of temperature...	2
1.2	Chemical structure of chlorophyll <i>a</i>	7
4.1	Temporal variation of ethyl oleate conversion	54
4.2	Parity plot of phenomenological model for hydrolysis experiments.....	61
4.3	Parity plot of phenomenological model validation for experiments conducted inside and outside parameter space.....	62
4.4	Mechanism explaining autocatalysis for ethyl oleate hydrolysis and oleic acid esterification.....	67
4.5	Schematic representation of hydrolysis and esterification mechanism.....	69
4.6	Schematic representation of simplified hydrolysis and esterification mechanism.....	72
4.7	Parity plot of mechanistic model for hydrolysis experiments.....	74
4.8	Parity plot of mechanistic model validation for experiments conducted inside and outside parameter space.....	76
4.9	Model validation at different pH for ethyl oleate hydrolysis at 280 °C and 40 min.....	77
5.1	LC-MS chromatograms for phenylalanine reaction products at different conditions.....	92
5.2	Reaction pathways for phenylalanine in HTW.....	92

5.3	Comparison of experimental (discrete points) and model (smooth curves) results for reactants and products at different conditions.....	95
5.4	Parity plot between experimental and model concentration.....	96
6.1	Total ion chromatogram for the product mixture obtained from the hydrothermal reaction of phytol 300 °C and 20 min.....	101
6.2	Representative MS fragmentation pattern of neophytadiene.....	103
6.3	First-order plot for phytol conversion in HTW.....	108
6.4	First-rank Delplot at 270 °C for different products.....	109
6.5	Reaction network for phytol in HTW.....	113
6.6	Simplified reaction network for kinetic modeling of phytol in HTW.....	114
6.7	Comparison of experimental (discrete points) and model (smooth curves) results for reactants and products at different conditions.....	118
6.8	Parity plot between experimental and model concentration for reactant and products.....	119
7.1	³¹ P-NMR spectrum of products from DOPC reaction at 200 °C and 60 min.....	125
7.2	Temporal variation of DOPC conversion.....	129
7.3	Parity plot for comparison of experimental and model concentration for DOPC.....	137
7.4	Parity plot for comparison of experimental and model concentration for oleic acid.....	138
7.5	Streamlined reaction network for DOPC in HTW.....	139
7.6	Comparison of experimental and calculated concentrations at 175 °C, 200 °C, 225 °C, and 350 °C.....	143
8.1	Effect of salts and boric acid on phenylalanine at 250 °C and 30 min in HTW.....	148

8.2	LC-MS chromatogram for phenylalanine and NaNO_3 reaction product in HTW at 250 °C, 30 min.....	149
8.3	Effect of ethyl oleate on molar yields of different products at 350 °C and 10 min.....	152
8.4	Conversion of phenylethylamine at 350 °C and different batch holding times.....	153
8.5	Effect of phenylalanine on ethyl oleate and oleic acid at 350 °C and 10 min.....	155
8.6	GC-MS chromatogram for binary mixture of phenylalanine and ethyl oleate (1.0 : 1.0) at 350 °C and 30 min.....	157
8.7.a.	Total yield of amides at 350 °C and 10 min for different initial molar ratios of phenylalanine to ethyl oleate.....	158
8.7.b.	Total yield of amide at various batch holding times and phenylalanine to ethyl oleate molar ratio of 5.0.....	158
8.8	Reaction network for binary mixture of ethyl oleate and phenylalanine in HTW.....	160
8.9	Comparison of experimental (discrete points) and model (smooth curves) results for different products for binary mixture of ethyl oleate with phenylalanine at 350 °C and different batch holding times.....	164
8.10	Parity plot of experimental and model concentrations at 350 °C and different batch holding times.....	165

List of Tables

Table

1.1 Chemical Composition (wt % dry basis) of <i>Nannochloropsis</i> sp.....	5
1.2 Structures of different model compounds for algae.....	11
4.1 Effect of initial addition of oleic acid and ethanol on ethyl oleate conversion (30 min, $C_{EO}^0 = 0.075$ mol/L).....	55
4.2 Effect of different pH on ethyl oleate conversion at 280 °C and 40 min ($C_{EO}^0 = 0.075$ mol/L, $R_w = 554$).....	56
4.3 Estimated Arrhenius parameters (min, L, mol) for unified hydrolysis and esterification.....	59
4.4 Comparison of experimental (Warabi <i>et al.</i>) and predicted ester conversion.....	64
4.5 Normalized sensitivity coefficients for phenomenological model.....	65
4.6 Estimated Arrhenius parameters for simplified mechanism Figure 4.6 (min, mol, L).....	73
4.7 Normalized sensitivity coefficients for mechanistic model.....	79
5.1 Conversion and molar yield of products for phenylalanine in HTW....	85
5.2 Conversion and yields of products for phenylalanine in HTW at different initial concentrations of phenylalanine.....	87
5.3 Rate constant and order for phenylalanine disappearance in HTW...	88
5.4 Arrhenius parameters for phenylalanine disappearance in HTW.....	89
5.5 Arrhenius parameters for phenylalanine reaction network.....	94

6.1 Products from the hydrothermal processing of phytol.....	102
6.2 Conversion and molar yield of products for phytol in HTW.....	106
6.3 Conversion and yield of major products for phytol in HTW at different initial concentration of phytol.....	107
6.4 First-order rate constants for phytol conversion in HTW.....	108
6.5 Arrhenius parameters for phytol reaction network.....	116
7.1 Conversion and molar yield of products from DOPC in HTW.....	126
7.2 Conversion of DOPC and yield of oleic acid with and without added acid at 200 °C and 15 min.....	130
7.3 Arrhenius parameters for phenomenological autocatalytic model (mol, min, L).....	136
7.4 Arrhenius parameters for DOPC reaction network.....	142
8.1 Conversion and yields of phenylalanine and phenylethylamine in presence of different additives at 250 °C and 30 min.....	147
8.2 Effect of ethyl oleate on yield of products from phenylalanine at 350 °C and different batch holding times.....	151
8.3 Effect of phenylalanine on yields of oleic acid, oleamides, and conversion of ethyl oleate at 350 °C and different batch holding times.....	151
8.4 Chemical names and structure of labels for GC-MS chromatogram for phenylalanine and ethyl oleate binary mixture (1.0 : 1.0) at 350 °C and 30 min.....	157
8.5 Rate constants at 350 °C for different initial ratios of ester to phenylalanine.....	162

List of Appendices

Table

A.1 Pressure and density of saturated liquid water at different temperatures.....	176
A.2 Conversion of ethyl oleate and yield of oleic acid at different temperatures and batch holding times.....	177

ABSTRACT

Hydrothermal liquefaction (HTL) refers to the process of converting biomass to bio-oil by contacting the biomass with water at high temperatures (> 200 °C) and sufficient pressures to maintain water in the liquid state. HTL process of algae producing bio-oil has the advantage of being energy efficient and capability of dealing with wet biomass. Very little is known about the mechanism of biomacromolecule reactions in high temperature water (HTW). In this thesis, we bridge this knowledge by studying ethyl oleate, phenylalanine, phytol, and 1,2-dioleoyl-sn-glycero-3-phosphocholine as representative model compounds for triglycerides, proteins, chlorophyll and phospholipid, respectively, in HTW from 175 – 350 °C.

We determined the kinetics for ethyl oleate hydrolysis in high-temperature water (HTW), which showed the reaction mechanism to be autocatalytic. The experimental data, from reactions at 150-300 °C, times from 5 to 1440 min, and with different initial concentrations of reactants and products, were used to estimate thermodynamically and thermochemically consistent Arrhenius parameters for the forward and reverse reactions in a phenomenological autocatalytic reaction model. The model correlated with the data and was also able to make quantitatively accurate predictions within the parameter space investigated. The model also predicted experimentally observed trends when extrapolated outside the original parameter space. We also elucidated the mechanism for ethyl oleate hydrolysis in HTW and its reverse reaction (oleic acid esterification in near- and supercritical ethanol) in the absence of any other added compounds. Hydrogen ions (from dissociation of water and oleic acid) and oleic acid serve as catalysts for hydrolysis. The rate equation arising from the

proposed mechanism provided a good fit of experimental conversion data for hydrolysis. The rate equation accurately predicted the influence of pH on hydrolysis for acidic and near-neutral conditions. The mechanistic model exhibits the ability to make quantitatively accurate predictions within and outside the original parameter space, especially for a multicomponent system. Sensitivity analysis shows that the values of the dissociation constant of oleic acid in ethanol, water, and ethanol-water systems strongly influence the predicted conversions. There is a need for experimental measurement of pK_a for fatty acids in both water and alcohols at elevated temperatures.

We examined the behavior of phenylalanine in HTW at 220, 250, 280, and 350 °C. Under these conditions, the major product is phenylethylamine. The minor products include styrene and phenylethanol (1-phenylethanol and 2-phenylethanol), which appear at higher temperatures and after longer batch holding times. Phenylethylamine forms via decarboxylation of phenylalanine, styrene forms via deamination of phenylethylamine, and phenylethanol forms via hydration of styrene. We quantified the molar yields of each product at the four temperatures, and the carbon recovery was between 80-100% for most cases. Phenylalanine disappearance follows first-order kinetics with activation energy of 144 ± 14 kJ/mol and pre-exponential factor of $10^{12.4 \pm 1.4} \text{ min}^{-1}$.

We also examined the behavior of phytol, an acyclic diterpene C_{20} -alcohol and a model compound for algal biomass, in HTW at 240, 270, 300, and 350 °C. Under these conditions, the major products include neophytadiene, isophytol, and phytone. The minor products include pristene, phytene, phytane, and dihydrophytol. Neophytadiene likely forms via dehydration of phytol, while isophytol can be obtained via an allylic rearrangement. We have quantified the molar yields of each product at the four temperatures, and the carbon recovery was greater than 90% for most cases. Phytol disappearance follows first order kinetics with an activation energy of 145 ± 20 kJ/mol and pre-exponential factor of $10^{11.7 \pm 1.9} \text{ min}^{-1}$. Delplot analysis discriminated between primary and non-primary products and led to a potential set of reaction pathways.

We examined the behavior of 1,2-dioleoyl-*sn*-glycero-3-phosphocholine (DOPC) in liquid water at 175, 200, 225, and 350 °C. DOPC hydrolyzed to give oleic acid and a number of phosphorus-containing products. The hydrolysis was catalyzed by oleic and phosphoric acids, which were also reaction products. DOPC formed 1-acyl and 2-acyl lyso-phosphatidylcholine (LPC) along with oleic acid as primary products. LPC subsequently formed other phosphorus-containing intermediates, which finally led to phosphoric acid as the ultimate P-containing product. At 350 °C, phosphoric acid and oleic acid were the only products observed. We observed an ester of oleic acid and glycerol (9-octadecenoic-2,3-dihydroxypropyl ester), which likely formed via the hydrolysis of LPC. A reaction network is proposed to explain the formation of the observed products. A quantitative kinetic model based on the proposed pathways was consistent with the experimental data for phenylalanine, phytol, and DOPC.

Effects of five different salts (NaCl, NaNO₃, Na₂SO₄, KCl, K₂HPO₄) and boric acid (H₃BO₃) on phenylalanine behavior at 250 °C have also been elucidated. These additives increase phenylalanine conversion, but decrease the yield of phenylethylamine, presumably by promoting the formation of high-molecular-weight compounds. Lastly, binary mixtures of phenylalanine and ethyl oleate have been studied at 350 °C and three different molar concentration ratios. The presence of phenylalanine enhances the conversion of ethyl oleate and molar yields of fatty acid. Higher concentration of ethyl oleate leads to increased deamination of phenylethylamine and hydration of styrene. Amides are also formed due to the interaction of oleic acid/ethyl oleate and phenylethylamine/ammonia and lead to a decrease in the fatty acid yields.

Taken collectively, these results provide new insights into the reactions of algae during its hydrothermal liquefaction to produce crude bio-oil.

CHAPTER 1

Introduction

1.1 Motivation

The world's population is expected to increase through 2050 to 9 billion [1], resulting in escalating energy demands. It is believed that fossil fuel reserves, such as coal, crude oil, natural gas, shale, etc., will peak out and become exhausted sooner than later. Given this scenario, there is considerable motivation to produce sustainable liquid fuels. Research is being conducted in the alternative and renewable energy sectors, and the production of fuel from biomass is one such area gaining momentum. Algae are potentially promising biofuel precursors and have advantages over other biomass energy sources. They have a higher (~20x) photosynthetic efficiency than terrestrial plants [2]. Algae can grow in brackish and saline water, thereby reducing the direct competition for land with conventional food crops [3]. Thirdly, algae have higher lipid content per area of land cultivated than other biomass sources such as soybean, sunflower, or palm oil [4]. Lastly, microalgae cultivation can be coupled with recycling of waste-water and refinery flue gases to make the process more economical and environmentally benign.

Hydrothermal processing of algal biomass has been widely reported in the past, comprising conversion of wet algal biomass to crude bio-oils (hydrothermal liquefaction) [3,5-7], carbonized solids (hydrothermal carbonization) [8, 9], and fuel gases (hydrothermal gasification) [10]. Of these processes, hydrothermal liquefaction (HTL) of microalgae is a potentially promising route to obtain high-energy-density, fungible advanced biofuels. This process involves treatment of

algal biomass in an aqueous medium at elevated temperatures (200 – 350 °C) and pressures (1.5 – 17 MPa). Water has distinctly different properties at high temperatures and pressures than at ambient conditions. Figure 1.1.a shows that the ion product of water (K_w) increases at high temperatures and then rapidly decreases at temperatures above the supercritical temperature of water (374 °C, 22.1 MPa). Figure 1.1.b illustrates that the dielectric constant of water continually decreases as the temperature is increased. These different properties of high temperature water (HTW) increase the solubility of organic compounds in water under these conditions compared to that at room temperature [11]. Thus, biomacromolecules in algae are more susceptible to hydrolytic attack in HTW.

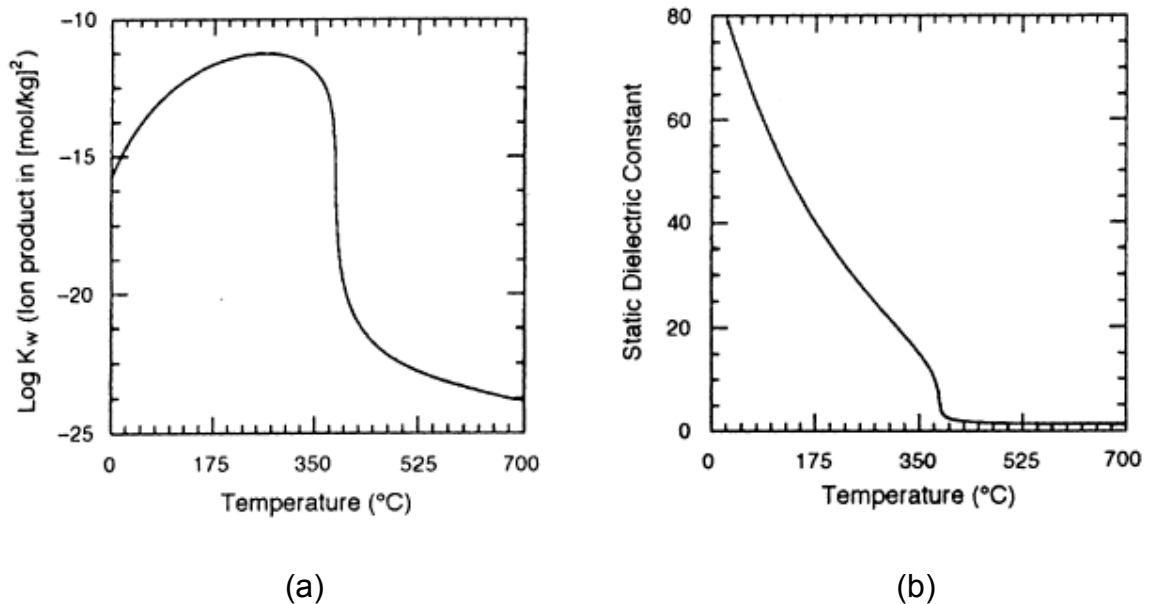


Figure 1.1 Properties of pure water at 250 bar as a function of temperature. a) Ionic product b) Dielectric constant [reprinted from ref. 12, with written permission]

Hydrothermal liquefaction is well suited for wet biomass because it obviates the need to dry the feedstock, an energy-intensive pretreatment step that lowers the overall efficiency of the process. Besides, the HTL process can be carried out at a lower temperature (200 – 350 °C) compared to pyrolysis (~500 °C) or gasification (~2000 °C), further saving energy.

Previous reports on HTL of algae have shown that the maximum bio-oil yield exceeds the crude lipid content of algae [3, 5, 6]. For instance, Brown *et al.* [3] have obtained a maximum bio-oil yield of 43 ± 2 wt% when they started with only 28% crude lipids in starting algae. This result suggests that not only the lipids but also the proteins and other components of algae must react to form the bio-oil. The literature provides qualitative and quantitative classification of bio-oil obtained from algae under various conditions. However, there is no elucidation of the chemistry and underlying pathways to explain the bio-oil formation due to the interactions of various components within algae. It can be very challenging to understand the chemistry of HTL if starting directly with algae because of algae's complex composition (see Section 1.2). To overcome this problem, one can instead study model compounds representing the complex biomacromolecules within algae. One expects these surrogate compounds to behave similarly to their corresponding biomacromolecules in HTW, because they contain the same functional groups as their representative biomacromolecules.

When initiating this research, there was very little information in the literature pertaining to the model compounds relevant to the algae system in HTW. Thus, we were motivated to study model compounds of algae in HTW from 175-350 °C, to provide useful insights into the reaction products, pathways, kinetics, and mechanisms for the bio-oil production during HTL of algae.

1.2 Relevance to Sustainability

Sustainability is generally referred to in terms of the triple bottom line of economic, environmental, and social dimensions. HTL of algae promises to be relevant to sustainability by influencing these dimensions either directly or indirectly. Many researchers have critically carried out a life-cycle assessment (LCA) of algae-derived biofuels [13-19] but a similar analysis for HTL process of algae to produce bio-oil does not exist. Nonetheless, one can use these results to obtain the relevance of HTL process to sustainability.

Algae growth requires carbon dioxide and nutrients. As envisioned on an industrial scale, recycling industrial flue gases and waste-water (rich in N, P, C, H, O) can help reduce overall costs, and potentially make the biofuel production process economical. Another advantage of using algae is that they do not necessarily require land for its growth but can be cultivated in brackish and saline water. Therefore, there is no competition with food crops. Moreover, HTL of algae has the potential for reduced life-cycle greenhouse gas emissions due to the incorporation of biogenic carbon into the bio-oil. Clearly, HTL of algae can have positive influences on society, ecology, and economy.

It has been recently shown in a LCA and energy analysis [13-15] that fertilizers consumption, harvesting and oil extraction from algae represent a high-energy debt, which may jeopardize the overall interest of algal biofuel compared to biofuels obtained from canola, corn, and switchgrass. However, one major criticism of these literatures is that they have used data on algal cultivation that is over 20 years old and significant improvements have been made since then. Besides, the choice of carbon dioxide source and location of the algae farms greatly affects the LCA. E.g.: Yang *et al.* [18] show in their analysis that recycling harvest water for algae cultivation can reduce the water and nutrients usage by 84% and 55%, respectively. On the other hand, using sea/waster-water decreases 90% water requirements and eliminates the need of all the nutrients except phosphate. LCA of algae biofuels suggest them to be environmentally better than fossil fuels but economically it is not yet so attractive [19]. An overall life-cycle analysis can help quantitate the advantages of HTL of algae.

1.3 Composition of Algae

Algae biomass is a complex mixture of biomacromolecules such as polysaccharides, triglycerides, lipids, and proteins. Becker [20] has summarized the general composition of different types of algae. Although the composition varies from strain to strain, algae primarily contain proteins and lipids (unlike conventional ligno-cellulosic biomass, containing mainly lignin and hemi-

cellulose). Table 1.1 shows a typical chemical composition of *Nannochloropsis* sp. [3].

Table 1.1 Chemical Composition (wt % dry basis) of *Nannochloropsis* sp. (Adapted from Brown *et al.* [3])

Carbohydrates	12
Proteins	52
Lipids	28
Ash	8
Elemental Analysis	
Carbon	43.3
Hydrogen	6.0
Oxygen	25.1
Nitrogen	6.4
Sulfur	0.5

Siegal *et al.* [21] reported in detail the chemical composition of the cell wall of at least ten different classes of algae. They found the cells of most algae to contain a wide variety of water-soluble monosaccharides, such as uronic acid, xylose, galactose and glucose. Abo-Shady *et al.* [22] classified neutral sugars in algal cell walls for *Chlorella vulgaris* and *Kirchneriella lunaris* as rhamnose, ribose, glucose, arabinose and mannose.

Proteins are another important constituent of algae (around 10-69 wt% in green algae [21]). Abo-Shady *et al.* [22] characterized cystine, proline, glutamic acid and leucine as the major amino acids in the cell walls of *Chlorella vulgaris* and *Kirchneriella lunaris*. A more recent review by Becker [20] gives an extended classification of other amino acids constituting various proteins in algae such as leucine, valine, lysine, phenylalanine, arginine, aspartic acid, glutamine, alanine, and glycine.

Lipids form the third major class of biomacromolecules in algae. Lipids can be classified either as non-polar (or neutral) lipids, such as triglycerides and free fatty acids, or polar lipids, such as phospholipids and glycolipids [23]. Triglycerides are esters composed of a glycerol backbone bound to three fatty acids. They can constitute between 11-68 wt% of the total lipids in algae, depending on its strain [23]. Fahl *et al.* [24] characterized the fatty acid composition of algae communities found in Weddell Sea (Antarctica). Thin-layer chromatography with flame ionization detector was used for characterization. They found that the fatty acid composition of microalgae was dominated by palmitoleic, palmitic, oleic and eicosapentaenoic fatty acids. Gatenby *et al.* [25] have compared the lipid contents for *Neochloris oleoabundans* and *Bracteacoccus grandis* at different growth stages and found a high percentage of C18 polyunsaturated fatty acids (PUFAs) in green algae. Brown *et al.* [3] have characterized fatty acids in *Nannochloropsis* sp. and shown that myristic acid (C14:0), palmitic acid (C16:0), palmitoleic acid (C16:1), eicosapentaenoic acid (C20:5), and arachidonic acid (C20:4) are the major fatty acids, with lesser amounts of oleic acid (C18:1), and linoleic acid (C18:2). These fatty acids would likely arise from the hydrolysis of the corresponding lipids in algae. Phospholipids, another class of lipids, can constitute between 10-50 wt% of the total lipids in algae [23]. Phospholipids contain a glycerol backbone with a diglyceride, a phosphate group, and an organic group. Bailey *et al.* [26] have studied the phospholipid composition of the plasma membrane of green algae *Hydrodictyon africanum*. Based on TLC and radioactive labeling experiments they found that phosphatidylcholine (PC) was the major phospholipid present in the cells. Lastly, glycolipids can constitute between 6-49 wt% of total lipids depending on the type of algae [23]. Glycolipids are lipids attached to a carbohydrate moiety.

Chlorophyll is a complex biomacromolecule present in algae and can constitute between 0.2-5 wt% of algae depending on the type of algae and the concentration of nitrogen in the nutrient media [27]. Structural features common to all the chlorophylls found in algae are the hydrophilic chlorin ring, which consists of a light-absorbing network of conjugated double bonds encased in a 4-

ion nitrogen ring, and the hydrophobic ester-linked phytol side chain [28]. Figure 1.2 shows the chemical structure of chlorophyll *a*, the most common chlorophyll type in green algae.

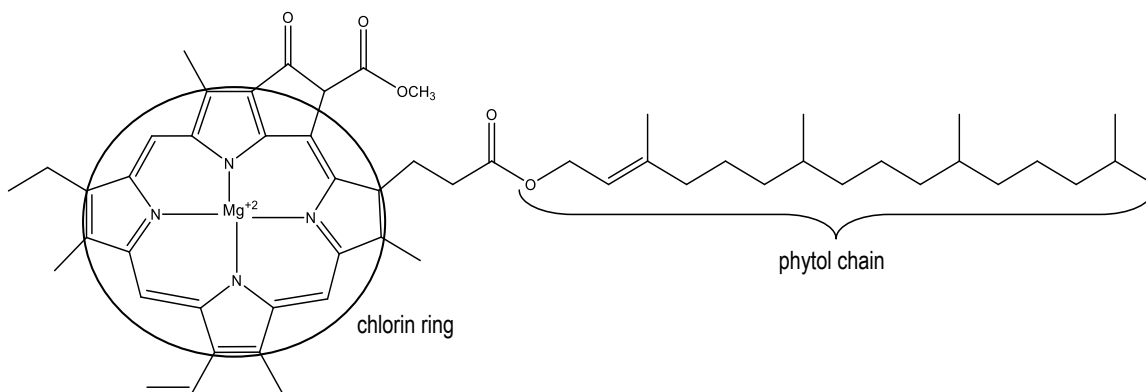


Figure 1.2 Chemical structure of chlorophyll *a*

Finally, the ash content of algae can be attributed to the accumulation of various inorganic compounds in the cells during the growth stage. Dried algal biomass can contain salts in varying amounts (5-20% wt ash content) [3]. These salts are taken in the cells from the nutrient medium used for the cultivation of algae [8]. The ash content and composition can vary from species to species. For instance, Minowa *et al.* [7] have characterized ash content as high as 24 wt% for *Dunaliella tertiolecta*, primarily containing sodium, potassium, magnesium, calcium, and chloride, whereas Brown *et al.* [3] report only up to 8 wt% of ash for their species, *Nannochloropsis* sp..

As mentioned previously, given the complex nature of algal cells, the underlying chemistry of biomacromolecules during HTL of algae can get very complicated. Therefore, to obtain a fundamental understanding of the reactions of biomacromolecules in algae during HTL process, we study different model compounds (ethyl oleate, phenylalanine, phytol, and dioleoylphosphatidylcholine (DOPC)) individually in HTW from 175 – 350 °C. Secondly, various biomacromolecules in algae could interact with each other to form additional products in the bio-oil. Therefore we also explore binary mixtures of phenylalanine and ethyl oleate and phenylalanine with various inorganic

additives (NaCl, NaNO₃, Na₂SO₄, KCl, K₂HPO₄, and H₃BO₃) at 350 °C (60 minutes) and 250 °C (30 minutes), respectively. The next section discusses the reasoning for choosing these model compounds.

1.4 Selection of Model Compounds

The choice of model compounds was one of the key challenges of this research, since there exist several possibilities (of representing the biomacromolecules in algae). The model compounds were selected such that they encompassed all the prominent classes of biomacromolecules in algae. An important factor governing the model compound selection was the similarity of the structural elements and chemical functional groups with the corresponding biomacromolecules so that the results of model compounds can provide useful information about the types and rates of chemical transformations of these biomacromolecules during HTL of algae. This section discusses the reasoning behind the selection of model compounds for this research, namely, 1) Ethyl oleate, 2) Phenylalanine, 3) Phytol, and 4) DOPC.

Triglycerides are the most important constituents of algae; they are directly responsible for forming the fatty acid components of the bio-oil. To understand the hydrolysis behavior of triglycerides, one can work with either a single ester, or glycerol and a fatty acid. We chose to do the former, using ethyl oleate as a model compound for triglycerides. The reason for choosing ethyl oleate was that it contains an oleic acid moiety, which is also one of the major fatty acids characterized in algae, possibly due to the hydrolysis of triglycerides containing an oleate moiety. Secondly, very little information has been documented for fatty acid esters in HTW. An understanding of ethyl oleate can lay the foundations for understanding triglyceride behavior in HTW.

Proteins comprise several amino-acid building blocks. During the HTL process, the proteins likely undergo hydrolytic depolymerization to release peptide fragments [29]. Thus, HTL of protein-containing algae can produce “bio-oil” containing either protein residues with amino acids, or new products obtained

through reactions of protein with other constituents of algae (e.g., glucose, triglycerides etc.). For instance, Brown *et al.* [3] and Dote *et al.* [6] have shown the bio-oil obtained during HTL of algae to contain several nitrogenous compounds, possibly originating from the amino acids contained in the algae feedstock. Researchers have also identified indole, pyrazine, pyridine, pyrrole, and their derivatives in the bio-oil obtained from liquefaction of algae from 200 - 600 °C [3, 5, 30-32]. These products likely arise from different amino acids. For example, Hwang *et al.* [33] have identified pyridines, pyrroles, oxazoles, and other N-containing compounds during the reaction of glucose and several amino acids in hot liquid water. To obtain a better understanding of the chemistry of bio-oil production during algae liquefaction, one needs to investigate the reactions of amino acids in high temperature water (HTW). Phenylalanine was chosen as model representative for amino acids because: 1) it is one of the most abundant amino acids in algae [20]; 2) It has an aryl substituent on a β -alanine backbone, which might lead to previously unexplored steric or electronic effects; 3) It has not been previously studied in great detail in HTW; 4) It exhibits the properties of both hydrophilic and hydrophobic amino acids; and 5) Phenylalanine and its products have better sensitivity and ease of detection by HPLC and GC in comparison to other amino acids. An understanding of phenylalanine can help lay the foundation for understanding the behavior of other amino acids and proteins during HTL of algae.

Chlorophyll is a complex molecule and can potentially form a number of products in the bio-oil. Thus, to model chlorophyll, we considered one of its simpler substituents, phytol. The ester group linking the phytol chain to the chlorin ring in the chlorophyll molecule can readily hydrolyze to release a phytol molecule [34]. Phytol is an acyclic diterpene alcohol, providing another class of functional groups to be explored in HTW. Moreover, no work has been reported previously for phytol behavior in sub-critical water. Researchers have also identified several components in bio-oil, such as phytane, phytene, neophytadiene, which can possibly be formed from phytol in HTW [3, 35]. Thus, a knowledge of the reactions of phytol in HTW could enable a better

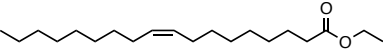
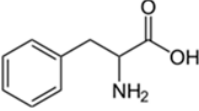
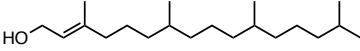
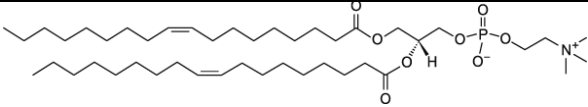
understanding of the pathways and mechanisms for formation of the constituents of bio-oil arising from phytol and hence chlorophyll during the HTL of algae. With this reasoning, phytol was selected as a model compound for chlorophyll.

Phospholipid chemistry can play an important role not only in the formation of the bio-oil, but also in the formation of several phosphorus compounds that are added to the aqueous phase during HTL of algae. It was mentioned earlier that phosphatidylcholine is one of the major phospholipids found in algae. Thus, we represented phospholipids by dioleoylphosphatidylcholine (DOPC). DOPC is a diglyceride with an oleate moiety that can readily form oleic acid on hydrolysis. Therefore, DOPC was chosen because of a similar reasoning to ethyl oleate (monoglyceride). Besides, there is no literature to elaborate on the behavior of phospholipids in HTW.

For the experiments with binary mixtures, we studied a system of phenylalanine and ethyl oleate because proteins and triglycerides constitute the major portion of an algal cell. This binary mixture would help us understand the interactions of these biomacromolecules in HTW. We also studied the effects of added inorganics (salts and boric acid) on phenylalanine. Various salts and boric acid were chosen because they are most abundant in the media used to culture algal cells.

It should be noted that we have not studied any model compounds for polysaccharides since they have been very widely studied in HTW previously alone and in binary mixtures with other model compounds [36-42]. With the above choice of model compounds and their binary mixtures major types of biomacromolecules in algae have been covered. Table 1.2 shows the structure of model compounds under consideration in this research.

Table 1.2 Structures of different model compounds for algae

Name	Structure
Ethyl Oleate	
Phenylalanine	
Phytol	
DOPC	

To sum up, we have extensively studied model compounds individually and in binary mixtures in HTW, to help lay the foundation to help better understand the process of hydrothermal liquefaction of algae in HTW. A review of literature for the selected model compounds is presented in Chapter 2. Chapter 3 discusses the experimental setup and the methodology used to carry out quantitative and qualitative analysis of the model compounds. Results pertaining to individual model compounds are discussed for ethyl oleate in Chapter 4, for phenylalanine in Chapter 5, for phytol in Chapter 6, and for DOPC in Chapter 7. The work carried out with binary mixture of phenylalanine with ethyl oleate and inorganic additives is summed up in Chapter 8. Chapter 9 summarizes the implications of this study to the understanding of HTL process for algae. Chapter 10 concludes with the key findings of this work and Chapter 11 gives direction for future work.

References

- [1] <http://www.un.org/News/Press/docs/2007/pop952.doc.htm>, Date last accessed, 5th May 2012
- [2] J. A. V. Costa, M. G. de Morais. The role of biochemical engineering in the production of biofuels from microalgae. *Bioresour. Technol.* 102, 2-9, 2011
- [3] T. M. Brown, P. Duan, P. E. Savage. Hydrothermal liquefaction and gasification of *Nannochloropsis* sp. *Energy Fuels* 24 (6), 3639-3646, 2010
- [4] T. M. Mata, A. A. Martins, N. S. Caetano. Microalgae for biodiesel production and other applications: A review. *Renewable Sustainable Energy Rev.* 14, 217-232, 2010
- [5] D. Zhou, L. Zhang, S. Zhang, H. Fu, J. Chen. Hydrothermal liquefaction of macroalgae *Enteromorpha prolifera* to bio-oil. *Energy Fuels* 24, 4054-4061, 2010
- [6] LadaY. Dote, S. Sawayama, S. Inoue, T. Minowa, S. Yokoyama. Recovery of liquid fuel from hydrocarbon-rich microalgae by thermochemical liquefaction. *Fuel* 73 (12), 1994
- [7] T. Minowa, S. Yokoyama, M. Kishimoto, T. Okakura. Oil production from algal cells of *Dunaliella tertiolecta* by direct thermochemical liquefaction. *Fuel* 74 (12), 1735-1738, 1995
- [8] R. B. Levine, T. Pinnarat, P. E. Savage. Biodiesel production from wet algal biomass through in situ lipid hydrolysis and supercritical transesterification. *Energy Fuels* 24, 5235-5243, 2010
- [9] S. M. Heilmann, H. T. Davis, L. R. Jader, P. A. Lefebvre, M. J. Sadowsky, F. J. Schendel, M. G. von Keitz, K. J. Valentas. Hydrothermal carbonization of microalgae. *Biomass Bioenergy* 34 (6), 875-882, 2010
- [10] Q. Guan, P. E. Savage. Gasification of *Nannochloropsis* sp. In supercritical water. *J. Supercrit. Fluids* 61, 139-145, 2012

- [11] P. E. Savage. Organic chemical reactions in supercritical water. *Chem. Rev.* 99, 603-621, 1999
- [12] J. W. Tester, J. A. Cline. Hydrolysis and oxidation in subcritical and supercritical water: Connecting process engineering science to molecular interactions. *Corrosion* 55 (11), 1088-1100, 1999
- [13] L. Lardon, A. Hélias, B. Sialve, J. Steyer, O. Bernard. Life-cycle assessment of biodiesel production from microalgae. *Environ. Sci. Technol.* 43 (17), 6475-6481, 2009
- [14] A. F. Clarens, E. P. Resurreccion, M. A. White, L. M. Colosi. Environmental life cycle comparison of algae to other bioenergy feedstocks. *Environ. Sci. Technol.* 44 (5), 1813-1819, 2010
- [15] A. F. Clarens, H. Nassau, E. P. Resurreccion, M. A. White, L. M. Colosi. Environmental impacts of algae-derived biodiesel and bioelectricity. *Environ. Sci. Technol.* 45, 7554-7560, 2011
- [16] P. K. Campbell, T. Beer, D. Batten. Life cycle assessment of biodiesel production from microalgae in ponds. *Bioresour. Technol.* 102, 50-56, 2011
- [17] P. Collet, A. Hélias, L. Lardon, M. Ras, R. Goy, J. Steyer. Life-cycle assessment of microalgae culture coupled to biogas production. *Bioresour. Technol.* 102, 207-214, 2011
- [18] J. Yang, M. Xu, X. Zhang, Q. Hu, M. Sommerfield, Y. Chen. Life-cycle analysis on biodiesel production from microalgae: Water footprint and nutrients balance. *Bioresour. Technol.* 102, 159-165, 2011
- [19] A. Singh, S. I. Olsen. A critical review of biochemical conversion, sustainability and life cycle assessment of algal biofuels. *Appl. Energy* 88 (10), 3548-3555, 2011
- [20] E. W. Becker. Micro-algae as a source of protein. *Biotechnol. Adv.* 25, 207-210, 2007

- [21] B. Z. Siegel, S. M. Siegel. The chemical composition of algal cell walls. *Crit. Rev. Microbiol.* 3 (1), 1-26, 1973
- [22] A. M. Abo-Shady, Y. A. Mohamed, T. Lasheen. Chemical composition of the cell wall in some green algae species. *Biologia Plantarum* 35 (4), 629-632, 1993
- [23] E. W. Becker. *Microalgae: Biotechnology and microbiology*. Cambridge University Press, Cambridge, 1994
- [24] K. Fahl, G. Kattner. Lipid content and fatty acid composition of algal communities in sea-ice and water from the Weddell Sea (Antarctica). *Polar Biol.* 13, 405-409, 1993
- [25] C. M. Gatenby, D. M. Orcutt, D. A. Kreeger, B. C. Parker, V. A. Jones, R. J. Neves. Biochemical composition of three algal species proposed as food for captive freshwater mussels. *J. Appl. Phycol.* 15, 1-11, 2003
- [26] D. S. Bailey, D. H. Northcote. Phospholipid composition of the plasma membrane of the green alga, *Hydrodictyon africanum*. *Biochem. J.* 156, 295-300, 1976
- [27] M. Piorreck, K. Baasch, P. Pohl. Biomass production: Total protein, chlorophylls, lipids and fatty acids of freshwater green and blue-green algae under different nitrogen regimes. *Phytochemistry* 23 (2), 207-216, 1984
- [28] S. Aronoff. The chemistry of chlorophyll (with special reference to foods). *Adv. Food Res.* 4, 134-179, 1953
- [29] T. Rogalinski, K. Liu, T. Albrecht, G. Brunner. Hydrolysis kinetics of biopolymers in subcritical water. *J. Supercrit. Fluids* 46, 335-341, 2008
- [30] P. Duan, P. E. Savage. Hydrothermal liquefaction of a microalga with heterogeneous catalysts. *Ind. Eng. Chem. Res.* 50, 52-61, 2011

- [31] Y. J. Bae, C. Ryu, J. Jeon, J. Park, D. J. Such, Y. Suh, D. Chang, Y. Park. The characteristics of bio-oil produced from the pyrolysis of three marine macroalgae. *Bioresour. Technol.* 102, 3512-3520, 2011
- [32] P. Biller, A. B. Ross. Potential yields and properties of oil from the hydrothermal liquefaction of microalgae with different biochemical content. *Bioresour. Technol.* 102, 215-225, 2011
- [33] H. Hwang, T. G. Hartman, C. Ho. Relative reactivities of amino acids in the formation of pyridines, pyrroles, and oxazoles. *J. Agric. Food Chem.* 43, 2917-2921, 1995
- [34] J. F. Rotani, J. Volkman. Phytol degradation products as biogeochemical tracers in aquatic environments. *Org. Geochem.* 34, 1-35, 2003
- [35] P. Valdez, J. G. Dickinson, P. E. Savage. Characterization of product fractions from hydrothermal liquefaction of *Nannochloropsis* sp. and the influence of solvents. *Energy Fuels* 25, 3235-3243, 2011
- [36] B. M. Kabyemela, T. Adschiri, R. M. Malaluan, K. Arai. Kinetics of glucose epimerization and decomposition in subcritical and supercritical water. *Ind. Eng. Chem. Res.* 36, 1552-1558, 1997
- [37] B. Kabyemela, T. Adschiri, R. M. Malaluan, K. Arai. Glucose and fructose decomposition in subcritical and supercritical water: Detailed reaction pathway, mechanisms, and kinetics. *Ind. Eng. Chem. Res.* 38, 2888-2895, 1999
- [38] T. Minowa, F. Zhen, T. Ogi. Liquefaction of cellulose in hot compressed water using sodium carbonate: Product distribution at different reaction temperatures. *J. Chem. Eng. Japan* 30 (1), 186-190, 1997
- [39] T. Minowa, F. Zhen, T. Ogi., G. Varhegyi. Decomposition of cellulose and glucose in hot compressed water under catalyst-free condition. *J. Chem. Eng. Japan* 31 (1), 131-134, 1998

[40] A. A. Peterson, R. P. Lachance, J. W. Tester. Kinetic evidence of the Maillard reaction in hydrothermal biomass processing: Glucose-glycine interactions in high-temperature, high-pressure water. *Ind. Eng. Chem. Res.* 49, 2107-2117, 2010

[41] A. Kruse, A. Krupka, V. Schwarzkopf, C. Gamard, T. Henningsen. Influence of proteins on the hydrothermal gasification and liquefaction of biomass. 1. Comparison of different feedstocks. *Ind. Eng. Chem. Res.* 44, 3013-3020, 2005

[42] A. Kruse, P. Maniam, F. Spieler. Influence of proteins on the hydrothermal gasification and liquefaction of biomass. 2. Model compounds. *Ind. Eng. Chem. Res.* 46, 87-96, 2007

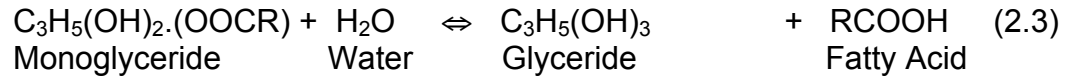
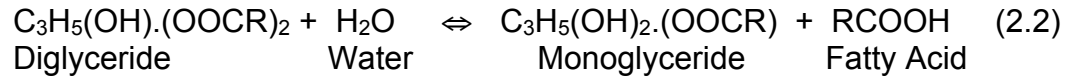
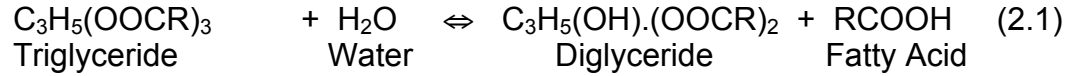
CHAPTER 2

Literature Review

The previous chapter summarized the reasoning behind selecting ethyl oleate, phenylalanine, phytol, and DOPC as model compounds for understanding hydrothermal liquefaction of algae. In this chapter we present a comprehensive literature review of the work done to date for each of these compounds in HTW. There exist numerous gaps in the literature pertaining to the study of individual and binary mixtures of model compounds in HTW. These provide a motivation for our research, which aims to establish a foundation for the comprehension of more complex systems relevant to algae processing.

2.1 Ethyl Oleate

Triglycerides are very important from the point of view of bio-oil production during HTL. Hydrolysis of triglycerides produces fatty acids and glycerol. Numerous studies have been undertaken to study this process with different kinds of vegetable oils in HTW [1-8]. Mills and McClain [4] studied the hydrolysis of beef tallow and coconut oil at 235 and 250 °C, and proposed a three-step reaction network, wherein the first step is hydrolysis of triglyceride to diglyceride, the second involves hydrolysis of the diglyceride to a monoglyceride, and the last involves the hydrolysis of monoglyceride to produce fatty acid and glycerol. This reaction scheme is summarized below. However, the authors did not report any kinetic data.



Patil *et al.* [1] have modeled hydrolysis of coconut oil between 180-280 °C using the above reaction network. Their model contained four parameters (three of which were overall equilibrium constants for the above reactions and one was the overall mass transfer coefficient) and one rate parameter for the hydrolysis of triglyceride. They determined that triglyceride hydrolysis (reaction 2.1) was the rate-controlling step and that mass transfer of glycerol and water across the phases was fast relative to the reaction rate. Alenezi *et al.* [3] also applied the above reaction scheme to obtain the hydrolysis kinetics for sunflower oil, using a continuous flow system in subcritical water at 20 MPa between 270-350 °C. Their results were comparable to those of Patil *et al.* [1]. Additionally, Alenezi *et al.* [3] proposed that the fatty acid produced above could act as a catalyst, auto-catalyzing the hydrolysis of triglycerides. This hypothesis was consistent with their experimental results. However, they do not consider any autocatalytic kinetics in their model.

Kocsisova *et al.* [8] studied the hydrolysis of refined edible rapeseed oil and a blend of higher fatty acids from 280-340 °C in a continuous reactor for a maximum residence time of 12 minutes and reported first-order kinetics. However, their kinetic data are not fully established since they modeled their triglyceride system with only one rate constant. Nonetheless, they report an interesting finding, wherein, the yields of the fatty acid decreased with an increase in temperature. They hypothesized dimerization of the fatty acid under their conditions, which was confirmed using IR measurements.

Although the kinetics of triglycerides has been reported in HTW, one needs to further study the individual reactions within the proposed scheme

(Eq.(2.1)-Eq.(2.3)), to get a more detailed mechanistic understanding about the system. In other words there is a need to explore the possible consequences of autocatalytic kinetics, fatty acid dimerization, and the reversibility or irreversibility of each step in the scheme. We overcome these gaps by studying the kinetics of ethyl oleate in HTW. Next, we present a till date literature review on hydrolysis of fatty acid esters in HTW.

Very little work has been done in the past on the kinetics of hydrolysis for individual fatty acid esters. Khuwijtjaru *et al.* [9] studied the hydrolysis of C₈-C₁₆ fatty acid methyl esters from 210 – 270 °C in a batch reactor. The kinetics of ester consumption was consistent with a rate equation that was first order in ester. We note, however, that the initial ester concentration was low ($\sim 5 \times 10^{-5}$ M) in this study, which means that kinetic features that become important at higher concentrations would have gone unobserved. Secondly, these authors have not considered the likelihood of the reverse reaction (esterification) in their work. In reality, hydrolysis and esterification are reversible and should be accounted together to fully elucidate this reaction pathway.

Day and Ingold [10] have classified hydrolysis of esters into eight possible mechanisms, depending on whether the reaction is (1) acid- or base- catalyzed (A or B), (2) acyl or alkyl cleavage (ac or al), and (3) unimolecular or bimolecular (1 or 2), depending upon whether the carbocation (formed as an intermediate) transforms to the product by itself or by the addition of an alcohol molecule to it [10]. Thus, the eight mechanisms that have been documented for esters (RCOOR') are Aac1, Aac2, Aal1, Aal2, Bac1, Bac2, Bal1 and Bal2. This classification is a useful starting point, but it strictly applies to reactions with added acid or added base. The system in which we are interested involves no added catalyst – just hydrolysis of TGs or fatty acid esters in neutral HTW.

For acid-catalyzed hydrolysis of esters, Aac2 is the most common mechanism. In the Aac2 mechanism, the first step is the protonation of the ester by H⁺ to generate a carbocation [10]. The carbocation is subsequently attacked by a water molecule and, after a series of steps, forms the corresponding fatty

acid and alcohol. Aal1 is the next common mechanism for esters having R' that give stable carbocations. Aac1 is rare, being found mostly with strong acids and sterically hindered R. Aal2 is even rarer. For base – catalyzed hydrolysis, Bac2 is almost universal. Bal1 occurs only with R' that give stable carbocations and only in weakly basic or neutral solutions. Bal2 is very rare and Bac1 has never been observed. More details regarding these mechanisms can be found in the literature [10].

There has been some previous mechanistic work on ester hydrolysis in near- neutral HTW, but none for long-chain fatty acid esters. Krammer and Vogel [11] proposed a modified form of the Aac2 mechanism for hydrolysis of ethyl acetate in neutral HTW. They suggest that reaction of two water molecules with a protonated ester intermediate is the rate-determining step. The presence of two water molecules, possibly due to hydrogen bonding, differentiates their mechanism from the conventional Aac2 mechanism. All other steps following the rate-determining step were taken to be fast and irreversible. The authors developed a kinetic model from their mechanism, but they only accounted for H⁺ arising from the dissociation of the acetic acid product. Since no acetic acid is present initially, the reaction rate at time (t), $t = 0$, would be zero according to this model. In reality, H⁺ from the dissociation of water would be available at $t = 0$ to begin the reaction. Secondly, if the reaction is solely catalyzed by H⁺, as suggested by Krammer and Vogel [11] then the pseudo-first order rate constant, k , for reactant disappearance should be directly proportional to the hydronium ion concentration in the solution. More specifically the slope of $\log k$ plotted against the pH should be -1 for such a H⁺-catalyzed reaction. Krammer and Vogel [11] did not check for this behavior by doing experiments at different initial pH values, but Comisar *et al.* [12] have carried out pH studies for hydrolysis of methyl benzoate at 200 °C and 300 °C. Their results indicated a dependence of the pseudo-first order rate constant on H⁺ much weaker than first-order in near-neutral HTW. To account for their observations, Comisar *et al.* [12] proposed a mechanism that included not only specific acid catalysis by H⁺ but also general acid catalysis by water molecules. They showed that such a mechanism led to a

rate equation that was quantitatively consistent with experimental results. The kinetics becomes first order in H^+ only at lower pH. Ravens [13] also showed that very low pH ($> 3N$ HCl) is needed to make ester hydrolysis specific acid catalyzed (for hydrolysis of polyethylene terephthalate fibers).

Oka *et al.* [14] proposed a base catalyzed pathway for ester hydrolysis in supercritical water (SCW), because adding a protic acid did not alter the hydrolysis rate of methyl 2-phenylpropionate at $390^\circ C$. Oka *et al.* [14] did not test their hypothesis by adding a base to the system, but given the findings of Comisar *et al.* [12], one expects little effect from either H^+ or added OH^- in near neutral SCW. The experimental result from Oka *et al.* [14] is consistent with the combination of general and specific acid catalysis proposed by Comisar *et al.* [12].

This review of the relevant literature indicates that ester hydrolysis can be catalyzed by H^+ , especially at very low pH, and by water molecules, especially at near-neutral pH. Moreover, it seems reasonable that if water can serve as a general acid catalyst, then the carboxylic acid formed by hydrolysis would be an even more effective general acid catalyst (although this hypothesis has not been previously tested). Furthermore, none of the mechanistic studies have considered hydrolysis and esterification in tandem.

2.2 Phenylalanine

Different strains of algae have varying composition of proteins ranging from as low as 6% wt to as high as 71% wt (on a dry algae basis) [15]. Rogalinski *et al.* [16] showed, using bovine serum albumin, that the proteins undergo hydrolytic depolymerization to release peptide fragments (amino acids), which decompose further in HTW. An understanding of the behavior of amino acids is important for comprehending the way proteins react in HTW. Thus, we study a model amino acid in our research and present next a literature review for amino acids in HTW.

Several researchers have studied the behavior of different amino acids in HTW [17-30]. Vallentyne [17] studied the decomposition of several amino acids

under subcritical water conditions ($T < 243\text{ }^{\circ}\text{C}$) and modeled the decarboxylation of amino acids using first-order kinetics. Despite the great efforts made in his research, he faced many technological problems due to the breaking of glass reactors employed in his work. Others too have mentioned decarboxylation as the main reaction of alanine and glycine in HTW and reported the first order rate constants [18-20].

Sato *et al.* [22] measured the decomposition of five amino acids (alanine, leucine, phenylalanine, serine and aspartic acid) at 200-340 $^{\circ}\text{C}$, 20 MPa and 20-180 s. They reported that decarboxylation to amines and deamination to organic acids were the two main pathways under these conditions. These authors suggest that alanine and glycine are produced as intermediates from serine. However, very short residence times were employed, preventing use of their work to broader studies of algae liquefaction.

Klinger and Vogel [23] studied alanine and glycine in hydrothermal conditions at 250-450 $^{\circ}\text{C}$, 34 MPa and 24 MPa, with residence times of 2.5-3.5 s. They too found organic acids and amines to be the main reaction products but they also suggested that glycine could dimerize to diketopiperazine. Other researchers have also reported trimers and tetramers of glycine and alanine at 200-350 $^{\circ}\text{C}$, 15-40 MPa and 120 s [31-33]. Cox and Seward [24] used a custom-built spectrophotometric cell and in situ observation to report dimerization and subsequent cyclization of alanine and glycine. They also fit a model of amino acid oligomerization kinetics to their experimental data using various reaction orders; they concluded that the best fit was obtained when oligomerization followed second-order kinetics. However, their study was conducted only at low temperatures (from 120-165 $^{\circ}\text{C}$). In a recent study, Otake *et al.* [34] reported oligomers up to pentamers for alanine and glycine at high temperatures (180-400 $^{\circ}\text{C}$), reaction times from 2 to 24 hours, and high pressure (1.0-5.5 GPa) without using a catalyst. However, these authors do not report rate constants for these oligomerization reactions starting from amino acids. Otake *et al.* [34] also report that under their experimental conditions, deamination of amino acids was

avored over decarboxylation. They attribute this difference in the pathways relative to others [17-20] to the high pressures (several GPa) they used. Sakata *et al.* [35] studied the effect of pH on the dimerization rate of glycine under hydrothermal conditions. They showed that the rate of dimerization increases with pH, with a maximum rate occurring at pH of 9.8 and 150 °C.

Abdelmoez *et al.* [25,26] studied the kinetics of 17 amino acids in saturated subcritical water (230-290 °C) and batch holding times ranging from 2.5-40 min, both individually and as mixtures. Glycine, alanine, valine, and proline were produced as intermediate products from other amino acids in their study. For phenylalanine in HTW, the authors propose a deamination pathway due to the formation of formic acid, carbonic acid, and ammonia. However, these authors may have overlooked the possibility of carbonic acid formation due to a decarboxylation pathway. They also report that amino acids in mixtures were less stable and had a decrease in their activation energy values. Furthermore, they conducted a pH study and found most amino acids to be labile at acidic and near-neutral pH values but more stable at basic pH 10. Li and Brill [28-30] have studied the kinetics of decarboxylation of aliphatic amino acids, effects of different side chain constituents, and effect of pH on the hydrothermal stability of these amino acids at 270-340 °C using an FT-IR spectroscopy flow reactor. They are also the only research group, to the best of our knowledge, to have studied the effect of addition of salt (KCl) on hydrothermal decarboxylation [28]. They found that the decarboxylation rate for α -alanine decreases with the addition of KCl. They hypothesized that either the transition state was less polar than the zwitterionic reactant due to solvent association on addition of salt or that K^+ or Cl^- ions formed complexes with the ionic sites of α -alanine thereby reducing its activity. However, the authors presented no experimental evidence in support their hypothesis.

Although a number of studies exist on the behavior of amino acids in HTW, no detailed characterization of products, pathways, and kinetics at high temperatures and longer batch holding times have been carried out in the past.

To the best of our knowledge, no study has been reported for amino acids above 340 °C and at times longer than 3 min [36]. These longer times are very relevant for hydrothermal liquefaction of algae because they lead to maximum yields of bio-oil. There has been no previous detailed exploration of all the possible products and pathways that may arise from amino acids under these conditions. Furthermore, different pathways, decarboxylation and deamination, have been proposed for reactions of amino acids in HTW but only on the basis of measuring carbon dioxide product yields. Measuring carbon dioxide evolution alone is not sufficient. Other products from amino acid reaction in and with HTW should be thoroughly identified to obtain a proper understanding of the reaction pathways. Furthermore, most of these previous studies are devoted to understanding primarily the behavior of simple amino acids such as alanine and glycine and not the more complicated amino acids.

2.3 Phytol

Our search of the literature found no previous work related to the reactions of chlorophyll in water at elevated temperatures and pressures. Previous work on phytol decomposition has either focused on its degradation by bacteria [37-39], its photodegradation in marine sediments and seawater [40-42], or its degradation in water at temperatures below 100 °C with and without a catalyst [43]. For instance, Gillian *et al.* [38] reported that phytol produces phytenic acid and phytone (6,10,14-trimethylpentadecan-2-one) when treated with bacteria under aerobic conditions at room temperature, whereas Rotani and Acquaviva [39] demonstrated that at 30 °C, phytol primarily formed phytone, while at 13 °C phytol gave phytenic acid as the major product. Rotani and coworkers [39-42, 44] also studied abiotic degradation of free phytol in seawater column at 11 °C and reported formation of phytone.

2.4 DOPC

The hydrothermal behavior of phospholipid is of interest to us since its chemistry is not clearly understood for algae liquefaction. We could not find any work reported on phospholipid at high temperatures in water. However, research has been conducted at much lower temperatures for phospholipids in liposomes. Zuidam and Crommelin [45] studied the kinetics of hydrolysis of phospholipid in liposomes comprising egg phosphatidylcholine (EPC), dimyristoyl phosphatidylcholine (DMPC), distearoyl phosphatidylcholine (DSPC), and dipalmitoyl phosphatidylcholine/cholesterol (DPPC/CHOL) at a pH of 4.0 and different temperatures (maximum 80 °C). They modeled the disappearance of the phospholipid with pseudo-first order kinetics. They have also shown that changes in fatty acid chains and size do not influence the hydrolysis rate constants significantly.

Kensil and Dennis [46] studied the alkaline hydrolysis (pH 12.7) of EPC and DPPC in liposomes and in mixed micelles, prepared using a 8:1 molar ratio of detergent (Triton X-100) to phospholipid between 15-60 °C. Free fatty acids and *sn*-glycerol-3-phosphorylcholine (GPC) were the main products of hydrolysis of these phospholipids. These authors proposed that GPC was formed through a lyso-phosphatidylcholine (LPC) intermediate. The first step of their proposed scheme involves the attack of a hydroxide ion at either the syn-1 or syn-2 positions of the PC to produce 2-acyl LPC and 1-acyl LPC isomers, respectively. The authors found equal hydrolysis rates at both positions over the first half-life of the hydrolysis process. The next step of the reaction scheme involves the hydrolysis of either of the LPCs (1-acyl and 2-acyl) to remove a second fatty acid moiety and to form GPC. The authors reported the kinetics to be first order for both the phosphatidylcholine and the hydroxide ions. They did not observe further hydrolysis of GPC and mentioned that this reaction was slow under their conditions. Hanahan [47] have also mentioned in their review that further hydrolysis of GPC is quite slow compared to acyl hydrolysis.

Grit and coworkers [48-50] studied the hydrolysis of different phosphatidylcholines (PC) in aqueous liposomal dispersions under acidic and alkaline conditions and reported pseudo-first order kinetics. They demonstrated that the rate of hydrolysis was acid- and base-catalyzed with a minimum rate occurring at a pH of 6.5 between 40-70 °C. They proposed a reaction scheme similar to Kensil and Dennis [46], except that they observed further hydrolysis of GPC to form glycerophosphoric acid (GPA) as the end product. GPA did not hydrolyze further under their conditions. The initial hydrolysis of PC gave an isomeric mixture of 1-acyl LPC and 2-acyl LPC. However, no rate constants were reported for the individual reaction steps of their network.

Koning and McMullan [51] studied the hydrolysis of DOPC using a 2 N HCl solution at 120 °C. They too proposed a reaction network similar to Kensil and Dennis [46], according to which the first steps involve removal of two fatty acids from the PC to form GPC. Additionally, they also suggest that GPC is further hydrolyzed via a cyclic ortho triester to form choline and cyclic glycerophosphate. Cyclic glycerophosphate was eventually converted to an equilibrium mixture of 85% α -glycerophosphate and 15% of β -glycerophosphate in the acidic medium. The authors obtained $80 \pm 5\%$ of the initial phosphorus in the combined α - and β -glycerophosphates. Maruo and Benson [52] have shown that the rate of hydrolysis of cyclic glycerophosphate to α - and β -glycerophosphate is rapid in 0.1 N HCl and 24 °C, with 50% conversion being achieved in less than 10 min under these conditions. Koning and McMullan [51] also quantified small amounts of phosphorylcholine ($15 \pm 5\%$ of total phosphorus). They proposed that phosphorylcholine could form via the hydrolysis of the phosphate group in GPC, a reaction parallel to the formation of cyclic glycerophosphate from GPC. Lastly, $5 \pm 3\%$ of inorganic phosphorus compound was quantified and hypothesized to originate via the hydrolysis of glycerophosphate and phosphorylcholine. However, no kinetics was reported for the individual steps of the reaction network.

It should be emphasized that although the above studies used liposomes and were performed at low temperatures, they give useful information about the

products that are formed during the hydrolysis of phosphatidylcholine (PC). However, the reaction chemistry and mechanism of PC is not well understood at higher temperatures (greater than 120 °C). A complete carbon or phosphorus balance remains elusive. Moreover, all of the above studies report an overall first-order rate constant for disappearance of PC. No one has yet explored the reaction at higher concentrations of PC, wherein some other kinetic phenomenon (e.g., autocatalysis) may become prominent (Changi *et al.* [53]). Although researchers have proposed different reaction networks for hydrolysis of phospholipids in acidic, neutral, and basic conditions, none of the reports mention the rate constants for all of the individual steps of the network.

2.5 Binary Mixtures

The last objective of this research is to explore binary mixture systems of phenylalanine and inorganic additives (salts and boric acid) and phenylalanine and an organic compound (ethyl oleate). This section talks about the previous work done with binary mixtures relevant to our chosen systems.

Effects of salts have been studied during hydrothermal gasification of amino acids or other carbon containing compounds, but very little work has been done with salts during the HTL process [54-57]. This work suggests that addition of salts could accelerate the decomposition of amino acids. To the best of our understanding, only Li *et al.* [28] has previously studied the effect of salts on amino acid reaction pathways and kinetics in water at high temperatures but for α -alanine. They observed a reduction in the decarboxylation rate on the addition of KCl (1 and 2 M). They hypothesized this reduction in the rate of decarboxylation due to either 1) the formation of a transition state less polar than the starting zwitterion of α -alanine, or 2) the formation of complexes of K^+ or Cl^- with ionic sites of α -alanine zwitterions. The authors have quantified the rate of decarboxylation by measuring CO_2 formation. It is quite possible that they may have overlooked the effects of salts on other parallel reactions of amino acid.

Regarding binary mixtures, glucose appears to be the only organic compound that has been studied together with amino acids in high-temperature, high-pressure water [58-60]. Peterson *et al.* [58] showed that a binary mixture of glucose and glycine at 250 °C and 10 MPa undergoes the Maillard reaction, where the sugar and amino acid combine to form the so-called Amadori compound. This product then undergoes a number of reactions to form polymeric compounds referred to as melanoidins. The authors also showed that the presence of glucose accelerated glycine disappearance, while the presence of glycine either increased or decreased glucose decomposition (depending on the initial glycine concentration). Clearly, the binary mixture behaves differently than either of the starting model compounds. Kruse *et al.* [59,60] have studied the influence of alanine on glucose in the presence of potassium salts but for hydrothermal gasification carried from 460 - 550 °C at 25 MPa and for reaction times between 5-9 s. They found that the gas yields decrease in the presence of amino acids and the dissolved organic carbon content increases, which they also attributed to the Maillard reaction.

For the algae system, triglycerides and proteins constitute more than 75% of the total cell composition. However, previous work has not focused on binary mixtures of ester and amino acids to enable us to elucidate interactions between triglycerides and proteins. It is possible that additional pathways may become important for binary mixtures compared to those for individual model compounds. E.g.: Brown *et al.* [36] and Valdez *et al.* [61] characterized and quantified fatty acid amides as products from the HTL of algae. Valdez *et al.* [61] reported that the yields of palmitic acid amide varied from 0.5 to 3 (mg/g of dry algae) depending on whether hexane or hexadecane was used, respectively, for recovery of bio-oil. These authors have proposed the reaction of fatty acids (product from ethyl oleate) with ammonia (product from amino acid) to account for the amide formation.

2.6 Summary of Gaps in Literature

The main objective of this thesis is to study various model compounds and their binary mixtures to obtain a better understanding of the biomacromolecules during HTL process. Based on the above literature review there are several aspects that have not been fully explored for either the biomacromolecules or the corresponding chosen model compounds in HTW.

Hydrolysis of fatty acid ester has not been studied to fully account for all the kinetics features at different conditions, i.e. autocatalysis and dimerization. Furthermore, kinetics of ester hydrolysis has been studied separately from esterification of fatty acid. In reality these are reverse reactions and should have coupled kinetics. Mechanistically, it has been established that ester hydrolysis proceeds via specific acid catalysis and general water catalysis. It is quite possible that other mechanisms (e.g. general acid catalysis by fatty acid) have been ignored in the past.

For amino acids, a through product characterization has not been documented at 350 °C (temperature of maximum bio-oil yield from algae). Besides, amino acid decomposition in HTW has been proposed to occur via different pathways (e.g. deamination and decarboxylation), and has been quantified through measurements of certain products, such as carbon dioxide. A 100% carbon balance remains elusive in literature because complete quantification of products and reactants has never been reported before. Moreover, only simple amino acids (e.g. glycine and alanine) have been studied in detail in HTW. It is possible that the kinetics features can be affected due to steric and electronic effects of complex amino acids.

On similar lines, reactions involving phytol and DOPC have also never been explored in HTW. There is no previous documentation of their product distribution, the pathways explaining product formation, or the rate constants associated with individual reaction steps in the overall product formation

pathways. Both of these compounds are likely to generate several products, not only in the bio-oil but also in the aqueous phase during HTL of algae.

Finally, binary mixtures of model compounds, besides glucose and amino acids have not been studied. From an algae perspective, triglycerides and proteins are the main constituents. Thus, one needs to understand the behavior of esters and amino acids together in HTW. It is possible that new products are formed via the interaction of model compounds and the rates of the individual steps are influenced by the presence of the new components in the mixtures.

Thus, this chapter summarizes the work done in the past relevant to model compounds in HTW and identifies the key gaps paving the road for carrying out additional research. The next chapter discusses the experimental setup used for various model compounds.

References

- [1] T. A. Patil, D. N. Butala, T. S. Raghunathan, H. S. Shankar. Thermal hydrolysis of vegetable oils and fats. 1. Reaction kinetics. *Ind. Eng. Chem. Res.* 27, 727-735, 1988
- [2] T. Fujii, P. Khuwijtjaru, Y. Kimura, S. Adachi. Decomposition kinetics of monoacyl glycerol and fatty acid in subcritical water under temperature-programmed heating conditions. *Food Chemistry* 94, 341-347, 2006
- [3] R. Alenezi, G. A. Leeke, R. C. D. Santos, A. R. Khan. Hydrolysis kinetics of sunflower oil under subcritical water conditions. *Chem. Eng. Res. Des.* 87, 867-873, 2009
- [4] V. Mills, H. K. McClain. Fat hydrolysis. *Ind. Eng. Chem. Res.* 47, 1982, 1949
- [5] R. L. Holliday, J. W. King, G. R. List. Hydrolysis of vegetable oils in sub- and supercritical water. *Ind. Eng. Chem. Res.* 47 (18), 6801-6808, 2008
- [6] J. W. King, R. L. Holliday, G. R. List. Hydrolysis of soybean oil in subcritical water flow reactor. *Green Chem.* 1 (6), 261-264, 1999
- [7] J. Sebastião S. Pinto, F. M. Lanças. Hydrolysis of corn oil using subcritical water. *J. Braz. Chem. Soc.* 17 (1) 85-89, 2006
- [8] T. Kocsisová, J. Juhaz, J. Cvengroš. Hydrolysis of fatty acid esters in subcritical water. *Eu. J. Lipid Sci. Technol.* 108, 652-658, 2006
- [9] P. Khuwijtjaru, T. Fujii, S. Adachi, Y. Kimura, R. Matsuno. Kinetics on the hydrolysis of fatty acid esters in subcritical water. *Chem. Eng. J.* 99, 1-4, 2004
- [10] J. N. E. Day, C. K. Ingold. Mechanism and kinetics of carboxylic ester hydrolysis and carboxyl esterification. *Trans. Faraday Soc.* 37, 685-705, 1941
- [11] P. Krammer, H. Vogel. Hydrolysis of esters in subcritical and supercritical water. *J. Supercrit. Fluids* 16, 189-206, 2000

- [12] C. Comisar, S. Hunter, A. Walton, P. E. Savage. Effect of pH on ether, ester, and carbonate hydrolysis in high-temperature water. *Ind. Eng. Chem. Res.* 47, 577-584, 2008
- [13] D. A. S. Ravens. The chemical reactivity of poly (ethylene terephthalate): heterogeneous hydrolysis by hydrochloric acid. *Polymer* 1, 375-383, 1960
- [14] H. Oka, S. Yamago, J. Yoshida, O. Kajimoto. Evidence for a hydroxide ion catalyzed pathway in ester hydrolysis in supercritical water. *Angew. Chem. Int. Ed.* 41 (4), 623-625, 2002
- [15] E. W. Becker. Micro-algae as a source of protein. *Biotechnol. Adv.* 25, 207-210, 2007
- [16] T. Rogalinski, K. Liu, T. Albrecht, G. Brunner. Hydrolysis kinetics of biopolymers in subcritical water. *J. Supercrit. Fluids* 46, 335-341, 2008
- [17] J. R. Vallentyne. Thermal reaction kinetics and transformation products of amino compounds. *Geochim. Cosmochim. Acta* 28, 157-188, 1964
- [18] Y. Qian, M. H. Engel, S. A. Macko, S. Carpenter, J. Deming. Kinetics of peptide hydrolysis and amino acid decomposition at high temperature. *Geochim. Cosmochim. Acta* 57, 3281-3293, 1993
- [19] E. Andersson, N. Holm. The stability of some selected amino acids under attempted redox constrained hydrothermal conditions. *Orig. Life Evol. Biosph.* 30 (1), 9-23, 2000
- [20] J. L. Bada, S. L. Miller, N. Zhao. The stability of amino acids at submarine hydrothermal vent temperatures. *Orig. Life Evol. Biosph.* 25, 111-118, 1995
- [21] H. C. Helgeson, J. P. Amend. Relative stabilities of biomolecules at high temperatures and pressures. *Thermochim. Acta* 245, 89-119, 1994
- [22] N. Sato, A. T. Quintain, K. Kang, H. Daimon, K. Fujie. Reaction kinetics of amino acid decomposition in high-temperature and high-pressure water. *Ind.*

Eng. Chem. Res. 43 (13), 3217-3222, 2004

[23] D. Klinger, J. Berg, H. Vogel. Hydrothermal reactions of alanine and glycine in sub- and supercritical water. *J. Supercrit. Fluids* 43, 112-119, 2007

[24] J. S. Cox, T. M. Seward. The reaction kinetics of alanine and glycine under hydrothermal conditions. *Geochim. Cosmochim. Acta* 71, 2264-2284, 2007

[25] W. Abdelmoez, T. Nakahasi, H. Yoshida. Amino acid transformation and decomposition in saturated subcritical water conditions. *Ind. Eng. Chem. Res.* 46, 5286-5294, 2007

[26] W. Abdelmoez, T. Nakahasi, H. Yoshida. Pathways of amino acid transformation and decomposition in saturated subcritical water conditions *Int. J. Chem. Reactor Eng.* 8 (A107), 1-19, 2010

[27] M. Faisal, N. Sato, A. T. Quintain, H. Daimon, K. Fujie. Hydrolysis and cyclodehydration of dipeptide under hydrothermal conditions. *Int. J. Chem. Kinet.* 39 (3), 175-180 2007

[28] J. Li, X. Wang, M. T. Klein, T. B. Brill. Spectroscopy of hydrothermal reactions, 19: pH and salt dependence of decarboxylation of α -alanine at 280-330 °C in an FT-IR spectroscopy flow reactor. *Int. J. Chem. Kinet.* 34 (4), 271-277, 2002

[29] J. Li, T. B. Brill. Spectroscopy of hydrothermal reactions 25: Kinetics of the decarboxylation of protein amino acids and the effect of side chains on hydrothermal stability. *J. Phys. Chem. A.* 107, 5987-5992, 2003

[30] J. Li, T. B. Brill. Spectroscopy of hydrothermal reactions 26: Kinetics of the decarboxylation of aliphatic amino acids and comparison with the rates of racemization. *Int. J. Chem. Kinet.* 35 (11), 602-610, 2003

[31] Ogata Y., E. Imai, H. Honda, K. Hatori, K. Matsuno. Hydrothermal circulation of seawater through hot vents and contribution of interface chemistry to prebiotic synthesis. *Origins of Life and Evolution of the Biosphere* 30, 527-537, 2000

- [32] D. K. Alargov, S. Deguchi, K. Tsujii, K. Horikoshi. Reaction behaviors of glycine under super- and subcritical water conditions. *Origins of Life and Evolution of the Biosphere* 32, 1-12, 2002
- [33] Md. N. Islam, T. Kaneko, K. Kobayashi. Reaction of amino acids in a supercritical water-flow reactor simulating submarine hydrothermal systems. *Bull. Chem. Soc. Jpn.* 76, 1171-1178, 2003
- [34] T. Otake, T. Taniguchi, Y. Furukawa, F. Kawamura, H. Nakazawa, T. Kakegawa. Stability of amino acids and their oligomerization under high-pressure conditions: Implications for prebiotic chemistry. *Astrobiology* 11 (8), 799-813, 2011
- [35] K. Sakata, N. Kitadai, T. Yokoyama. Effects of pH and temperature on dimerization rate of glycine: Evaluation of favorable environmental conditions for chemical evolution of life. *Geochim. Cosmochim. Acta* 74, 6841-6851, 2010
- [36] T. M. Brown, P. Duan, P. E. Savage. Hydrothermal liquefaction and gasification of *Nannochloropsis* sp. *Energy Fuels* 24 (6), 3639-3646, 2010
- [37] P. W. Brooks, J. R. Maxwell. Early stage fate of phytol in a recently-deposited lacustrine sediment, in: B. Tissot, F. Biennier (Eds.). *Advances in Organic Geochemistry* 1973, Technip, Paris, France, 977-991. 1974
- [38] F. T. Gillian, P. D. Nichols, R. B. Johns, H. Bavor. Phytol degradation by marine bacteria. *Appl. Environ. Microbiol.* 45 (5), 1423-1428, 1983
- [39] J. F. Rotani, M. Acquaviva. The aerobic bacterial metabolism of phytol in seawater: Temperature dependence of an abiotic intermediate step and its consequences. *Chemosphere* 26 (8), 1513-1525, 1993
- [40] J. F. Rotani, J. Volkman. Phytol degradation products as biogeochemical tracers in aquatic environments. *Org. Geochem.* 34, 1-35, 2003

- [41] J. F. Rotani, I. Combe, P. Giral. Abiotic degradation of free phytol in the water column: A new pathway for the production of acyclic isoprenoids in the marine environment. *Geochim. Cosmochim. Acta* 54, 1307-1313, 1990
- [42] J. F. Rotani, G. Bailet. Production of acyclic isoprenoid compounds during the photodegradation of chlorophyll-a in seawater. *J. Photochem. Photobiol., A* 59, 369-377, 1991
- [43] J. W. De Leeuw, V. A. Correa, P. A. Schenck. On the decomposition of phytol under simulated geological conditions and in the top-layer of natural sediments, in: B. Tissot and F. Bienner (Eds.) *Advances in Organic Geochemistry*, Technip, Paris, France, 993-1004, 1974
- [44] J. F. Rotani, P. C. Bonin, J. K. Volkman. Biodegradation of free phytol by bacterial communities isolated from marine sediments under aerobic and denitrifying conditions. *Appl. Environ. Microbiol.* 65(12), 5484-5492, 1999
- [45] N. J. Zuidam, D. J. A. Crommelin. Chemical hydrolysis of phospholipids *J. Pharm. Sci.* 84 (9) 1113-1119, 1995
- [46] C. R. Kensil, E. A. Dennis. Alkaline hydrolysis of phospholipids in model membranes and the dependence on their state of aggregation *Biochemistry* 20, 6079-6085, 1981
- [47] D. J. Hanahan. *Lipide Chemistry*. John Wiley & Sons, Inc., New York, 1960
- [48] M. Grit, J. H. de Smidt, A. Struijke, D. J. A. Crommelin. Hydrolysis of phosphatidylcholine in aqueous liposome dispersions. *Int. J. Pharm.* 50, 1-6, 1989
- [49] M. Grit, D. J. A. Crommelin. The effect of aging on the physical stability of liposome dispersions. *Chem. Phys. Lipids* 62, 113-122, 1992
- [50] M. Grit, D. J. A. Crommelin. Chemical stability of liposomes: implications for their physical stability. *Chem. Phys. Lipids* 64, 3-18, 1993

- [51] A. J. De Koning, K. B. McMullan. Hydrolysis of phospholipids with hydrochloric acid. *Biochim. Biophys. Acta* 106, 519-526, 1965
- [52] B. Maruo, A. A. Benson. Cyclic glycerophosphate formation from the glycerolphosphatides. *J. Biol. Chem.* 234 (2), 254-256, 1959
- [53] S. Changi, T. Pinnarat, P. E. Savage. Modeling hydrolysis and esterification kinetics for biofuel processes. *Ind. Eng. Chem. Res.* 50, 3206-3211, 2011
- [54] D. Xu, S. Wang, X. Hu, C. Chen, Q. Zhang, Y. Gong. Catalytic gasification of glycine and glycerol in supercritical water. *Int. J. Hydrogen Energy* 34, 5357-5364, 2009
- [55] O. T. Onsager, M. S. A. Brownrigg, R. Lødeng. Hydrogen production from water and CO via alkali metal formate salts. *Int. J. Hydrogen Energy* 21 (10), 883-885, 1996
- [56] A. A. Peterson, F. Vogel, R. P. Lachance, M. Fröling, M. J. Antal Jr., J. W. Tester. Thermochemical biofuel production in hydrothermal media: A review of sub- and supercritical water technologies. *Energy Environ. Sci.* 1, 32-65, 2008
- [57] A. Kruse, E. Dinjus. Influence of salts during hydrothermal biomass gasification: The role of the catalyzed water-gas shift reaction. *Z. Phys. Chem.* 219, 341-366, 2005
- [58] A. A. Peterson, R. P. Lachance, J. W. Tester. Kinetic evidence of the Maillard reaction in hydrothermal biomass processing: Glucose-glycine interactions in high-temperature, high-pressure water. *Ind. Eng. Chem. Res.* 49, 2107-2117, 2010
- [59] A. Kruse, A. Krupka, V. Schwarzkopf, C. Gamard, T. Henningsen. Influence of proteins on the hydrothermal gasification and liquefaction of biomass. 1. Comparison of different feedstocks. *Ind. Eng. Chem. Res.* 44, 3013-3020, 2005

[60] A. Kruse, P. Maniam, F. Spieler. Influence of proteins on the hydrothermal gasification and liquefaction of biomass. 2. Model compounds. *Ind. Eng. Chem. Res.* 46, 87-96, 2007

[61] P. Valdez, J. G. Dickinson, P. E. Savage. Characterization of product fractions from hydrothermal liquefaction of *Nannochloropsis* sp. and the influence of solvents. *Energy Fuels* 25, 3235-3243, 2011

CHAPTER 3

Experimental Setup

This chapter discusses the experimental setup used for individual model compounds and the binary mixtures. It provides the reader with information about the conditions used for different experiments (concentrations, temperatures, and batch holding times), procedures employed for getting maximum recovery of the material from the reactors and post-recovery analysis using different analytical techniques such as, gas chromatography with mass spectrometry or flame ionization detector (GC-MS or GC-FID), high pressure liquid chromatography (HPLC), and nuclear magnetic resonance (NMR). One can use this information for reproducing the experiments, if so desired.

3.1 Materials

All the chemical reagents used in this work were ordered of the highest available purity and used as received. Ethyl oleate ($\geq 98\%$), oleic acid ($\geq 99\%$), phenylalanine-L ($\geq 99\%$), and phytol ($\geq 97\%$) were purchased from Sigma Aldrich, while DOPC ($\geq 99\%$) was purchase from Avanti Polar Lipids Inc. Other chemicals and standards such as, phenylethylamine, phenylethanol, styrene, sodium chloride, sodium nitrate, sodium sulfate, potassium chloride, dipotassium hydrogen phosphate, boric acid, phosphoric acid (85 wt%), hydrochloric acid (0.1N), glacial acetic acid, trifluoroacetic acid, and sodium hydroxide (0.1N) were purchased from Sigma Aldrich ($\geq 99\%$), while lyso-phosphatidylcholine (18:1) ($\geq 99\%$) was purchased from Avanti Polar Lipids Inc.

Methanol, dicholormethane, acetonitrile, and chloroform were purchased from Fisher Scientific ($\geq 99\%$) and used as received either for recovering

materials from the reactor post-reaction or as mobile phase for HPLC. Distilled water of HPLC grade was used for carrying out all the reactions.

3.2 General Experimental Setup

All reactions were carried out in stainless steel (SS-316) batch reactors assembled using Swagelok tube fittings (one port connector and two caps). Two different sizes of reactors were used for this work, 3/8" (with an internal volume of 1.5 mL) for ethyl oleate, phenylalanine and DOPC and 1/4" (with an internal volume of 0.59 mL) for phytol. Prior to using the reactors, they were filled with water and heated in a fluidized sand bath at a high temperature (between 250-300 °C) for 30-60 minutes to remove any residual materials and expose the reactor walls to the HTW environment. The conditioned reactors were cooled by quenching them in a cold-water bath. Each uncapped reactor was then washed thoroughly with methanol before use. The residual methanol was removed by several flushing of the reactors with water.

Reactants were added either directly or using a certain amount of a freshly prepared stock solution to the reactor in a pre-decided amount (see sections 3.3.1-3.3.5). Note that for maintaining uniformity throughout the text, the initial molar concentrations of model compounds (in mol/L) are based on 95% of the respective reactor volume. Water was loaded into the reactor such that the total fluid phase in the reactor at reaction condition occupied around 95% of the reactor volume. This volume of water, determined using Eq. (3.1), ensures that majority of the reactor is occupied with a liquid phase at the reaction condition. Under these operating conditions, one can assume that the transfer between the liquid and vapor phases does not affect the kinetics of the reaction. The density of the water at the reaction condition is calculated from steam tables (Refer Appendix, Table A.1).

$$V_{RoomT} = 0.95V_{Reactor} \frac{\rho_{ReactionT}}{\rho_{RoomT}} \quad (3.1)$$

The loaded reactors were sealed and placed in a preheated, fluidized sand bath (Techne SBL-2D) for a desired batch holding time and maintained at the desired temperature using a temperature controller (Techne TC- 8D). The sand bath was isothermal within $\pm 1^\circ \text{C}$. Pressures at reaction conditions were determined from the saturated steam tables (Refer Appendix, Table A.1). The heat-up time for 1.5 mL reactor was found to be 2-3 min, which is small relative to the typical batch holding times used in this study. The 0.59 mL reactor will have an even shorter heat-up time. Upon reaching the desired batch holding time, the reactors were removed from the sand bath and quenched by immersion in a cool water bath. The reactors were opened and the contents were recovered using a suitable solvent system (see Sections 3.3.1-3.3.5). This solvent solution was able to dissolve both the reactants and the products formed during the reaction, thereby giving a clear homogeneous phase suitable for further analysis. For uniformity, each sample was diluted up to 10 mL in a volumetric flask using the appropriate solvent. To determine experimental error, experiments were performed in triplicate for most cases. The experimental uncertainties reported represent the run-to-run variations, quantified by the standard deviations of experimental replicates.

3.3 Individual Model Compound Experimental Setup

This section describes in detail the experimental procedure used for each model compound and the binary mixtures in HTW.

3.3.1 Ethyl Oleate

Hydrolysis of ethyl oleate was carried out at 240, 260, 280, 300, and 350 °C for batch holding times between 0 and 180 min. The reactors (capacity 1.5 mL) were loaded at room temperature with 40 μL of ethyl oleate, such that the initial concentration of ester (C_{EO}^0) based on 95% reactor volume in these experiments was 0.075 mol/L. The amount of water loaded in the reactors, calculated using Eq.(3.1), was 1.16, 1.12, 1.08, 1.04, and 0.92 mL at 240, 260, 280, 300, and 350 °C. The loaded and sealed reactors were then immersed in a

preheated isothermal fluidized sand bath for the desired batch holding time. After the reaction was over, the reactors were opened and contents recovered using methanol solvent.

We performed a control experiment at room temperature to determine the recovery of ethyl oleate by loading 40 μL of ethyl oleate and 1.16 mL water into a reactor. The reactor was sealed and kept at room temperature for 30 minutes and then opened. The post-reaction work-up procedure used for the experiments at the elevated temperatures was then performed.

Additional experiments were performed to test the effect of products (oleic acid and ethanol) and variation of pH on the conversion of ethyl oleate. The necessity for carrying out these experiments will become clearer in Chapter 4 when we discuss the results of ethyl oleate hydrolysis. To test the effect of oleic acid, a set of three experiments was conducted at 240 $^{\circ}\text{C}$ (30 min) with varying amounts of oleic acid added initially into the system ($R_{\text{OA}} = 0.25, 0.5, \text{ and } 1.0$) and $R_{\text{w}} = 569$. Here R stands for the initial ratio of moles of oleic acid (OA), water (W), and ethanol (EtOH) to the limiting reactant, ethyl oleate. To test the effect of added ethanol on ethyl oleate, another set of three experiments was conducted at 300 $^{\circ}\text{C}$ (30 min) with varying amounts of ethanol added initially into the system ($R_{\text{EtOH}} = 25$ and $R_{\text{w}} = 450$, $R_{\text{EtOH}} = 50$ and $R_{\text{w}} = 375$, and $R_{\text{EtOH}} = 75$ and $R_{\text{w}} = 300$). Lastly, to see the effects of pH on ethyl oleate conversion, stock solutions of pH less than 7 were prepared by adding appropriate amounts of 0.1 N hydrochloric acid in water and those with pH greater than 7 were prepared by adding appropriate amounts of 0.1 N sodium hydroxide in water. The pH of the stock solution was confirmed at room temperature using a pH meter. The reactors were loaded with 40 μL of ethyl oleate and 1.08 ml of each of the above stock solutions and heated at 280 $^{\circ}\text{C}$ and 40 minutes with the rest of the procedure for post-recovery and analysis similar to that outlined previously.

Ethyl oleate and oleic acid (the main product of ethyl oleate hydrolysis) were quantitatively analyzed on HPLC with a UV detector using the analytical procedure outlined previously but with a few modifications [1]. We used a Zorbax

ODS HPLC column (4.6 mm id x 250 mm length) with 5 μm particle size packing. The mobile phase consisted of two solvent systems. Solvent A was methanol acidified with acetic acid (0.05% v/v) and solvent B comprised water acidified with phosphoric acid (0.1% v/v). The elution method involved an isocratic flow of 85% solvent A and 15% solvent over a period of 30 minutes at a total flow rate of 1 mL/min, which gave peaks corresponding to oleic acid and ethyl oleate at around 6 and 11 mins, respectively at 200 nm.

Calibration curves, generated using ethyl oleate and oleic acid standards in known quantities, were used to quantify these compounds. In all cases, the conversion of ethyl oleate is calculated using the yields of the reactant and product and assuming that the small difference between their sum and 100% (perfect mass balance) can be apportioned equally between the two yields. Furthermore, hydrolysis of ethyl oleate at all temperatures and 60 minutes, experiments with added oleic acid and added ethanol, and four pH experiments were repeated in triplicates and experimental uncertainty was calculated as standard deviation of the run-to-run variability.

3.3.2 Phenylalanine

Phenylalanine in HTW was studied at 220, 250, 280, and 350 $^{\circ}\text{C}$ for batch holding times between 0 and 240 min. Prior to loading the reactors, we prepared a stock solution by dissolving 1500 mg of phenylalanine completely in 100 mL of water (15000 ppm). Fresh stock solutions were made every two weeks. The reactors (capacity 1.5 mL) were then loaded at room temperature with suitable amounts of the stock solution. The initial concentration of phenylalanine (C°_{phe}) based on 95% reactor volume in these experiments was 0.075 mol/L. The amount of water loaded in the reactors, calculated using Eq.(3.1), was 1.20, 1.14, 1.08, and 0.92 mL at 220, 250, 280, and 350 $^{\circ}\text{C}$. Upon completion of the reaction at a desired temperature and batch holding time in a fluidized sand bath, the reactors were opened and the contents were recovered using methanol.

We performed a control experiment at room temperature to determine the recovery of phenylalanine. We loaded 1 mL of the stock solutions into a reactor and then sealed the reactor. The reactor was kept at room temperature for 30 minutes and then opened. The post-reaction work-up procedure used for the experiments at the elevated temperatures was then performed. Experiments were also performed to determine the effect of concentration of phenylalanine on its conversion and the yield of its products at 250 and 350 °C and different batch holding times. We examined phenylalanine in HTW at 4000 and 22000 ppm under these conditions.

To quantify phenylalanine, we used HPLC with a UV detector. A Zorbax ODS HPLC column (4.6 mm id x 250 mm length) with 5 µm particle size packing was used for the separation of phenylalanine. The mobile phase consisted of two solvent systems. Solvent A was water containing trifluoroacetic acid (0.1% v/v) and solvent B comprised acetonitrile containing trifluoroacetic acid (0.1% v/v). The elution method involved an isocratic flow of 90% solvent A and 10% solvent over a period of 30 minutes at a total flow rate of 1 mL/min, which gave phenylalanine peak at ~7 min at 205 nm.

We used an Agilent Technologies model 6890N GC equipped with an autosampler, autoinjector, and mass spectrometric detector to identify the main products from the HTW treatment of phenylalanine. Phenylalanine was not amenable to GC analysis, as it gave very poor peak resolution on the GC. A Wiley mass spectral library was used for compound identification by matching the mass fragments of observed peaks with those in the library. An Agilent Technologies model 6890 GC equipped with a FID was used to quantify the products. The reaction products were separated on a HP-5MS fused silica, non-polar capillary column (50 m length x 0.20 mm inner diameter x 0.33 µm film thickness). We used an inlet temperature of 300 °C, a split ratio of 5:1, and an injection volume of 1.0 µL. The temperature program involved an initial oven temperature of 40 °C followed by heating to 150 °C at a rate of 10 °C /min (isothermal for 4 min), then ramping at 10 °C /min to 225 °C (isothermal for 5

min), and a final ramp of 10 °C/min to 300 °C (isothermal for 15 min), giving a total run time of 50 min. Helium served as the carrier gas (1 mL/min).

To detect high molecular weight compounds and oligomers of phenylalanine in the product mixture, an Agilent Q-TOF LC-MS system, with an Agilent 1290 binary pump was used. Agilent Zorbax Eclipse Plus C-18 column (2.1 x 50 mm, 1.8 µm particle size, as stationary phase) was used. One Solvent (A) comprised water with 0.1% formic acid. Another solvent (B) comprised 95% acetonitrile, 5% water, and 0.1% formic acid. A gradient method starting with 5% solvent B (hold 1 min) transitioning to 100% B over 9 min (hold 2 min) was used. The flow rate to the column was maintained at 0.4 ml/min. Representative samples from reactions conducted at 250 °C and 30 min and 350 °C and 60 min were analyzed. These samples were recovered in a 1:1 (v/v) mixture of methanol to chloroform (to give a homogenous phase with water) and diluted to 10 mL, to ensure that all the oligomers are soluble in chloroform phase.

We generated calibration curves using standards of pure phenylalanine, phenylethylamine, styrene, and phenylethanol to determine the corresponding concentrations of each of these compounds. Product molar yields were calculated by dividing the number of moles of the product formed by the number of moles of phenylalanine initially loaded into the reactor. Experiments for phenylalanine at 220 °C and 150 min, 250 °C and 30, 60, and 90 min, 280 °C and 30 min, and 350 °C and 10, 20, and 30 min were reproduced three times to obtain experimental errors.

3.3.3 Phytol

The behavior of phytol in HTW was studied at 240, 270, 300, and 350 °C for batch holding times between 0 and 300 min. The reactors (capacity 0.59 mL) were loaded at room temperature with 50 µL of phytol, such that the initial concentration of phytol (C_{phytol}^0) based on 95% reactor volume in these experiments was 0.26 mol/L. The amount of water loaded in the reactors, calculated using Eq.(3.1), was 0.43, 0.41, 0.39, and 0.35 mL at 240, 270, 300,

and 350 °C. Upon completion of the reaction at a desired temperature and batch holding time in a fluidized sand bath, the reactors were opened and the contents were recovered using a 3:1 (v/v) solution of dichloromethane to methanol. This solvent solution was chosen because it was able to dissolve both the reactants and the products formed during the reaction, thereby giving a clear homogeneous phase for further analysis.

We performed a control experiment at room temperature to determine the recovery of phytol. We loaded a reactor with 50 µL of phytol and about 0.40 mL of water and sealed the reactor. The reactor was kept at room temperature for 60 minutes. The post-reaction work-up procedure used for the experiments at the elevated temperatures was then performed.

We used an Agilent Technologies model 6890N GC equipped with an autosampler, autoinjector, and mass spectrometric detector to identify the major products from the HTW treatment of phytol. A Wiley mass spectral library was used for compound identification by matching the mass fragments of observed peaks with those in the library. An Agilent Technologies model 6890 GC equipped with a FID was used to quantify the products. The reaction products were separated on a HP-5MS fused silica, non-polar capillary column (50 m length x 0.20 mm inner diameter x 0.33 µm film thickness). We used an inlet temperature of 300° C, a split ratio of 10:1, and an injection volume of 1.0 µL. The temperature program involved an initial oven temperature of 60° C (isothermal for 2 minutes) followed by heating to 200° C at a rate of 20° C/min and then ramping at 5° C/min to 280° C (isothermal for 10 minutes), giving a total run time of 35 minutes. Helium served as the carrier gas (1 mL/min). High molecular weight oligomers were detected (but not quantified) using a DB-5-HT fused silica, non-polar capillary column (30 m length x 0.25 mm inner diameter x 0.1 µm film thickness) on an Agilent 7890N GC-FID. We used a cool-on-column injection with an injection volume of 1.0 µL. The temperature program involved an initial oven temperature of 35° C (isothermal for 2 minutes) followed by heating to 280° C at a rate of 20° C/min and then ramping at 10° C/min to 380° C

(isothermal for 5 minutes), giving a total run time of 29 minutes. Helium served as the carrier gas (1 mL/min).

We generated a calibration curve for phytol by measuring the peak areas for standards of known concentrations, using GC-FID. This calibration, which was linear, was used to estimate the concentrations (and hence conversion) of phytol post-reaction. Nearly all of the reaction products contained 20 carbon atoms and were structurally similar to phytol. Hence one can approximate the FID response factors of these products to be similar to that of phytol. Therefore, we used the calibration curve for phytol to estimate the concentrations of these products post-reaction as well. Product molar yields were then calculated by dividing the number of moles of the product formed by the number of moles of phytol initially loaded into the reactor. Experiments at 240° C and 180 minutes, 270° C and 45 minutes, 300° C and 20 minutes, and 350° C and 10 minutes were carried out in triplicate to assess reproducibility.

3.3.4 DOPC

The reaction chemistry of DOPC in HTW was studied at 175, 200, 225, and 350 °C for batch holding times between 0 and 150 min. Higher temperatures were avoided for kinetics because the hydrolysis of DOPC gave complete conversion rapidly. The reactors (capacity 1.5 mL) were loaded at room temperature with approximately 75 mg of DOPC. The exact weight of DOPC added to the reactor was calculated as the difference in the weight of the reactor before and after loading. The initial concentration of DOPC (C°_{DOPC}) based on 95% reactor volume in these experiments was 0.07 mol/L. The amount of water loaded in the reactors, calculated using Eq.(3.1), was 1.27, 1.23, and 1.18 at 175, 200, and 225 °C. Upon completion of the reaction at a desired temperature and batch holding time in a fluidized sand bath, the reactors were opened and the contents were recovered using methanol.

We performed a control experiment at room temperature to determine the recovery of DOPC. We loaded a reactor with 20 mg of DOPC and 1.23 mL of

water and sealed the reactor. The reactor was kept at room temperature for 30 minutes. The post-reaction work-up procedure used for the experiments at the elevated temperatures was then performed.

We analyzed oleic acid (hydrolysis product of DOPC) using the HPLC and UV detector method outlined previously in Section 3.3.1. We generated a calibration curve for oleic acid by using pure oleic acid standards of known concentrations. This calibration, which was linear, was used to estimate the unknown concentrations of oleic acid. We used an Agilent Technologies model 6890N GC equipped with an autosampler, autoinjector, and mass spectrometric detector to identify the major products from the HTW treatment of DOPC. A Wiley mass spectral library was used for compound identification by matching the mass spectra of observed chromatogram peaks with those in the library. An Agilent Technologies model 6890 GC equipped with a FID was used to quantify the products. The reaction products were separated on a HP-5MS fused silica, non-polar capillary column (50 m length x 0.20 mm inner diameter x 0.33 μm film thickness). We used an inlet temperature of 300 $^{\circ}\text{C}$, a split ratio of 5:1, and an injection volume of 1.0 μL . The temperature program involved an initial oven temperature of 50 $^{\circ}\text{C}$ followed by heating to 300 $^{\circ}\text{C}$ at a rate of 25 $^{\circ}\text{C}/\text{min}$ (isothermal for 10 min), giving a total run time of 20 min. Helium served as the carrier gas (1 mL/min). As will be discussed in Chapter 7, the major products identified using the GC were glycerol and an ester of oleic acid and glycerol, 9-octadecenoic-2,3-dihydroxypropyl ester (referred to as OPE here onwards). We quantified OPE using a calibration curve generated with different known amounts of ethyl oleate. However, the glycerol peak was not well resolved, especially at high temperatures and long batch holding times. Thus, glycerol was not quantified. For detecting diglycerides (if any), we used a high temperature ASTM 6584 column installed in Agilent GC-FID 7890 equipment using the procedure outlined previously by Levine *et al.* [2].

We identified and quantified a number of the phosphorus-containing compounds generated during the reaction of DOPC by using ^{31}P -NMR at 25 $^{\circ}\text{C}$

on a Varian MR-400 NMR spectrometer at 161.7 MHz. The inverse gated decoupling technique was used to suppress the Nuclear Overhauser Effect (NOE). An observation frequency of 1619.2 Hz was used for acquisition. A pulse angle of 90° and a relaxation delay of 10 s were utilized. Typically, we obtained 128 scans before Fourier transformation was carried out. Agilent's VnmrJ 3 software *qEstimate* tool enabled us to estimate the absolute concentration (in terms of phosphorus equivalent) for any sample. This capability is based on the linearity of the digital receiver and does not require the use of reference signals or the addition of reference standard compounds to the NMR sample. A one-point external calibration was performed for the probe before using the quantification tool. This calibration was set up using a phosphorus standard of 1000 mg/L or 32.26 mM equivalent of phosphorus (obtained from Sigma Aldrich) and the methodology outlined for calibrating the probe [3]. We tested the validity of this calibration by running phosphorus standards of known concentrations, which gave concentrations within $\pm 5\%$ of the actual concentration. Having established confidence in the external calibration, we quantified DOPC and other phosphorus-containing compounds using this technique. Next, we identified the products corresponding to different peaks in the NMR spectrum by matching their chemical shifts with those of pure compounds that were expected as products from the hydrolysis of DOPC. To confirm these identities, we added small amounts of these pure compounds to a sample obtained from reaction at 175 °C and 150 min. No new peaks appeared in the NMR spectrum. Rather, the areas of existing peaks increased, thereby confirming the product identities.

Product molar yields were calculated by dividing the number of moles of the product formed by the number of moles of DOPC initially loaded into the reactor. Experiments at 175° C and 30 minutes, 200° C and 45 minutes, and 225° C and 45 minutes were carried out in triplicate to assess reproducibility.

3.3.5 Binary Mixtures

We studied binary mixtures of phenylalanine with different inorganic additives, such as, 1) NaCl, 2) NaNO₃, 3) Na₂SO₄, 4) KCl, 5) K₂HPO₄, 6) H₃BO₃,

and with an organic compound, 7) ethyl oleate. The purpose of this study is to understand how salts and triglycerides could interact with proteins during HTL of algae.

We performed experiments with phenylalanine and inorganic additives, at 250 °C and 30 minutes each. Stock solutions were made by dissolving 40 mg of a salt (or boric acid) in 10 mL of the phenylalanine stock solution. The concentration of each additive in the phenylalanine solution was 4000 mg/L. The concentration of salt was chosen such that the ratio of salt to phenylalanine was between 20-25% (w/w), which is a typical ratio of ash/proteins in algae [4].

Reactions of a binary mixture were performed at 350 °C (10, 20, 30, 40, and 60 minutes) at three different molar ratios of phenylalanine to ethyl oleate (~0.2 : 1; ~1 : 1; and ~5 : 1). Depending on the desired molar ratio of phenylalanine to ethyl oleate, we added 0.92 mL of stock solution (either 4000 ppm, or 15000 ppm, or 22000 ppm) along with the corresponding amount of ethyl oleate (either 10 µL or 40 µL) to the reactor. Phenylalanine stock solution was prepared fresh for each mixture.

We performed two control experiments at room temperature to determine the recovery of phenylalanine with K_2HPO_4 and ethyl oleate, respectively. We loaded 1 mL of the phenylalanine and K_2HPO_4 stock solution into a reactor and then sealed the reactor. In another reactor, 1 mL of phenylalanine (15000 ppm) was taken with 40 µL of ethyl oleate and sealed. These reactors were kept at room temperature for 30 min. For each of these reactions, the post recovery procedure similar to that of phenylalanine alone in HTW was followed (Section 3.3.2).

Analysis of phenylalanine and its products were done with GC-FID, using the methods outlined previously in Section 3.3.2. However, for quantification of ethyl oleate and oleic acid, we obtained poor peak separation using the HPLC method outlined in Section 3.3.1, probably due to the presence of additional products (from phenylalanine). Therefore, we developed a new method for

quantification using an Agilent Technologies model 7890N GC-FID. The separation was carried out on a DB-FFAP column (30 m length x 0.32 mm inner diameter x 0.25 μm film thickness). The inlet temperature was set at 220 °C with split ratio of 5:1, and injection volume of 1.0 μl . The temperature program involved an initial oven temperature of 50 °C followed by heating to 120 °C at a rate of 5 °C /min and ramping at 20 °C to 220 °C (isothermal for 6 min), giving a total run time of 25 min. Helium served as the carrier gas (1 mL/min).

We generated calibration curves for phenylalanine, its products, ethyl oleate and oleic acid using standards of known concentration, to determine corresponding concentrations of each in a reaction sample. Molar yields of the products were calculated by dividing the number of moles of the product formed by the number of moles of the limiting reactant initially loaded into the reactor. All experiments with phenylalanine and inorganic additives at 250 °C and 30 min, and experiments with phenylalanine and ethyl oleate at 350 °C at 10, 20, and 30 min (for all three molar ratios (0.2:1, 1:1, and 5:1)), were conducted in triplicate to assess experimental uncertainties.

Thus, we conclude summarizing the experimental setup used for different model compounds. Next, we next discuss the results of these experiments with individual model compounds and their mixtures (Chapters 4-9).

References

- [1] T. Pinnarat, P. E. Savage. Noncatalytic esterification of oleic acid in ethanol. *J. Supercrit. Fluids* 53, 53-59, 2010
- [2] R. B. Levine, T. Pinnarat, P. E. Savage. Biodiesel production from wet algal biomass through in situ lipid hydrolysis and supercritical transesterification. *Energy Fuels* 24, 5235-5243, 2010
- [3] <http://www.umich.edu/~chemnmr/docs.html>, Date last accessed 12th April, 2012
- [4] T. M. Brown, P. Duan, P. E. Savage. Hydrothermal liquefaction and gasification of *Nannochloropsis* sp. *Energy Fuels* 24 (6), 3639-3646, 2010

CHAPTER 4

Behavior of Ethyl Oleate in HTW

As mentioned previously, one of the objectives of this project was to study the kinetics of hydrolysis of ethyl oleate and esterification of oleic acid in unison. In this chapter we first describe the preliminary work that was done to validate the experimental methods. We then report the effect of temperature, batch holding time, initial concentration of the products (oleic acid and ethanol), and pH on the conversion of ethyl oleate. Next, we develop a quantitative phenomenological kinetics model to fit the experimental observations, which is then followed by a mechanistic model giving valuable insights of the underlying chemistry for hydrolysis of fatty acid ester.

4.1 Control Experiment

A control experiment (as mentioned in 3.3.1) was done to assess our ability to measure accurately the amount of ethyl oleate in the reactor. This experiment, which was essentially a run performed at room temperature, gave an ethyl oleate recovery of 95%, thereby verifying the suitability of the methods used for quantifying the amount of ethyl oleate.

We were also concerned with the possibility that two immiscible liquid phases might be present in the reactor at the experimental conditions since ethyl oleate is insoluble in water at room temperature. We could not find solubility data for ethyl oleate in water for the reaction temperatures of interest in this study, so we used ASPEN Plus version 2006.5 for fluid phase equilibrium calculations. We used the RK-ASPEN thermophysical properties model, which is suitable for a mixture of polar and nonpolar compounds at high temperatures and pressures [1].

A FLASH3 block was used in ASPEN to do the vapor-liquid equilibrium calculations, with conditions set to those of the experiments. Although ethyl oleate is not in the Aspen Plus chemical library, we performed the calculations using methyl oleate, which is very similar to the compound of interest. The results of performing these calculations showed that a single liquid phase would exist at the experimental conditions for methyl oleate. Thus, we infer that a single homogeneous liquid phase also existed for ethyl oleate in water at the reaction conditions investigated.

4.2 Effect of Reaction Conditions

This section discusses the results pertaining to hydrolysis of ethyl oleate under different conditions. We remind the reader that in all cases, the conversion of ethyl oleate (X) is calculated using the yields of the reactant and product and assuming that the small difference between their sum and 100% (perfect mass balance) can be apportioned equally between the two yields. Also, note that the conversion of ethyl oleate and molar yield of oleic acid are also tabulated independently in Appendix, Table A.2. Note that we also used several experimental data for the reverse reaction (esterification of oleic acid) for obtaining a combined kinetics. Tanawan Pinnarat, who worked jointly on this project, carried out these esterification experiments. The experimental results for esterification of oleic acid are presented elsewhere [2-5].

4.2.1 Temperature and Batch Holding Time

In this section, we present the results for effect of temperature and batch holding time on the conversion of ethyl oleate. Figure 4.1 shows the conversion of ethyl oleate at different batch holding times and 240, 260, 280, 300 and 350 °C. The initial concentration of ester (C_{EO}^0) in these experiments was 0.075 mol/L. The line segments connecting sequential data points serve to make the trends more apparent.

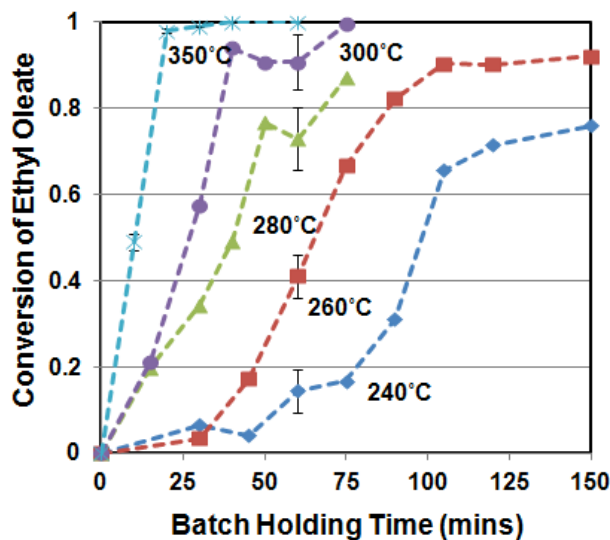


Figure 4.1 Temporal variation of ethyl oleate conversion. Legends are ◆ 240 °C, ▲ 260 °C, ■ 280 °C, ● 300 °C, and * 350 °C

At the lower temperatures, the trend of conversion with time exhibits sigmoidal behavior. That is, the rate at 240 °C is slow for the first 60 min or so, but then the rate increases sharply. This type of behavior is entirely inconsistent with a simple power-law rate equation used by previous researchers [6]. Rather, it is indicative of autocatalysis. The literature does provide precedent for autocatalysis during ester hydrolysis in high temperature water [7,8]. The carboxylic acid product is generally viewed as the autocatalytic agent. Khuwijtjaru *et al.*, the only other group who have studied fatty acid ester hydrolysis, use low concentrations of ester (three order of magnitude less) that probably prevented them from observing this kinetic feature that becomes important at higher concentrations [6].

At higher temperatures, the sigmoidal shape becomes less pronounced, indicating that temperature effects are dominant compared to autocatalysis. It should be noted that at 350 °C, we have plotted directly the conversion of ethyl oleate without taking its average with the yield of oleic acid. At this temperature, the yield of oleic acid first increases and then decreases. (see Appendix, Table A.2). One could explain the decrease in the yield of oleic acid to arise due to dimerization at high temperatures. Kocsisová *et al.* observed dimers of

unsaturated fatty acids at high temperatures (above 310 °C) using IR measurements, thereby leading to a decrease in the yield of fatty acids [9]. Their findings are in line with our observations. It should be noted that for the purpose of obtaining the unified kinetics of hydrolysis and esterification, we have not considered the dimerization of fatty acid.

4.2.2 Initial Addition of Oleic Acid and Ethanol

To test for autocatalysis by the fatty acid produced during hydrolysis, we conducted three additional experiments at 240 °C (30 min) with varying amounts of oleic acid present initially. We denote the initial molar ratios (R) of oleic acid (OA) and water (W) to the limiting reactant (ethyl oleate, EO) to be R_{OA} and R_W , respectively. As shown in the first four rows of Table 4.1, the conversion of the ester increases with an increasing initial amount of oleic acid present. This increase is so large that an equimolar addition of oleic acid is functionally equivalent to about a 60 °C increase in temperature. That is, both changes lead to a conversion of about 60% after 30 min. The results in Table 4.1 clearly demonstrate that the presence of oleic acid catalyzes the hydrolysis reaction.

Table 4.1 Effect of initial addition of oleic acid and ethanol on ethyl oleate conversion (30 min, $C_{EO}^0 = 0.075$ mol/L)

T (°C)	R_{OA}	R_{EtOH}	R_W	X
240	0	0	569	0.07 ± 0.03
240	0.25	0	569	0.27 ± 0.07
240	0.5	0	569	0.41 ± 0.05
240	1.0	0	569	0.61 ± 0.09
300	0	0	495	0.57 ± 0.08
300	0	25	450	0.35 ± 0.07
300	0	50	375	0.23 ± 0.05
300	0	75	300	0.18 ± 0.07

We also determined the effect of added ethanol (EtOH), one of the hydrolysis products, on the extent of hydrolysis. We used three different conditions with varying initial molar ratios of ethanol to ethyl oleate at a fixed temperature of 300°C (30 min). The molar ratio of water to ethyl oleate (R_W) necessarily decreased in these runs as the ethanol ratio increased because the

total fluid volume was roughly constant. The final four rows of Table 4.1, which show the results, indicate that an increase in the ethanol ratio leads to a decrease in conversion. This effect is probably due to the reverse reaction (esterification), becoming more important, which reduces the hydrolysis rate.

4.2.3 Different pH

Based on the observations reported in Figure 4.1, one of the goals of this project was to obtain the mechanism for autocatalysis for the hydrolysis of ethyl oleate. In order to validate the proposed mechanism (as will be discussed later in section 4.4), we carried out experiments at various pH, ranging from strongly acidic to near- and neutral and finally strongly basic conditions, using the procedure described previously in section 3.3.1. Note that we calculated the pH of neutral HTW at 280 °C to be 5.82, using the ion product correlation developed by Marshall and Franck [10]. This correlation is accurate for HTW, which was used in this work, but it is less reliable under some supercritical conditions. For the hydrolysis with added acid (pH < 5.82 at reaction condition) or base (pH > 5.82 at reaction condition), we assumed complete dissociation of the acid/base when calculating the pH at reaction conditions.

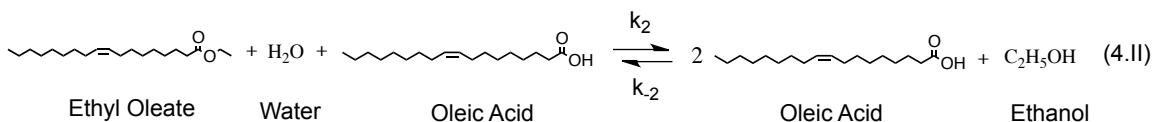
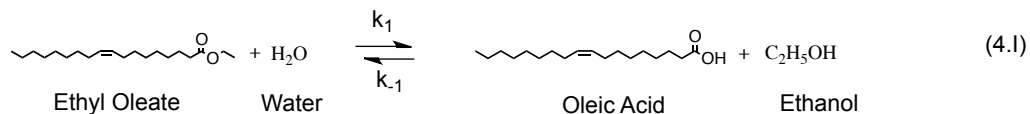
Table 4.2 Effect of different pH on ethyl oleate conversion at 280 °C and 40 min ($C_{EO}^0 = 0.075$ mol/L, $R_w = 554$)

pH at reaction temperature	X
1.42	0.99
2.12	0.98 ± 0.15
4.11	0.29 ± 0.10
5.65	0.41 ± 0.06
5.82	0.49 ± 0.07
8.34	0.36
9.89	0.59
11.88	0.94

Table 4.2 shows the effect of different pH on conversion of ethyl oleate. We observe that at very low pH (< 4), the conversion of ethyl oleate rapidly increases, such that complete conversion is obtained at a pH value equal to 1.42. It can be concluded that the system is strongly acid catalyzed (specific catalysis by [H⁺]) under these conditions. However, for near- and neutral pH, the conversion remains similar given the experimental error, indicating that some other route is involved other than specific acid catalysis by [H⁺] for the autocatalytic hydrolysis of ethyl oleate. These results are in line with the findings of Ravens [11]. Finally under strongly basic conditions (pH > 8.34), there is an increase in the conversion of ethyl oleate, indicating a base-catalyzed mechanism (specific catalysis by [OH⁻]), as was suggested previously by Oka et al [12]. Thus, the pH experiments give valuable insights for developing a mechanism to explain autocatalysis for the hydrolysis of ethyl oleate.

4.3 Phenomenological Autocatalytic Kinetics

In this section, we use the experimental data from the previous section, as well as and that reported in Figure 5 of Pinnarat and Savage [2], to develop and validate a unified kinetic model for hydrolysis and esterification. The sigmoidal trends in Figure 4.1 and the acceleration of hydrolysis upon addition of oleic acid lead us to propose an autocatalytic model for this hydrolysis/esterification system. The phenomenological model comprises two reversible reactions as shown below:



The first reaction is a reversible hydrolysis of ester to produce the fatty acid. In the second step, the fatty acid formed can catalyze the reaction to give another mole of the acid and ethanol. We assumed that the reaction orders are

equal to the stoichiometric coefficients, ϑ_i . Thus, rate equations for the consumption of ester (for hydrolysis experiments) and the consumption of oleic acid (for esterification experiments) can be written. For example, the rate equation for ethyl oleate hydrolysis is given below in Eq.(4.1), where subscripts EO, OA, W, and EtOH represent ethyl oleate, oleic acid, water, and ethanol, respectively.

$$-r_{EO} = k_1 C_{EO} C_W - k_{-1} C_{OA} C_{EtOH} + k_2 C_{EO} C_W C_{OA} - k_{-2} C_{OA}^2 C_{EtOH} \quad (4.1)$$

We next combined the rate equations with the design equation for a constant volume batch reactor. Substituting the expressions for the concentration of each component (C_i) in terms of the conversion of the limiting reactant, $C_i = C_i^0 (R_i + \vartheta_i X_{EO})$, into Eq.(4.2) leads to a differential equation that describes how the ethyl oleate conversion changes with batch holding time.

$$\begin{aligned} \frac{dX}{dt} = & k_1 C_{EO}^0 (1-X)(R_w - X) - k_{-1} C_{EO}^0 (R_{OA} + X)(R_{EtOH} + X) \\ & + k_2 C_{EO}^0{}^2 (1-X)(R_w - X)(R_{OA} + X) - k_{-2} C_{EO}^0{}^2 (R_{OA} + X)^2 (R_{EtOH} + X) \end{aligned} \quad (4.2)$$

One can write a similar equation for oleic acid esterification. We assume that the rate constants follow Arrhenius form (Eq.(4.3)), where 10^{a_i} and E_i are the respective pre-exponential factor and activation energy.

$$k_i = 10^{a_i} \exp\left(\frac{-E_i}{RT}\right) \quad (4.3)$$

The ratios of forward and reverse rate constants for the first (uncatalyzed) and second (catalyzed) reactions should be the same, because both steps rely on a common equilibrium constant. This thermodynamic constraint leads to Eq.(4.4) and Eq.(4.5), and it reduces the total number of adjustable parameters in the model to six.

$$a_{-1} = a_1 - a_2 + a_{-2} \quad (4.4)$$

$$E_{-1} = E_1 - E_2 + E_{-2} \quad (4.5)$$

We numerically integrated the differential equations using Euler's method and simultaneously performed parameter estimation to get estimates for a_1 , a_2 , a_{-2} , E_1 , E_2 , and E_{-2} . These calculations were performed using Microsoft Excel 2007 and its Solver function. The objective function to be minimized was the sum of the squared differences between the experimental and calculated conversions. We combined and used together the experimental data for hydrolysis of ethyl oleate in Figure 4.1 (except the data at 60 minutes for 240-300 °C and all data at 350 °C), added oleic acid in Table 4.1 (first four rows), and also the experimental data for esterification of oleic acid reported elsewhere (Table 2 [ref. 4] and Figure 5 [ref. 2]), to estimate numerical values for the parameters in the model. To the best of our knowledge, this report is the first to treat ester hydrolysis and fatty acid esterification data together to develop a unified model for this reaction system. Table 4.3 displays the parameter estimates.

Table 4.3 Estimated Arrhenius parameters (min, L, mol) for unified hydrolysis and esterification

Reaction i	a_i	E_i (kJ/mol)
1	4.3	86.7
2	3.1	51.1
-1	8.6	123.6
-2	7.5	87.9

4.3.1 Validation of Phenomenological Model

Having obtained the Arrhenius parameters for the phenomenological model proposed above, our next task was to ensure that these parameters are consistent and not only fit the experimental data but also predict the conversion of ethyl oleate for conditions both inside and outside the parameter space. This section describes in detail different tests used to validate the model and its parameters.

4.3.1.a Thermodynamic Consistency

To verify that the parameters in Table 4.3 are reasonable on a thermochemical basis, we calculated the heat of reaction for hydrolysis of ethyl oleate (using the estimated activation energies) and compared it to the value obtained using heats of formation of the reactants and products. The heat of reaction is simply the difference between the activation energies for the forward and reverse reaction. The activation energies in Table 4.3 lead to $\Delta H_R = -36.9$ kJ/mol. Heats of formation for ethyl oleate, water, oleic acid, and ethanol were taken from Vatanai *et al.* [13] to obtain the theoretical $\Delta H_R = -42.4$ kJ/mol (at 298 K). Our experimental estimate for ΔH_R is in good agreement with this thermochemical estimate.

Khuwijitjaru *et al.* used a first order model to describe the hydrolysis kinetics for different fatty acid esters (acyl chain length C₈-C₁₆) [6]. They observed no autocatalysis at their low initial concentrations, so our Reaction 4.1 probably provides an appropriate comparison with their results. They reported the activation energy for hydrolysis of methyl palmitate to be 70 kJ/mol. This value is similar to but slightly lower than our E₁ value of 87 kJ/mol for uncatalyzed hydrolysis of ethyl oleate. The difference likely exists because the two studies used different fatty acid esters, different experimental conditions, and different kinetic models.

Pinnarat and Savage report activation energies for hydrolysis of ethyl oleate as 66 ± 14 kJ/mol and that for esterification of oleic acid to be 56 ± 2 kJ/mol [2]. Since their experiments had a high concentration of fatty acid, it is probably most appropriate to compare their activation energies with E₂ and E₋₂. Our estimate for E₂ (51 kJ/mol) is within the uncertainty of their value, whereas our estimate for E₋₂ (89 kJ/mol) is not. This discrepancy possibly arises because Pinnarat and Savage used only the esterification data to estimate the activation energies, whereas the present model uses both the hydrolysis and esterification

data simultaneously. Pinnarat and Savage also did not explicitly consider autocatalysis.

4.3.1.b Model Fit to Experimental Data

Figure 4.2 demonstrates the ability of the model with the parameters in Table 4.3 to correlate the experimental results for hydrolysis of ethyl oleate. These parity plots compare the calculated and experimental conversions. If the model provided a perfect fit for all the data, all points would fall on the diagonal line. Clearly, the model fit is not perfect, but it is very good, implying that the estimated parameters are consistent with the experimental data. Moreover, the data are scattered on both sides of the diagonal indicating the absence of systematic errors. Similar ability of the model to fit experimental data for esterification of oleic acid is reported in Figure 3 of Changi *et al.* [4].

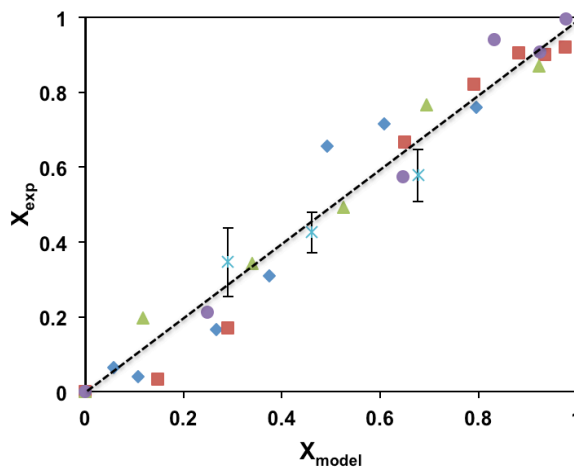


Figure 4.2 Parity plot of phenomenological model for hydrolysis experiments. Legends are ♦ 240 °C, ▲ 260 °C, ■ 280 °C, ● 300 °C, and * initially added oleic acid

4.3.1.c Model's Predictive Capability

We used most of the experimental results to determine reliable values for the model parameters. Several sets of results were reserved, however, to test the predictive ability of the model. These data are the points at 60 min batch holding time at 240, 260, 280, 300 °C, all the data points for 350 °C from Figure

4.1 and the results displayed in the final four rows of Table 4.1 (effect of ethanol on hydrolysis of ethyl oleate). We also used data for esterification of oleic acid, which were not used for parameter estimation. These results came from experiments done both within and outside the parameter space used to determine the model parameters. Thus, they provide an opportunity to assess the predictive ability of the model as it interpolates within the parameter space and also as it extrapolates beyond. The parity plot in Figure 4.3 summarizes the results from this model validation study.

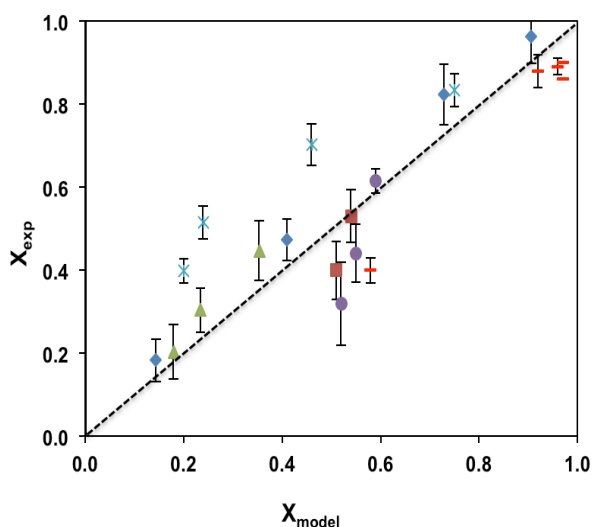


Figure 4.3 Parity plot of phenomenological model validation for experiments conducted inside and outside parameter space. Legends are ♦ hydrolysis, 60 min at 240, 260, 280, and 300 °C (Figure 4.1), ■ esterification, 10 min, 270 °C and 290 °C (Figure 5, [ref. 2]), ▲ hydrolysis with added ethanol (Table 4.1), ● esterification with added ethyl oleate (Table 3, [ref. 4]), and * esterification with added water (Table 3, [ref. 4]), – hydrolysis, 10, 20, 30, 40, and 60 min at 350 °C (Figure 4.1)

First, we tested the ability of the model to predict the outcome of experiments done within the parameter space used to determine the model parameters. The diamonds in Figure 4.3 compare model predictions and experimental results from hydrolysis for 60 min at 240, 260, 280, and 300 °C. The squares show the results for esterification at 270 °C and 290 °C for 10 min

each. It is clear that the points nearly fall on the diagonal, indicating that the model can be used to predict experimental conversions for such cases.

Next, we tested the ability of the model to predict experimental conversions outside the parameter space for the temperature variable used for hydrolysis. The hyphens in Figure 4.3 show results of hydrolysis conducted at different batch holding times and 350 °C. These points lie close to the diagonal, indicating that the model can be used to predict experimental conversions for hydrolysis for temperatures outside those used to estimate the parameters. We also tested the model's predictive ability for cases where one of the reaction products was added to the reactor. No data from experiments with added product ethanol, ester, or water were used to determine the model parameters. Thus, the comparisons test the predictive ability of the model outside its parameter space. The triangles in Figure 4.3 show results from hydrolysis experiments with added ethanol, and these outcomes are predicted well by the model. The circles and asterisks in Figure 4.3 show results from esterification experiments with varying initial ester and water amounts, respectively. The model does a poorer job of predicting the experimental conversions in these cases, but it does predict the proper trends (i.e. adding ester and water reduces the conversion for esterification). One possible reason for the model's lack of quantitative predictive ability in these cases when extrapolated is that the model is phenomenological and is not based on the elementary steps that govern the reaction chemistry. One needs to build a detailed mechanistic model that includes charged intermediates, dissociation of oleic acid in high temperature water, and catalysis by H^+ . These modifications will be discussed in Section 4.4.

As a final test of the predictive ability of the model, we use it to predict results in the literature. Warabi *et al.* report yields of ethyl oleate from oleic acid esterification at 300°C, 150 bar, and $R_{EtOH} = 42$ [14]. Table 4.4 compares their experimental results at different batch holding times with the yields predicted by the above kinetics model. Even though the experimental conditions used by

Warabi *et al.*¹⁶ are not within our parameter space, the model still gives nearly quantitatively accurate prediction of the product yields, except at the longest time.

Table 4.4 Comparison of experimental (Warabi *et al.* [14]) and predicted ester conversion

Reaction Time (min)	Warabi <i>et al.</i> [14]	Model
4	0.49	0.51
6	0.57	0.61
8	0.67	0.68
10	0.74	0.73
14	0.96	0.79

To sum up this section on model validation, we have demonstrated that the model makes quantitatively accurate predictions within, and at times outside, the parameter space. It also accurately predicts trends when extrapolated outside the original parameter space.

4.3.2 Sensitivity Analysis

Having obtained the Arrhenius parameters in Table 4.3, our next objective was to determine the sensitivity of the calculated conversion to small changes in the estimated Arrhenius parameters. For this purpose, we calculated normalized sensitivity coefficients as shown in Eq.(4.6), where P represents one of the parameters.

$$S = \frac{\partial(\ln X)}{\partial(\ln P)} \quad (4.6)$$

These coefficients indicate the relative change in conversion that would result from some small change in a parameter. A normalized sensitivity coefficient of unity, for example, indicates that a small relative change (say 1%) in a parameter leads to an identical relative change in conversion. We used Berkeley Madonna 8.3.18 to compute the sensitivity coefficients, which are functions of the initial concentrations, reaction time, and temperature. We conducted this sensitivity analysis at the experimental conditions used to test the

predictive capability of the model, as discussed in the previous section. Table 4.5 summarizes the sensitivity analysis results.

Table 4.5: Normalized sensitivity coefficients for phenomenological model

Run	Reaction	t (mins)	T (°C)	X	R _w	R _{EtOH}	R _{EO}	Normalized Sensitivity Coefficient					
								a ₁	E ₁	a ₂	E ₂	a ₋₂	E ₋₂
1	Hyd.	60	240	0.18	569	0	0	7.70	-16.47	7.01	-11.07	0.00	0.00
2	Hyd.	60	300	0.96	510	0	0	0.29	-0.57	0.88	-1.30	-0.26	0.28
3	Est.	10	270	0.40	0	35	0	0.00	0.00	0.00	0.00	5.07	-5.68
4	Hyd.	30	300	0.45	450	25	0	3.93	-7.62	5.49	-7.84	-2.94	3.10
5	Est.	30	250	0.62	0	10	2	0.01	0.01	-0.15	0.23	6.68	-7.88
6	Est.	30	250	0.70	10	10	0	-0.04	0.08	-1.34	2.14	7.52	-8.90

Run 1 shows that for hydrolysis, at a lower temperature, the model is highly sensitive to a_1 , E_1 , a_2 , and E_2 , i.e. to the forward rate constants for both reactions 4.I and 4.II, but not sensitive to a_{-2} and E_{-2} . This result is reasonable since the calculated conversion is low under these conditions as are the product concentrations. One would not expect the reverse reaction to be important under these conditions. Run 2, however, shows that at a higher temperature (and higher conversion), not only does the model become sensitive to all six parameters, but also the magnitude of the sensitivity to the parameters decreases. Again this outcome is reasonable because at high conversion, products are present in higher concentration, and the reverse reaction should have some influence on the calculated conversion. Moreover, the magnitude of the sensitivity coefficients decreases because as the conversion approaches unity, it is not capable of undergoing much additional increase. Run 3 shows that for esterification at moderate conversion, the model is sensitive to only a_{-2} and E_{-2} , the kinetics for the esterification reaction. Collectively, runs 1-3 show that to estimate reliable values for all six of the model parameters one needs to use data from both hydrolysis and esterification reactions.

Run 4 shows the normalized sensitivity coefficients for hydrolysis with added ethanol. The calculated conversion is still most sensitive to E_1 and E_2 (as in Run 1), but the added ethanol brings with it sensitivity to the Arrhenius

parameters for esterification (a_{-2} and E_{-2}). This sensitivity arises because of an increase in the esterification rate under those conditions.

Runs 5 and 6 list the normalized sensitivity coefficients for the cases of added ester and water, respectively, for esterification. The calculated conversion is sensitive not only to E_{-2} and a_{-2} but it is also modestly sensitive to E_2 and a_2 . This result implies that the hydrolysis path is also important when water or ester is present during esterification under those conditions.

To summarize, this section describes the sensitivity of the calculated conversions to the model parameters under different conditions. For hydrolysis, E_1 and E_2 are most important with a_{-2} and E_{-2} being least important. The latter becomes important only in the presence of added ethanol. Similarly for esterification, a_{-2} and E_{-2} are most important. Thus, one needs a combination of both the hydrolysis and esterification data to get accurate estimates for all of the kinetics parameters.

4.4 Mechanistic Autocatalytic Kinetics

The previous section described a phenomenological model to explain autocatalysis during hydrolysis of ethyl oleate. However, this model was not able to predict accurately the conversion for esterification involving ternary mixtures. To overcome this limitation of the phenomenological model to quantitatively predict the conversion of ethyl oleate for esterification of oleic acid with added ester or water and to obtain a fundamental understanding of autocatalysis at a molecular level, we study in detail the mechanism for this system. Such a model is useful because we can adjust the reaction condition in the system to accelerate the reaction in the desired direction, which can be useful for industrial process development. This section elucidates on the mechanistic modeling of a unified system for hydrolysis of ethyl oleate and esterification of oleic acid. This study was also jointly conducted with Tanawan Pinnarat.

In Chapter 2.1, we had reviewed different possible mechanisms that have been proposed for hydrolysis of ester. Based on this literature search, the Aac2

mechanistic framework is the most likely option of fatty acid ester hydrolysis in HTW in the absence of an added acid or base. We build on this foundation by noting that specific acid catalysis is probably not the sole mechanism for fatty acid ester hydrolysis, as is also evident from the results of the pH experiments shown in Table 4.2. We include the possibility of general acid catalysis by water molecules, as proposed by Comisar *et al.* [15], and also by the fatty acid hydrolysis product, which should be an even better proton donor than water.

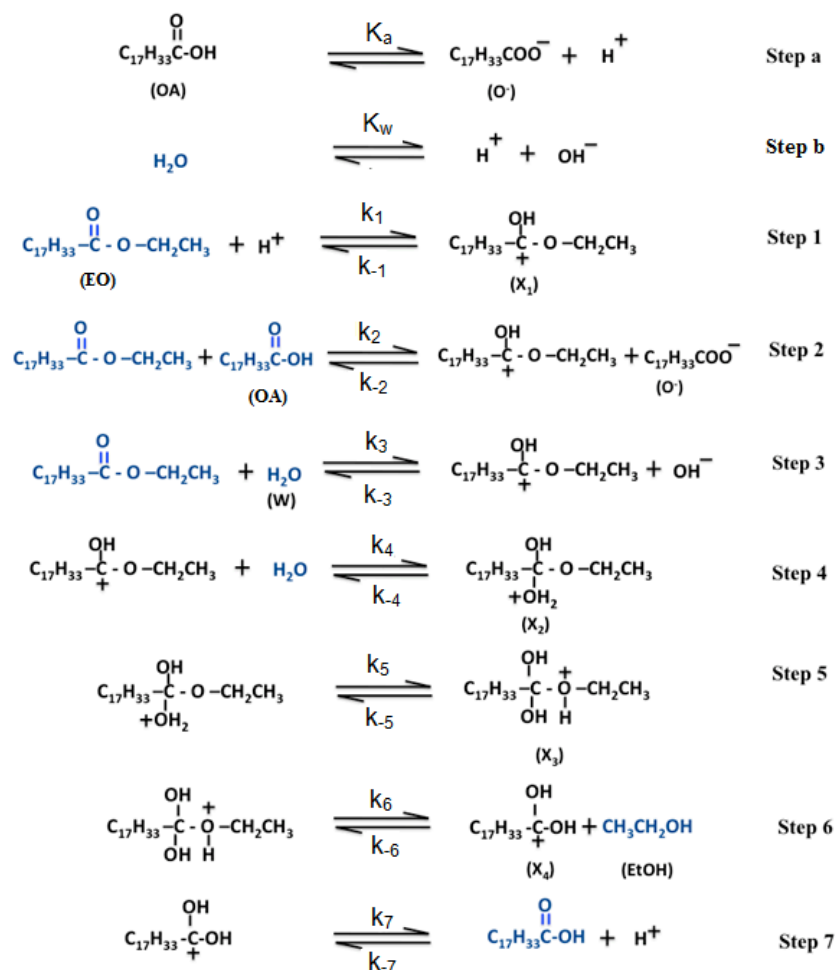


Figure 4.4 Mechanism explaining autocatalysis for ethyl oleate hydrolysis and oleic acid esterification

Figure 4.4 shows all the steps of the proposed mechanism. The forward reactions pertain to fatty acid ester hydrolysis, while the reverse reactions describe fatty acid esterification. Again, we emphasize that this mechanism is intended to describe hydrolysis and esterification in the absence of added mineral acid or base. In step a, oleic acid (the specific fatty acid used in this study) dissociates to give $[H^+]$ and $[C_{17}H_{33}COO^-]$. The dissociation constant (K_a) of the acid at the reaction conditions governs the formation of H^+ ions. Step b shows the dissociation of water into H^+ and OH^- , and the extent of this dissociation is quantified through the ion product of water, K_w . Ester hydrolysis is initiated by one of the parallel steps 1-3. We consider the possibility that the hydrolysis is catalyzed by H^+ (step 1), obtained from dissociation of either fatty acid or water as shown in steps a and b, by oleic acid (step 2), and by water (step 3).

Steps 1-3 all generate the same protonated ester intermediate X_1 , which in step 4 adds a water molecule to produce another intermediate X_2 . In step 5, proton transfer takes place within the intermediate X_2 to form intermediate X_3 , which then forms a carbocation X_4 through the loss of ethanol in step 6. This carbocation subsequently forms the product oleic acid (OA) and regenerates H^+ , as shown in step 7.

From the reverse reaction perspective, esterification starts with protonation of oleic acid (OA) in the reverse of step 7 to give a carbocation intermediate (X_4), which is then attacked by ethanol to form intermediate (X_3) in the reverse of step 6. This intermediate X_3 undergoes rearrangement to give intermediate X_2 in the reverse of step 5. In the reverse of step 4, water (W) is released to form a carbocation (X_1). Intermediate X_1 can subsequently form the product ester (EO) through the reverse of either the steps 1, 2, or 3. In the reverse of step 1, X_1 forms ester and regenerates $[H^+]$. In the reverse of step 2, X_1 reacts with $C_{17}H_{33}COO^-$ (denoted O^- in Figure 1) to produce ethyl oleate and oleic acid. In reverse of step 3, X_1 reacts with OH^- to produce ethyl oleate and water. The reaction mechanism can be written in a simpler manner as shown in

Figure 4.5. Note that the co-reactants are written above the arrows for each step and the co-products are written below the arrows.

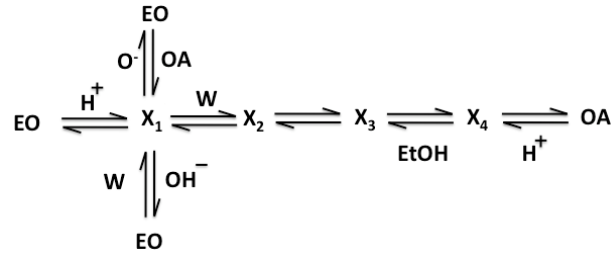


Figure 4.5: Schematic representation of hydrolysis and esterification mechanism

4.4.1 Reaction Rate Equation

The rate equation for ethyl oleate or oleic acid can be written analytically using the streamlined method outlined by Helfferich [16]. The only assumptions made are that each step is an elementary reaction and that each intermediate is present in trace levels and in a quasi-stationary state. No assumptions need to be made regarding the identity or existence of any rate determining steps. Moreover, all steps are taken to be reversible. Eq.(4.7) shows the rate equation. Note that k_i and k_{-i} refer to the rate constants for the forward and reverse step i in Figure 4.4 and K_i refers to the ratio k_i/k_{-i} .

$$r_{EO} = -r_{OA} = \frac{Qk_{-7}C_{H^+}C_{EtOH}C_{OA} - k_bC_W(k_1C_{H^+}C_{EO} + k_2C_{OA}C_{EO} + k_3C_WC_{EO})}{k_bC_W + Q(C_{EtOH} + k_c + k_d + k_e)} \quad (4.7)$$

$$Q = k_{-3}C_{OH^-} + k_{-1} + k_{-2}C_{O^-} \quad (4.8)$$

$$k_b = k_7K_4K_5K_6, \quad k_c = \frac{k_7}{k_{-6}}, \quad k_d = \frac{k_7}{k_{-5}}K_6, \quad k_e = \frac{k_7}{k_{-4}}K_6K_5 \quad (4.9)$$

The rate equation given by Eq.(4.7) is more general and hence more complex than any previous rate equations considered for ester hydrolysis in near- neutral HTW [7, 15]. However, Eq.(4.7) reduces to the simple power-law form given by Krammer and Vogel [7] if we incorporate their simplifying assumptions (step 4 is the rate-limiting step with two water molecules, steps 5, 6

and 7 are irreversible, and steps 2 and 3 do not occur). Eq.(4.7) also simplifies to the form given by Comisar *et al.* [15] when we incorporate their assumptions (similar assumptions as Krammer and Vogel except that step 3 does occur as proposed in our scheme in Figure 4.4).

4.4.2 Kinetic Modeling of Autocatalytic Mechanism

If the proposed mechanism in Figure 4.4 is correct then the corresponding rate equation should be consistent with the experimental data. In this section, we develop a mechanistic kinetics model and fit it to experimental data to test for the consistency. The model will also provide insight into the rates of each step. The mechanistic kinetics model can be obtained (Eq.(4.11)) by combining the rate equation (Eq.(4.7)) with the design equation for a constant volume batch reactor (Eq.(4.10)).

$$\frac{dC_i}{dt} = r_i \quad (4.10)$$

$$\frac{dC_{EO}}{dt} = -\frac{dC_{OA}}{dt} = \frac{Qk_{-7}C_{H^+}C_{EtOH}C_{OA} - k_bC_W(k_1C_{H^+}C_{EO} + k_2C_{OA}C_{EO} + k_3C_WC_{EO})}{k_bC_W + Q(C_{EtOH} + k_c + k_d + k_e)} \quad (4.11)$$

One can substitute expressions for concentration for each component (C_i) in terms of the conversion (X) of the limiting reactant, $C_i = C_i^0 (R_i + \vartheta_i X)$ into Eq.(4.11), where R_i = initial molar ratio of component i to that of the limiting reactant and ϑ_i = stoichiometric coefficient of component i , to obtain a differential equation that describes how conversion changes with the batch holding time for fatty acid ester (during hydrolysis) and fatty acid (during esterification). We assume that the rate constants and equilibrium constants follow Arrhenius/Van't Hoff form (Eq.(4.12)), where 10^{a_i} and E_{a_i} are the respective pre-exponential factor and activation energy.

$$k_i = 10^{a_i} \exp\left(\frac{-E_i}{RT}\right) \quad (4.12)$$

The value of the dissociation constant of water K_w is temperature dependent and calculated using the correlation from Marshall and Franck [10]. We found no literature values for K_a for oleic acid in water, ethanol, or ethanol-water mixtures at the temperatures of interest in this work. Therefore we treat K_a as an adjustable parameter. One expects the value of K_a to be different in water, ethanol, and water-ethanol mixtures. On the basis of the experimental results of Rahman *et al.* [17] for the K_a of saturated fatty acids in ethanol-water mixtures, we expect a linear relationship between $\log K_a$ and the mole fraction of ethanol. Therefore, we calculated the dissociation constant of oleic acid in ethanol-water mixture as the mole fraction weighted average of its value estimated in pure water ($K_{a,w}$) and pure ethanol ($K_{a,e}$), as is shown in eq.(4.13), where, $x_e = 1 - x_w$ and x_w is mole fraction of water.

$$\log K_a = x_w \log K_{a,w} + x_e \log K_{a,e} \quad (4.13)$$

We numerically integrated the differential equations for hydrolysis and esterification using Euler's method and performed simultaneously parameter estimation to determine numerical values for the various Arrhenius parameters. These calculations were performed using Microsoft Excel 2007 and its Solver function. The objective function to be minimized was the sum of the squared differences between the experimental and calculated conversions, from both hydrolysis and esterification experiments. We varied the size of the time step used in the numerical integration from 0.1 to 0.5 to 1 minute and found that there was no difference in either the conversions or the estimated parameters. Thus, Euler's method with a step size of 0.1 min was used as a suitable means of numerically integrating the differential equations. For hydrolysis, we used the data in Figure 4.1 (except those at 60 min for 240, 260, 280, and 300 °C and all the data for 350 °C) and Table 4.1 and for esterification we used the data reported in Figure 5 of Pinnarat and Savage [2] and Tables 2 and 3 of Changi *et al.* [4].

Using the methodology outlined above, we solved the kinetics model (Eq.(4.11)) and obtained values of the Arrhenius parameters for the different

collections of rate and equilibrium constants. The model results were largely insensitive to the precise numerical values for the Arrhenius parameters in k_3 , k_{-3} , k_c , k_d and k_e , and the numerical values of these parameters were very small ($< 10^{-4}$). Removing these parameters from the model did not diminish its ability to fit the experimental data. This result means that the completely general rate equation in Eq.(4.11) is not required to describe the behavior of esterification and hydrolysis under the conditions in the present experiments. A more simplified rate equation can suffice. That k_3 and k_{-3} are not kinetically significant implies that step 3 in Figure 4.4, protonation of ester by water, is not competitive with the competing parallel paths of protonation by H^+ and by oleic acid. Neglecting the less significant parameters (k_c , k_d , k_e , k_3 , k_{-3}) permits the reaction pathway to be simplified to the form shown in Figure 4.6.

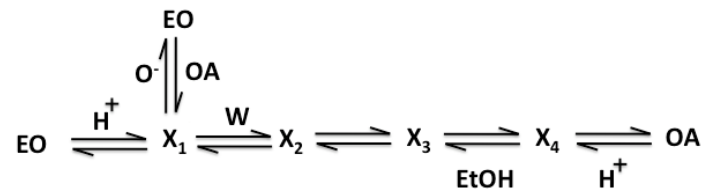


Figure 4.6 Schematic representation of simplified hydrolysis and esterification mechanism

Incorporating the simplifications reduces the rate equation from Eq.(4.7) to Eq.(4.14). The only rate constants appearing in Eq.(4.14) are for steps 1, 2, and 7. Steps 4, 5, and 6 contribute only equilibrium constants, through the term k_b in the denominator. This result, which emerged by confronting the general rate equation with the experimental data, indicates that under the conditions of the present experiments, steps 4, 5, and 6 are in a quasi-equilibrium state. In addition to noting that the stoichiometry for hydrolysis requires that the rate of consumption of ethyl oleate (steps 1 and 2 of Figure 4.4) equal the rate of formation of oleic acid (step 7 of Figure 4.4), the simplified kinetics model provides the additional insights that step 3 is too slow to be significant and steps 4, 5, and 6 are in quasi-equilibrium.

$$r_{EO} = -r_{OA} = \frac{k_{-7}(k_{-1} + k_{-2}C_{O^-})C_{H^+}C_{EtOH}C_{OA} - k_bC_w(k_1C_{H^+}C_{EO} + k_2C_{OA}C_{EO})}{k_bC_w + (k_{-1} + k_{-2}C_{O^-})C_{EtOH}} \quad (4.14)$$

We obtain the concentration of O^- in the above equation from the dissociation equilibrium of oleic acid. In a similar manner, we obtain the concentration for H^+ using the definition of K_w and K_a . For hydrolysis, these concentrations can be given as shown in Eq. (4.15) below.

$$C_{O^-} = \frac{K_a C_{EO}^0 (R_{OA} + X)}{\sqrt{K_a C_{EO}^0 (R_{OA} + X) + K_w}}, \quad C_{H^+} = \sqrt{K_w + K_a C_{EO}^0 (R_{OA} + X)} \quad (4.15)$$

Once again, one can use the design equation for a constant volume batch reactor to obtain the corresponding differential equation that describes how conversion changes with batch holding time. We next use this simplified rate equation and kinetics model to estimate again the parameter values using the same data set and method as listed previously. Table 4.6 shows the values of the Arrhenius parameters in the simplified kinetics model.

Table 4.6 Estimated Arrhenius parameters for simplified mechanism Figure 4.6 (min, L, mol)

Parameter	a_i	E_i (kJ/mol)	$k_{260^\circ C}$
k_1	4.3	40.7	2.29
k_2	3.7	42.5	0.31
k_{-1}	2.2	47.4	3.4×10^{-3}
k_{-2}	2.1	65.2	4.2×10^{-5}
k_{-7}	4.4	42.2	1.76
k_b	1.5	48.8	5.5×10^{-4}
$K_{a,w}$	1.5	45.6	1.1×10^{-3}
$K_{a,e}$	2.1	43.8	5.3×10^{-3}

To assess whether the numerical values obtained for $K_{a,w}$ and $K_{a,e}$ are reasonable, we extrapolated them to room temperature, where experimental values of pK_a are available for some fatty acids. We calculate the pK_a of oleic acid to be between 6 and 7 at room temperature for various mole fractions of ethanol and water. This range is slightly lower than the pK_a of 7 to 9.24 reported for palmitic acid and 7.47 to 9.35 reported for stearic acid at different mole fractions of ethanol at room temperature [17]. These differences might be due to

the use of different fatty acids (unsaturated versus saturated), but more likely it is a simple manifestation of the error that can result when extrapolating by nearly 200 °C, via the Van't Hoff equation.

4.4.3 Validation of Mechanistic Model

Similar to the validation for the phenomenological model, we conduct a series of exercises to test the consistency of the parameters for the mechanistic model to fit the experimental data and also predict the conversion of ethyl oleate for conditions both inside and outside the parameter set. This section describes different methods used to validate the mechanistic model and its parameters.

4.4.3.a Model Fit to Experimental Data

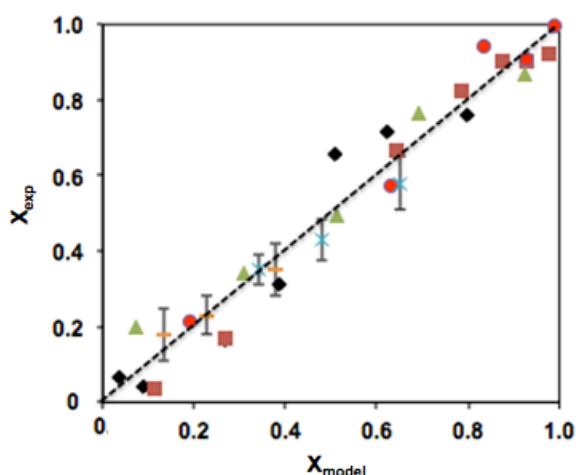


Figure 4.7: Parity plot of mechanistic model for hydrolysis experiments. Legends are ♦ 240 °C, ■ 260 °C, ▲ 280 °C, ● 300 °C, except 60 minutes (Figure 4.1), ✱ with added oleic acid at 240 °C, and – with added ethanol at 300 °C (Table 4.1)

Figure 4.7 demonstrates the ability of the simplified rate equation with the parameters in Table 4.6 to correlate the experimental results for ethyl oleate hydrolysis. The parity plot compares the calculated and experimental conversions. If the model provided a perfect fit for all the data, all points would fall on the diagonal line. Clearly, the model fit is not perfect, but it is very good. Moreover, the data are scattered on both sides of the diagonal indicating the absence of systematic errors. Note that the error bars, when shown, represent

standard deviations as determined from three replicated experiments. Similar ability of the model to fit experimental data for esterification of oleic acid are reported in Figure 4 of Changi *et al.* [5]

4.4.3.b Model's Predictive Capability

As mentioned in the previous section, the model fit well with the experimental data from both hydrolysis and esterification. We next used the mechanistic model to predict the conversion from experiments done both within and outside the parameter space used to determine the model parameters. For this purpose, we used experimental results for hydrolysis at 60 minutes between 240-300 °C and all data at 350 °C (Figure 4.1) and experimental data for hydrolysis at different pH (Table 4.2). Additional experiments were also conducted for esterification of oleic acid, which have been tabulated elsewhere (see supporting information, Tables 3-6 of Changi *et al.* [5]). This exercise provides an opportunity to assess the predictive ability of the model as it interpolates within the parameter space and also as it extrapolates beyond the parameter space.

Figure 4.8 shows the parity plot comparing experimental conversions with conversions calculated from the mechanistic kinetics model at different conditions both within and outside the parameter space used to regress the model parameters.

First, we tested the ability of the model to predict the outcome of experiments done within the parameter space. Good agreement can be seen of the model and experimental conversions (diamonds, triangles, circles, asterisks), indicating that the model can be used to predict experimental conversions for such cases. The model's predictive capability was also tested for experiments done outside the parameter space. Once again very good agreement can be seen in Figure 5 (squares, hyphens, and crosses), indicating that the model can be used to predict experimental conversions for such cases. We also used the model to predict experimental conversions reported in the literature (plusses) [14].

From Figure 5, it can be seen that the model does a reasonable job of predicting these conversions measured in a different lab.

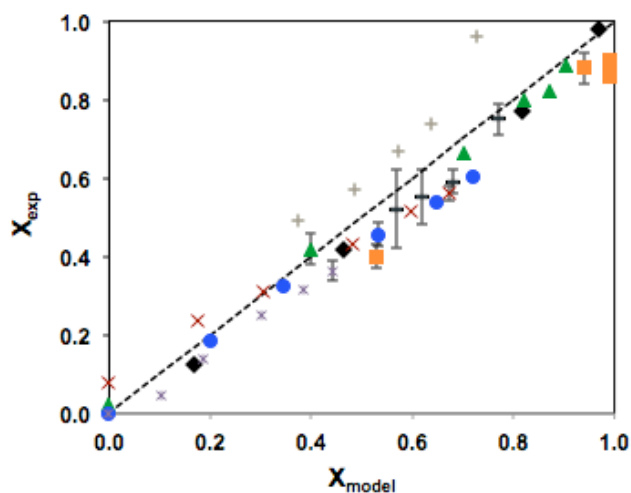


Figure 4.8 Parity plot of mechanistic model validation for experiments conducted inside and outside parameter space. Legends are ♦ hydrolysis at 240, 260, 280 and 300 °C and 60 min (Figure 4.1), ▲ esterification at 200 °C and $R_{EtOH} = 9:1$ (see SI, Table 3 [ref. 5]), ● esterification at 230 °C and $R_{EtOH} = 7:1$ (see SI, Table 4 [ref. 5]), * esterification with added water at 230 °C, $R_{EtOH} = 9.85:1$ and $R_w = 8.82:1$ (see SI, Table 5 [ref. 5]), ■ hydrolysis at 350 °C and 10, 20, 30, 40, and 60 min (Figure 4.1), – esterification with added ester at 250 °C and $R_{EtOH} = 10$ (Table 3, [ref. 4]), x esterification with added water at 230 °C, $R_{EtOH} = 9.75:1$ and $R_w = 0.61:1$ (see SI, Table 6 [ref. 5]), and + Esterification at 300 °C, 150 bar and $R_{EtOH} = 42:1$ [ref. 14]

We also tested the ability of the model to predict the influence of pH on hydrolysis. If the mechanism proposed in Figure 4.4 is correct, then the kinetics model built on this foundation should be able to predict the effect of the pH for acid-catalyzed hydrolysis reaction. Experimentally, the rate constant for hydrolysis (Figure 4.9) is largely insensitive to pH at near neutral conditions (pH~4 to ~8). It increases sharply, however, both below pH of 3.8 (strongly acidic) and above pH 10 (strongly basic). These experimental trends are fully consistent with the findings of Comisar *et al.* [15] for methyl benzoate hydrolysis. More significant at present, however, is that the mechanistic model predicts precisely the trends observed at near-neutral and acidic pH.

The experimental data in Figure 4.9 show a sharp increase in the rate constant in the presence of base, which is consistent with base-catalyzed pathway being available at those conditions. E.g.: Comisar *et al.* [15] used a $k_B C_{OH^-}$ term to successfully fit their data for hydrolysis of methyl benzoate at high pH. Obviously, the mechanistic model presented here, which focuses on the acid catalyzed mechanisms operative in near- neutral and acid HTW, cannot capture the effect at strongly basic conditions. To sum up, we have demonstrated that the model makes quantitatively accurate predictions within and, at most times, outside the parameter space.

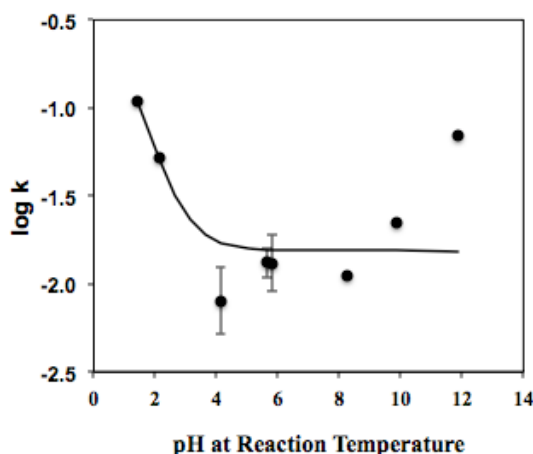


Figure 4.9 Model validation at different pH for ethyl oleate hydrolysis at 280 °C and 40 min

4.4.4 Sensitivity Analysis

We carried out sensitivity analysis using the method outlined in section 4.3.2 to identify the parameters to which conversion is most sensitive under different conditions. Table 4.7 lists the normalized sensitivity coefficients (calculated using Eq.(4.7)), for hydrolysis and esterification at different conditions. Run 1 corresponds to hydrolysis at 300 °C and 30 minutes starting with only ethyl oleate and a large excess of water. The model is highly sensitive to a_1 , E_1 , a_2 , E_2 , a_{aw} and E_{aw} and largely insensitive to the other parameters. In other words, the rate constants for protonation of the ester by oleic acid and by H^+ (steps 1 and 2 of Figure 4.4), and $K_{a,w}$ are most important for accurately estimating the conversion. Run 2 shows similar results for the case where oleic acid is also

present initially. These results indicate that only k_1 and k_2 are kinetically significant under these conditions, suggesting that the protonation of the ester by H^+ or oleic acid to form intermediate X_1 compete for the rate-determining step. This process being rate-limiting differs from Krammer and Vogel [7] wherein addition of water to the intermediate X_1 was assumed to control the overall rate of the reaction. However, if one takes the protonation of ester as the rate-determining step in the Krammer and Vogel [7] mechanism, then one arrives at a rate equation with precisely the same form as the one used to fit their data.

Run 3 is hydrolysis with a large amount of added ethanol. The sensitivity analysis shows that the model is most sensitive to Arrhenius parameters for the reverse reactions (a_b , E_b , a_{-1} , E_{-1} , a_{-2} , E_{-2}) along with a_{aw} and E_{aw} , and moderately sensitive to a_{-7} , E_{-7} , a_2 and E_2 , a_{ae} and E_{ae} . In this case, there does not appear to be any single rate-determining step.

Runs 4, 5 and 6 represent esterification reactions under different conditions. Run 4 is esterification without addition of any components other than the two reactants. Sensitivity analysis shows that the rate constant for protonation of oleic acid (reverse of step 7) and $K_{a,e}$ are most important. Under these conditions, protonation is the rate-determining step. For run 5, esterification with added water, the calculated conversion becomes sensitive to all parameters, and no rate-determining step exists. Likewise, the results for run 6, esterification with added ester, indicate sensitivity to nearly all of the relevant model parameters and hence the absence of any single rate determining step. Note that in all cases the model is insensitive to k_{-1} , since sensitivity coefficients related to a_{-1} and E_{-1} are very small ($< 2 \times 10^{-3}$).

Under all conditions examined, the dissociation constant of oleic acid plays an important role for determining conversion. To the best that we know, dissociation constants have not been reported for oleic acid in water, ethanol, and ethanol-water mixtures at high temperatures. There is a need for studies to obtain the dissociation constants of fatty acids in high temperature water and alcohol systems.

Table 4.7 Normalized sensitivity coefficients for mechanistic model

Run	T (C)	X _{model}	C ^o (mol/L)	R _w	R _{OA}	R _{EROH}	a ₀₃	E ₀₃	a ₁₃	E ₁₃	a ₃₀	E ₃₀	a ₃₁	E ₃₁	a _{7s}	E _{7s}	a _b	E _b	a _{AV}	E _{AV}	a _{ae}	E _{ae}
1	300	0.63	0.08	569	0	0	9.25	-7.91	2.56	-2.69	-0.02	0.05	0.00	0.00	-0.01	0.01	0.02	-0.05	1.56	-4.41	0.00	0.00
2	240	0.65	0.08	569	1	0	2.51	-2.38	3.46	-4.07	-0.02	0.05	0.00	0.00	-0.02	0.02	0.02	-0.05	0.42	-1.32	0.00	0.00
3	300	0.16	0.08	300	0	75	18.46	-15.55	2.11	-2.21	-6.53	13.01	<3x10 ⁻³	<10 ⁻³	-1.19	1.04	4.58	-13.31	2.32	-6.53	0.79	-1.57
4	250	0.77	0.61	0	0	10	-0.07	-0.05	0.06	0.00	0.08	-0.17	<8x10 ⁻⁵	<8x10 ⁻²	3.06	-2.96	-0.05	0.17	0.00	0.00	0.69	-1.50
5	250	0.2	0.31	50	0	10	-1.60	1.48	-2.80	3.23	3.25	-7.05	<6x10 ⁻⁴	<-2x10 ⁻³	8.55	-8.17	-2.28	7.29	0.97	-2.99	0.26	-0.57
6	250	0.57	0.18	0	6	10	-0.50	0.47	-0.27	0.31	0.42	-0.92	<10 ⁻⁴	<-10 ⁻⁴	5.13	-4.93	-0.30	0.94	0.00	0.00	1.06	-2.31

4.5 Conclusions

This study is the first to explore the dynamics of ester hydrolysis and fatty acid esterification reactions in tandem. The kinetics is autocatalytic, and a two-step phenomenological model with six adjustable parameters, fit the experimental conversion data obtained over a range of temperatures, initial concentrations, and batch holding times. The parameter values are thermodynamically consistent and reasonable on a thermochemical basis. The model makes reliable quantitative predictions within the experimental conditions used to determine its parameters. It also makes reliable qualitative predictions when extrapolated outside this parameter space. Sensitivity analysis showed that the model is mostly sensitive to the forward rate constants for the catalyzed reaction step (4.II) for hydrolysis and the reverse rate constants for the catalyzed reaction step (4.II) for esterification. Sensitivity analysis also confirms the need of using both hydrolysis and esterification data to obtain reliable estimates of the kinetic parameters for each forward and reverse reaction.

We have also elucidated the common mechanism for fatty acid ester hydrolysis and fatty acid esterification without added acid or base catalysts. Ethyl oleate hydrolysis is both specific acid catalyzed and general acid catalyzed by oleic acid but not by water molecules. Esterification is primarily via specific acid catalysis. The reaction rate equation based on the mechanism was consistent with experimental data for both hydrolysis and esterification. It also provided reliable quantitative predictions both within the experimental conditions used to determine its parameters and outside this parameter space (including different pH values) and for a multicomponent system of fatty acid, ester, water and alcohol. The conversion predicted by the mechanistic model is very sensitive to the dissociation constant K_a , for oleic acid. Accurate determination of dissociation constants of fatty acids in ethanol, water, and ethanol-water systems at high temperatures would enable more accurate mechanistic kinetics models. The rate-limiting steps for ester hydrolysis in HTW with no added acid or products are protonation by H^+ (step 1 Figure 4.4) and by oleic acid (step 2 Figure 4.4), while

for esterification in hot compressed ethanol it is protonation of oleic acid by H^+ (reverse of step 7 of Figure 4.4). There is no rate-determining step in many instances where all components are simultaneously present.

References

- [1] N. Akiya, P. E. Savage. Kinetics and mechanism of cyclohexanol dehydration in high-temperature water. *Ind. Eng. Chem. Res.* 40, 1822-1831, 2001
- [2] T. Pinnarat, P. E. Savage. Noncatalytic esterification of oleic acid in ethanol. *J. Supercrit. Fluids* 53, 53-59, 2010
- [3] T. Pinnarat. Noncatalytic esterification for biodiesel production. *PhD thesis* University of Michigan, Michigan (U.S.), 2011
- [4] S. Changi, T. Pinnarat, P. E. Savage. Modeling hydrolysis and esterification kinetics for biofuel processes. *Ind. Eng. Chem. Res.* 50, 3206-3211, 2011
- [5] S. Changi, T. Pinnarat, P. E. Savage. Mechanistic modeling hydrolysis and esterification kinetics for biofuel processes. *Ind. Eng. Chem. Res.* 50, 12471-12478, 2011
- [6] P. Khuwijitjaru, T. Fujii, S. Adachi, Y. Kimura, R. Matsuno. Kinetics on the hydrolysis of fatty acid esters in subcritical water. *Chem. Eng. J.* 99, 1-4, 2004
- [7] P. Krammer, H. Vogel. Hydrolysis of esters in subcritical and supercritical water. *J. Supercrit. Fluids* 16, 189-206, 2000
- [8] O. Jogunola, T. Salmi, K. Eranen, J. Warna, M. Kangas, J. P. Mikkola. Reversible autocatalytic hydrolysis of alkyl formate: kinetic and reactor modeling. *Ind. Eng. Chem. Res.* 49, 4099-4106, 2010
- [9] T. Kocsisová, J. Juhaz, J. Cvengroš. Hydrolysis of fatty acid esters in subcritical water. *Eu. J. Lipid Sci. Technol.* 108, 652-658, 2006
- [10] W. Marshall, E. Franck. Ion product of water substance 0-1000 °C, 1-10,000 bar, new international formulation and its background. *J. Phys. Chem. Ref. Data* 10 (2), 295-304, 1981
- [11] D. A. S. Ravens. The chemical reactivity of poly (ethylene terephthalate): heterogeneous hydrolysis by hydrochloric acid. *Polymer* 1, 375-383, 1960

- [12] H. Oka, S. Yamago, J. Yoshida, O. Kajimoto. Evidence for a hydroxide ion catalyzed pathway in ester hydrolysis in supercritical water. *Angew. Chem. Int. Ed.* 41 (4), 623-625, 2002
- [13] A. Vatani, M. Mehrpooya, F. Gharagheizi. Prediction of standard enthalpy of formation by a QSPR model. *Int. J. Mol. Sci.* 8, 407-432, 2007
- [14] Y. Warabi, D. Kusdiana, S. Saka. Reactivity of triglycerides and fatty acids of rapeseed oil in supercritical alcohols. *Bioresour. Technol.* 91, 283-287, 2004
- [15] C. Comisar, S. Hunter, A. Walton, P. E. Savage. Effect of pH on ether, ester, and carbonate hydrolysis in high-temperature water. *Ind. Eng. Chem. Res.* 47, 577-584, 2008
- [16] F. G. Helfferich. Comprehensive chemical kinetics. N. J. B. Green Ed., vol. 40 *Kinetics of Multistep Reactions*, 2nd ed., Elsevier Science and Technology, 2004
- [17] M. Rahman, A. Ghosh, R. Bose. Dissociation constants of long chain fatty acids in methanol-water and ethanol-water mixtures. *J. Chem. Tech. Biotechnol.* 29, 158-162, 1979

CHAPTER 5

Behavior of Phenylalanine in HTW

In this chapter we first describe the preliminary work that was done to validate the experimental methods. We then report the effect of temperature, batch holding time, and initial concentration of phenylalanine on the product distribution. Next, we elucidate the reaction pathways, and develop a corresponding quantitative phenomenological kinetics model to fit the experimental observations.

5.1 Control Experiment

A control experiment (as mentioned in 3.3.2) was done to assess our ability to measure accurately the amount of phenylalanine in the reactor. This experiment, which was essentially a run performed at room temperature, gave a phenylalanine recovery of 98%, thereby verifying the suitability of the methods used for quantifying the amount of phenylalanine.

5.2 Effect of Reaction Conditions

5.2.1 Temperature and Batch Holding Time

Experiments were performed at different temperatures (220-350 °C) and batch holding times (0-240 min) to determine how these variables affect phenylalanine conversion, product yields, and reaction kinetics. In general phenylalanine conversion increased with increasing temperature and batch holding times, however, the yield of the products showed a different trend.

Table 5.1 presents the product molar yields and phenylalanine conversion at different times and temperatures. The uncertainties reported are the standard deviation determined from triplicate runs conducted at different batch holding time for each temperature. Phenylethylamine was the major product at all but the most severe conditions examined. Small amounts of styrene and phenylethanol formed as minor products when conversion was < 95%. Both 1- and 2-phenylethanol appeared in these experiments, but we summed their yields and report that sum hereafter, as phenylethanol. To the best of our knowledge, neither styrene nor phenylethanol has been observed previously as a product from hydrothermal treatment of phenylalanine.

Table 5.1 Conversion and molar yield of products for phenylalanine in HTW

T (°C)	Time (mins)	Phenylalanine Conversion	Phenylethylamine Yield	Styrene Yield	Phenylethanol Yield	C-balance (%)
220	60	0.12	0.10	0.001	0	99
	120	0.20	0.10	0.001	0	90
	150	0.23 ± 0.04	0.11 ± 0.007	0.001 ± 9.6E-5	0	89 ± 4
	180	0.25	0.12	0.001	0.0011	87
	240	0.27	0.13	0.001	0.0018	88
250	30	0.33 ± 0.03	0.20 ± 0.04	0.001 ± 9E-4	0.0018 ± 0.001	88 ± 8
	60	0.53 ± 0.04	0.28 ± 0.04	0.002 ± 6E-4	0.0017 ± 0.001	77 ± 11
	90	0.60 ± 0.02	0.38 ± 0.008	0.003 ± 9E-4	0.0010 ± 0.001	86 ± 3
	120	0.66	0.41	0.005	0.0014	84
	150	0.70	0.41	0.005	0.0016	80
	180	0.73	0.44	0.007	0.0017	81
280	10	0.62	0.43	0.002	0	85
	15	0.80	0.55	0.003	0	80
	20	0.84	0.59	0.005	0	82
	30	0.91 ± 0.01	0.64 ± 0.005	0.001 ± 4E-4	0.0014 ± 0.0004	81 ± 1
	40	0.95	0.67	0.027	0.0022	80
	60	0.97	0.68	0.044	0.0030	81
	60	0.97	0.68	0.044	0.0030	81
350	5	0.63	0.36	0.001	0.0015	76
	10	1.00 ± 0.003	0.62 ± 0.03	0.09 ± 0.02	0.0016 ± 0.0003	68 ± 9
	15	1.00	0.60	0.07	0.0033	70
	20	1.00	0.45 ± 0.05	0.20 ± 0.05	0.0124 ± 0.002	64 ± 3
	30	1.00	0.33 ± 0.04	0.27 ± 0.04	0.0244 ± 0.004	61 ± 5
	40	1.00	0.30	0.28	0.0242	57
	60	1.00	0.23	0.38	0.0342	60

The yields of phenylethylamine increased with increasing batch holding times for runs at 220, 250, and 280 °C. The highest yield for phenylethylamine was about 0.68 at 280 °C and 60 min. At 350 °C, the yield of phenylethylamine

increased from 0.36 at 5 min to 0.62 at 10 min and then decreased thereafter. This behavior suggests that phenylethylamine decomposes to secondary products under severe conditions. The yields of styrene were low (< 0.01) at 220, 250, and 280 °C (until 30 min). However, the yield of styrene increased to 0.044 at 280 °C and 60 min. At 350 °C the yield of styrene increased from 0.001 at 5 min to 0.38 at 60 min. At this condition, the yield of styrene exceeded that of phenylethylamine, and styrene was the major product.

Phenylethanol was not formed with yields exceeding 0.003 except at longer batch holding times at 350 °C. At this temperature the yield of phenylethanol increased from about 0.002 at 5 min to nearly 0.034 at 60 min.

The conversion of phenylalanine was below 0.30 at mild conditions (e.g., 220 °C (< 240 min), 250 °C (< 30 min)). In general, the conversion increased with both temperature and time. Nearly complete conversion was observed at 280 °C at a batch holding time of 60 min and at 350 °C for batch holding times greater than 10 min.

The carbon balance was $90\% \pm 10\%$ in most cases, and fell below 80% only for experiments at 350 °C. The conversion of phenylalanine was very high under these conditions. It is likely that the more severe conditions led to the formation of higher molecular weight products via oligomerization, as will be explained in the next section. It should be noted that there was considerable gas formation (most likely carbon dioxide), especially under severe conditions. Although, we have not quantified CO_2 , we account for it in the carbon balance by assuming its yield was equal to the yield of phenylethylamine, since CO_2 would form in parallel with phenylethylamine during the decarboxylation of phenylalanine.

5.2.2 Initial Concentration of Phenylalanine

As mentioned previously, the above results have been reported for a base case concentration of phenylalanine of 15000 ppm. It was necessary to determine the effects of the initial concentration of phenylalanine on the products

before we develop a kinetics model for the reaction network and study the behavior of binary mixtures involving phenylalanine. In this section we present the results of the product yields for different initial concentrations of phenylalanine. The initial concentrations were varied to 4000 and 22000 ppm because we use these exact concentrations for the study of the binary mixture of phenylalanine with ethyl oleate (Chapter 8).

Table 5.2 Conversion and yields of products for phenylalanine in HTW at different initial concentrations of phenylalanine

Temp (°C)	Initial Loading (ppm)	Time (min)	Phenylalanine Conversion	Phenylethylamine Yield	Styrene Yield	Carbon Balance (%)
250	4000	30	0.38	0.22	0	84
		60	0.53	0.27	0	73
		90	0.60	0.33	0	74
		120	0.64	0.42	0.01	79
		150	0.77	0.37	0.02	62
	22000	30	0.34	0.24	0	90
		60	0.48	0.35	0	88
		90	0.59	0.39	0.01	81
		120	0.66	0.40	0.01	75
		150	0.70	0.39	0.02	73
350	4000	10	0.98	0.58	0.04	63
		20	0.98	0.44	0.22	68
		30	0.99	0.43	0.23	68
		40	0.98	0.39	0.27	69
		60	1.00	0.13	0.35	48
	22000	10	1.00	0.71	0.08	78
		20	1.00	0.40	0.21	60
		30	1.00	0.32	0.26	57
		40	1.00	0.24	0.27	50
		60	1.00	0.12	0.43	53

Table 5.2 summarizes the phenylalanine conversion and product yields at two different initial concentrations of phenylalanine (4000 ppm, and 15000 ppm) and two temperatures (250 and 350 °C) at different batch holding times. Comparing Tables 5.1 and 5.2, we can conclude that similar yields of phenylethylamine and styrene were obtained for different initial loading of

phenylalanine, under similar conditions. These results indicate that the yield of phenylethylamine and styrene are independent of the initial phenylalanine concentration, suggesting a first-order reaction for their formations.

5.3 Kinetics of Phenylalanine Disappearance

To compare the present rate data for the disappearance of phenylalanine with previous work [1-3], which indicated first-order kinetics, we fit the phenylalanine conversion data of Table 5.1 to Eq.(5.1), which is the integrated form of the batch reactor design equation coupled with a n^{th} -order rate equation, and k_n is the n^{th} -order rate constant.

$$C_{PA} = \left[C_{PA,initial}^{(1-n)} - (1-n)k_n t \right]^{\frac{1}{1-n}} \quad (5.1)$$

The residual for minimization was the summation of squared errors (SSE) between the calculated and experimental phenylalanine concentrations (Eq.(5.2)), where, j is the number of discrete reaction times at any particular temperature.

$$SSE = \sum_j [C_{j,mod} - C_{j,exp}]^2 \quad (5.2)$$

A non-linear regression was carried out using the SOLVER add-in in Excel 2007, to obtain the values of k_n and n , as displayed in Table 5.3. The overall reaction order for phenylalanine is almost unity at all temperatures under consideration, which is consistent with the previous work. Hence, we reanalyzed the data using first order kinetics to obtain the corresponding first-order rate constants (k_{first}) at different temperatures (Table 5.3).

Table 5.3 Rate constant and order for phenylalanine disappearance in HTW

T (°C)	Order (n)	k_n (mol, min, L)	k_{first} (min ⁻¹)
220	0.94	0.0008	0.0015
250	0.97	0.0065	0.0083
280	0.98	0.0600	0.0692

An Arrhenius plot (based on first order rate constants) gave the activation energy to be 144 ± 14 kJ/mol and the pre-exponential factor to be $10^{12.4 \pm 1.4} \text{ min}^{-1}$.

Table 5.4 compares these Arrhenius parameters with those reported previously for phenylalanine in HTW. Though there is some variability in the Arrhenius parameters, the rate constants calculated at a given temperature (250 °C is used in Table 5.4) compare very well for the results from this work and that of Li and Brill [3] and Abdelmoez *et al.* [2]. The small differences between these parameters probably arise from systematic differences in operating temperatures, pressures, process times, and procedures for data collection. These rate constants, however, are six to seven times higher than those calculated using the Arrhenius parameters reported by Vallentyne [1]. Li and Brill [4] had also noted discrepancies between their rate constants and those computed by Vallentyne [1] for other amino acids, such as glycine. They attribute these discrepancies to differences in the reactor surface materials. Li and Brill used a titanium flow cell, whereas Vallentyne used glass reactors. The analytical procedures used by Vallentyne were not as advanced as the current methods for quantification, which could also result in some discrepancies between the rate constants.

Table 5.4 Arrhenius parameters for phenylalanine disappearance in HTW

Source	A_0 (min^{-1})	E_a (kJ/mol)	$k_{250^\circ\text{C}}$ (min^{-1})
This work	$10^{12.4 \pm 1.4}$	144 ± 14	0.0083
Li and Brill [3]	$10^{15.1 \pm 2.5}$	171 ± 8	0.0095
Abdelmoez [2]	$10^{10.5}$	126	0.0092
Vallentyne [1]	$10^{10.1}$	129	0.0014

5.4 Reaction Pathways

Section 5.2 showed that phenylalanine in HTW produced phenylethylamine as its main product, while styrene and phenylethanol were produced in minor amounts at most of the conditions under consideration. However, at 350 °C and 60 min, the yield of styrene becomes greater than that of phenylethylamine. We desired to discover the complete set of reaction pathways for phenylalanine and these products.

Phenylethylamine can form via decarboxylation of phenylalanine. Decarboxylation mechanisms for amino acids can be complicated and several have been proposed. Direct decarboxylation of the zwitterions of carboxylic acid

and carboxylate ion, such as occurs in amino acids, has been reported [4-7]. Li and Brill [4] mentioned that that an aromatic ring at the β -carbon can act as an electron sink that dissipates the developing negative charge on the α -carbon atom during the decarboxylation reaction, as would be applicable for phenylalanine. Researchers have also proposed a general water-molecule-catalyzed transition state involving a six-membered ring for decarboxylation [4, 8, 9].

Styrene or a corresponding alkene has not been reported in the past as a product from amino acid conversion in HTW. We hypothesize that phenylethylamine undergoes deamination at severe conditions to form styrene, because the yield of phenylethylamine decreases and the yield of styrene increases. To test this hypothesis, we reacted 20 μ L of phenylethylamine (equivalent to the amount of phenylethylamine formed at complete conversion of phenylalanine) in water at 350 $^{\circ}$ C and 30 min. The phenylethylamine conversion was 0.51 ± 0.04 and the yield of styrene was 0.31 ± 0.02 . The above results indicate formation of styrene as a secondary product (from phenylethylamine) during treatment of phenylalanine in HTW.

Phenylethanol isomers, which were minor products, could be obtained via hydration of styrene in HTW. 1-phenylethanol, which can form via Markovnikov's rule, was more abundant than 2-phenylethanol, the anti-Markovnikov product. These observations are consistent with An *et al.* [10], who report hydration of some olefins without any added catalysts at 250 $^{\circ}$ C in high temperature water and also mention that the alcohol formed via Markovnikov's rule is the more abundant alcohol. We tested whether this pathway would be operative for styrene by reacting 20 μ L of styrene in HTW at 350 $^{\circ}$ C and 30 min. Styrene conversion under these conditions was 0.35, and it formed phenylethanol in a yield of 0.05. It is interesting to note that under these conditions styrene mostly formed several high molecular weight products, including 1,3-diphenylbutane, a styrene dimer. Styrene oligomerization under these conditions is reasonable. Erdmenger *et al.* [11] reported polymerization of styrene under near-critical water

conditions to produce polystyrene, with a number-average molecular weight (M_n) of 25,790 Da, in yields of 0.31. They mention that polystyrene has a high decomposition temperature (~ 310 °C) and thus can be polymerized up to 300 °C. Furthermore, the polymerization of styrene is auto-initiating at high temperatures and no additional initiator is required [12]. The polymerization process can start initially as a [2+4] Diels-Alder reaction between two styrene molecules, which results in a non-aromatized Mayo adduct. This adduct can further react with another styrene molecule to generate chain-propagating molecules [11, 12].

We also expect that phenylethanol can dehydrate in HTW to form styrene. There is ample evidence in the literature for alcohol dehydration in HTW [13-15]. Commonly established mechanisms for alcohol dehydration are E1cB, E1, and E2. These notations stand for elimination (“E”) with a rate-limiting step that is either unimolecular (“1”) or bimolecular (“2”). Depending on the reaction conditions used, a given alcohol can undergo dehydration by any one of these mechanisms. More details about these mechanisms can be found elsewhere [13-15].

Similar to styrene, phenylalanine could also dimerize at high temperatures and longer batch holding times, as has been mentioned for other amino acids [16-20]. LC-MS chromatograms of the products from phenylalanine at 250 °C and 30 min and at 350 °C and 60 min (Figure 5.1), indicate the presence of not only phenylethylamine (main decarboxylation product), but also oligomers of phenylalanine (up to 706 amu).

Comparing Figures 5.1a and 5.1b shows that more of the higher molecular weight oligomers are obtained at the higher temperature and longer batch holding time. Since we did not quantify the yields of the many oligomers of phenylalanine and styrene, the carbon balances shown in Table 5.1 are not 100%. The propensity for more oligomerization at the higher temperatures and longer times is consistent with the carbon balance being lower at more severe conditions.

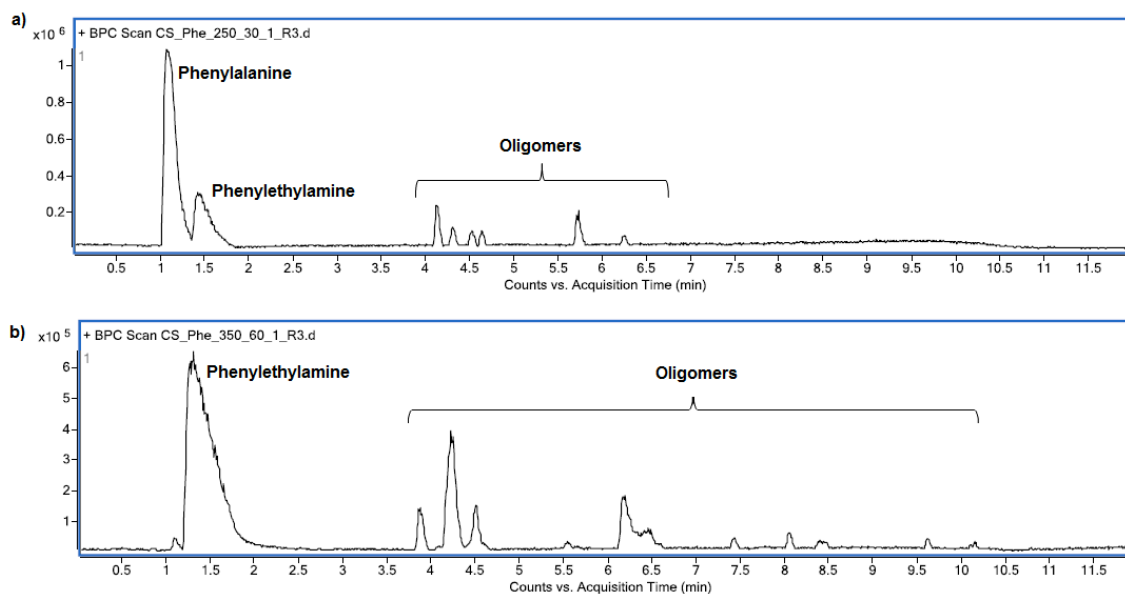


Figure 5.1 LC-MS chromatograms for phenylalanine reaction products at different conditions. a) 250° C and 30 min, and b) 350° C and 60 min

Based on the reasoning provided in this section, we propose the reaction network in Figure 5.2 to describe the reactions of phenylalanine in HTW. The reactions include decarboxylation, hydration/dehydration, and oligomerization, all of which have been previously documented in HTW.

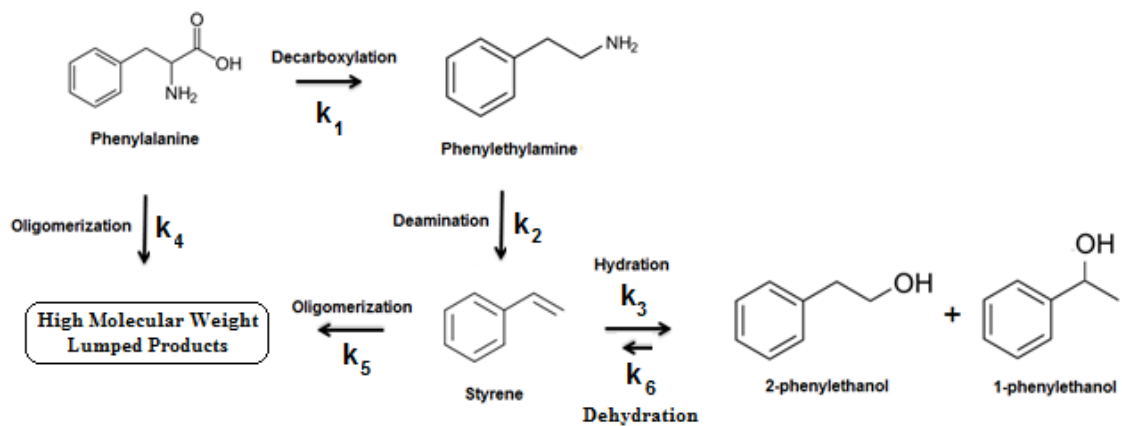


Figure 5.2 Reaction pathways for phenylalanine in HTW

5.5 Kinetic Model

The reaction network in Figure 5.2 provides different pathways that interconnect the observed reaction products. Our focus now turns to constructing a chemical kinetic model based on a proposed reaction network. All reactions in the network were treated as being irreversible and proceeding through first order kinetics, except oligomerization of phenylalanine, which was taken to follow second-order kinetics, as suggested by Cox and Seward [16] for alanine and glycine. The model can be represented by differential equations (given through Eq. (5.3) – Eq. (5.6)), which apply to reactions in a constant-volume batch reactor.

$$\frac{dC_{PA}}{dt} = -k_1 C_{PA} - k_4 C_{PA}^2 \quad (5.3)$$

$$\frac{dC_{PEA}}{dt} = k_1 C_{PA} - k_2 C_{PEA} \quad (5.4)$$

$$\frac{dC_{STY}}{dt} = k_2 C_{PEA} - k_3 C_{STY} - k_5 C_{STY} + k_6 C_{PEOH} \quad (5.5)$$

$$\frac{dC_{PEOH}}{dt} = k_3 C_{STY} - k_6 C_{PEOH} \quad (5.6)$$

where, C is the concentration and the subscripts PA , PEA , STY , and $PEOH$ represent phenylalanine, phenylethylamine, styrene, and phenylethanol respectively.

We used MATLAB 2010 to solve simultaneously the set of ordinary differential equations above and perform parameter estimation to obtain the values of the rate constants at each temperature. We used *fmincon* to perform the optimization using the *optimtool* GUI. The minimization algorithm uses a sequential quadratic programming active set optimization method [21]. The objective function for minimization was the summation of squared relative error (SSRE) between the calculated and experimental product concentrations at a given reaction temperature. This quantity was calculated using Eq. (5.8), where, j

is the number of discrete reaction times at a particular temperature and i is the number of components.

$$SSRE = \sum_j \sum_{i=1}^4 \left[\frac{C_{j,i,model} - C_{j,i,exp}}{(C_{j,i,model} + C_{j,i,exp}) / 2} \right]^2 \quad (5.8)$$

The rate constants at each temperature were then fit to the linearized form of the Arrhenius equation to get A_i and E_{a_i} along with the associated standard errors for each rate constant.

Table 5.5: Arrhenius parameters for phenylalanine reaction network

Rate Constant (k_i) in Fig. 2	Units	A	E_a (kJ/mol)	$k_{250} \text{ } ^\circ\text{C}$
1	min^{-1}	$10^{12.5 \pm 0.6}$	146 ± 6	$7.49\text{E-}3$
2	min^{-1}	$10^{7.7 \pm 1.1}$	113 ± 11	$2.77\text{E-}4$
3	min^{-1}	$10^{10.6 \pm 0.3}$	155 ± 4	$1.12\text{E-}5$
4	$\text{L mol}^{-1} \text{ min}^{-1}$	$10^{13.9 \pm 4.3}$	153 ± 12	$4.17\text{E-}2$
5	min^{-1}	$10^{7.3 \pm 0.4}$	132 ± 4	$1.25\text{E-}6$
6	min^{-1}	$10^{8.5 \pm 0.5}$	140 ± 6	$3.23\text{E-}6$

Table 5.5 displays the Arrhenius parameters that provided the best description of the experimental data. It also displays the values of the rate constants at 250 °C, so that the relative rates of the different paths can be easily discerned. The rate constant for decarboxylation, k_1 , is largest of the first-order rate constants at all temperatures. It is also larger than the pseudo-first-order rate constant for oligomer formation from phenylalanine ($k_4 C_{\text{PA}, \text{initial}} \sim 3\text{E-}3 \text{ min}^{-1}$). These observations indicate that decarboxylation of phenylalanine to phenylethylamine is always the main pathway. The rate constants k_2 and k_3 , which govern formation of styrene and phenylethanol are one and two orders of magnitude lower than k_1 at 250 °C. Of course this result is consistent with these products being in low yields at this temperature. The rate constants k_5 and k_6 are three orders of magnitude lower than that for decarboxylation of phenylalanine, consistent with these pathways for styrene oligomerization and dehydration of phenylethanol being minor ones.

Figure 5.3 shows the experimental concentrations and those calculated from the model for phenylalanine, phenylethylamine, styrene, and phenylethanol at all four temperatures investigated. The model accurately describes the trends in the data and typically provides the species concentrations within experimental errors.

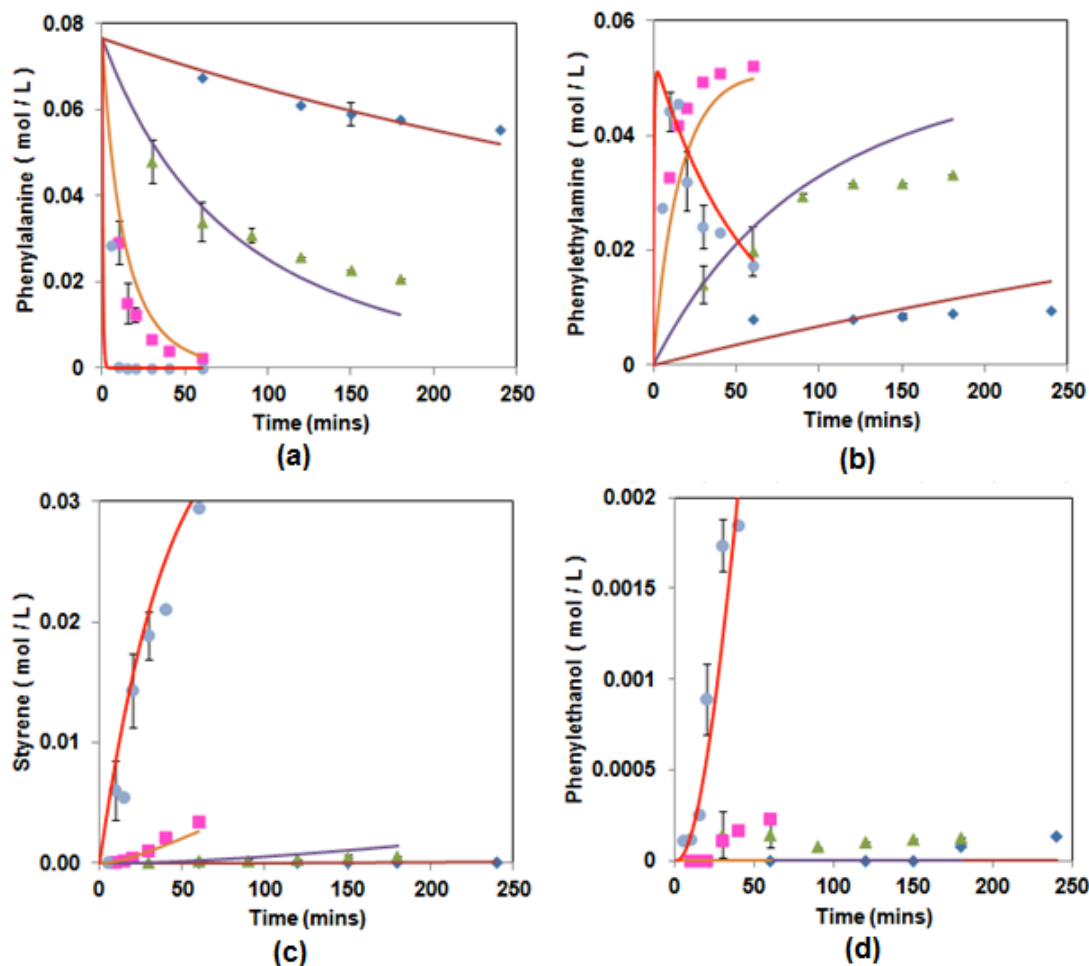


Figure 5.3 Comparison of experimental (discrete points) and model (smooth curves) results for reactants and products at different conditions. Legends are a) phenylalanine, b) phenylethylamine, c) styrene, and d) phenylethanol at \blacklozenge 220 °C, \blacktriangle 250 °C, \blacksquare 280 °C, and \bullet 350 °C

Figure 5.4 shows a parity plot of the experimental and model-calculated concentrations for all species at all conditions. There is good agreement of the model with the data, given the experimental uncertainty. The data are scattered on both sides of the diagonal line, indicating the absence of systematic errors in the data fitting.

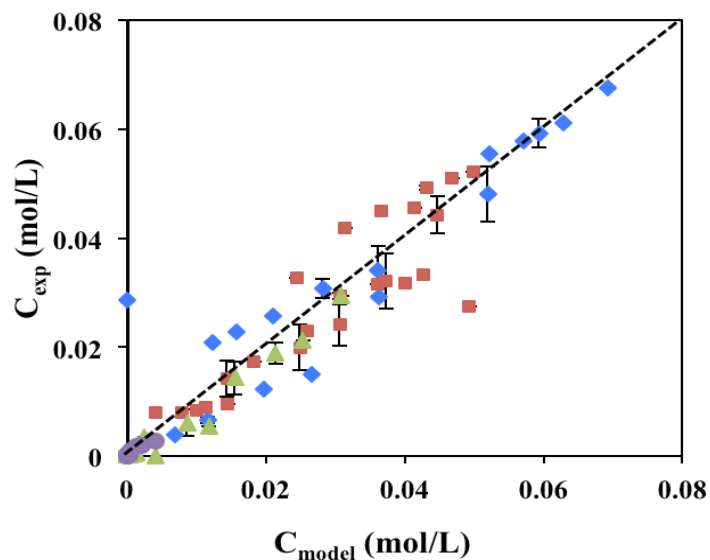


Figure 5.4 Parity plot between experimental and model concentration. Legends are ◆ phenylalanine, ▲ phenylethylamine, ■ styrene, and ● phenylethanol at 220° C, 250° C, 280° C, and 350° C

5.6 Conclusions

Under the conditions studied, phenylalanine readily underwent decarboxylation to form phenylethylamine. Subsequently, phenylethylamine underwent deamination to styrene (favored at high temperatures), and styrene underwent either hydration to form phenylethanol or oligomerization. Phenylethanol can dehydrate to a small extent in HTW to styrene. Phenylalanine can also oligomerize at high temperatures and longer batch holding times.

We propose a reaction network based on the above observations. A phenomenological kinetics model based on the proposed network accurately describes the trends in the data and typically estimates the concentrations of the reactant and products within their experimental errors. All the rate constants are typically first-order except oligomerization of phenylalanine, which follows second order kinetics. The rate constant for phenylethylamine formation is largest amongst all the first order rate constants. Thus, we elucidate broadly through this study of phenylalanine that many different types of reactions (e.g., decarboxylation, hydration, oligomerization, and dehydration) can occur for other amino acids during HTL of algae.

References

- [1] J. R. Vallentyne. Thermal reaction kinetics and transformation products of amino compounds. *Geochim. Cosmochim. Acta.* 28, 157-188, 1964
- [2] W. Abdelmoez, T. Nakahasi, H. Yoshida. Amino acid transformation and decomposition in saturated subcritical water conditions. *Ind. Eng. Chem. Res.* 46, 5286-5294, 2007
- [3] J. Li, T. B. Brill. Spectroscopy of hydrothermal reactions 25: Kinetics of the decarboxylation of protein amino acids and the effect of side chains on hydrothermal stability. *J. Phys. Chem. A.* 107, 5987-5992, 2003
- [4] J. Li, T. B. Brill. Spectroscopy of hydrothermal reactions 26: Kinetics of the decarboxylation of aliphatic amino acids and comparison with the rates of racemization. *Int. J. Chem. Kinet.* 35 (11), 602-610, 2003
- [5] R. D. Bach, C. Canepa. Electronic factors influencing the decarboxylation of β -keto acids. A model enzyme study. *J. Org. Chem.* 61, 6346-6353, 1996
- [6] D. Sicinska, D. G. Truhlar, P. Paneth. Solvent-dependent transition states for decarboxylations. *J. Am. Chem. Soc.* 123, 7683-7686, 2001
- [7] L. M. Phillips, J. K. Lee. Theoretical studies of mechanisms and kinetic isotope effects on the decarboxylation of orotic acid and derivatives. *J. Am. Chem. Soc.* 123, 12067-12073, 2001
- [8] P. Ruelle. Ab initio quantum-chemical study of the unimolecular pyrolysis mechanisms of acetic acid. *Chem. Phys.* 110, 263-274, 1986
- [9] P. Ruelle. Ab initio study of the unimolecular pyrolysis mechanisms of formic acid: additional comments based on refined calculations. *J. Am. Chem. Soc.* 109, 1722-1725, 1987

- [10] J. An, L. Bagnell, T. Cablewski, C. R. Strauss, R. W. Trainor. Applications of high-temperature aqueous media for synthetic organic reactions. *J. Org. Chem.* 62, 2505-2511, 1997
- [11] T. Erdmenger, C. R. Becer, R. Hoogenboom, U.S. Schubert. Simplifying the free-radical polymerization of styrene: Microwave-assisted high-temperature auto polymerizations. *Aust. J. Chem.* 62, 58-63, 2009
- [12] J. D. Campbell, J. A. Allaway, F. Teymour, M. Morbidelli. High-temperature polymerization of styrene: Mechanism determination with preparative gel permeation chromatography, matrix-assisted laser desorption/ionization time-of-flight mass spectrometry, and ^{13}C nuclear magnetic resonance. *J. Appl. Polym. Sci.* 94 (3), 890-908, 2004
- [13] N. Akiya, P. E. Savage. Kinetics and mechanism of cyclohexanol dehydration in high-temperature water. *Ind. Eng. Chem. Res.* 40, 1822-1831, 2001
- [14] X. Xu, M. J. Antal. Mechanism and temperature-dependent kinetics of the dehydration of *tert*-butyl alcohol in hot compressed liquid water. *Ind. Eng. Chem. Res.* 36 (1), 23-41, 1997
- [15] S. E. Hunter, C. E. Ehrenberger, P. E. Savage. Kinetics and mechanism of tetrahydrofuran synthesis via 1,4-butanediol dehydration in high-temperature water. *J. Org. Chem.* 71, 6229-6239, 2006
- [16] J. S. Cox, T. M. Seward. The reaction kinetics of alanine and glycine under hydrothermal conditions. *Geochim. Cosmochim. Acta.* 71, 2264-2284, 2007
- [17] Ogata Y., E. Imai, H. Honda, K. Hatori, K. Matsuno. Hydrothermal circulation of seawater through hot vents and contribution of interface chemistry to prebiotic synthesis. *Origins of Life and Evolution of the Biosphere* 30, 527-537, 2000

- [18] D. K. Alargov, S. Deguchi, K. Tsujii, K. Horikoshi. Reaction behaviors of glycine under super- and subcritical water conditions. *Origins of Life and Evolution of the Biosphere* 32, 1-12, 2002
- [19] Md. N. Islam, T. Kaneko, K. Kobayashi. Reaction of amino acids in a supercritical water-flow reactor simulating submarine hydrothermal systems. *Bull. Chem. Soc. Jpn.* 76, 1171-1178, 2003
- [20] T. Otake, T. Taniguchi, Y. Furukawa, F. Kawamura, H. Nakazawa, T. Kakegawa. Stability of amino acids and their oligomerization under high-pressure conditions: Implications for prebiotic chemistry. *Astrobiology* 11 (8), 799-813, 2011
- [21] <http://www.mathworks.com/help/toolbox/optim/ug/fmincon.html>. Date last accessed, 3rd September 2011

CHAPTER 6

Behavior of Phytol in HTW

In this chapter we first describe the preliminary work that was done to validate the experimental methods for phytol. We then report the effect of temperature, batch holding time, and initial concentration of phytol on the product distribution. Finally we mention the identities and amounts of the different products, elucidate the reaction pathways, and develop a corresponding quantitative phenomenological kinetics model to fit the experimental observations.

6.1 Control Experiments

A control experiment (as mentioned in 3.3.3) was done to assess our ability to measure accurately the amount of phytol in the reactor. This experiment, which was essentially a run performed at room temperature, gave a very good phytol recovery of about 94%, thereby verifying the suitability of the methods used.

We were also concerned with the possibility that two immiscible liquid phases might be present in the reactor at the experimental conditions since phytol is insoluble in water at room temperature. We could not find solubility data for phytol in water for the reaction temperatures of interest in this study, so we used ASPEN Plus version 2006.5 for fluid phase equilibrium calculations. We used the RK-ASPEN thermophysical properties model, which is suitable for a mixture of polar and nonpolar compounds at high temperatures and pressures [1]. A FLASH3 block was used in ASPEN to do the vapor-liquid-liquid equilibrium calculations, with conditions set to those of the experiments. Phytol is not in the Aspen Plus chemical library, so we performed the calculations first using

eicosane (the n-alkane analogue of phytol) and then using eicosanoic acid (which contains the same number of carbon atoms as phytol but is more polar). The calculations showed that a single liquid phase would exist at the experimental conditions for both eicosane and eicosanoic acid. Thus, this modeling exercise helped us infer that a single homogeneous liquid phase existed for phytol in water at the reaction conditions investigated.

6.2 Effect of Reaction Conditions

6.2.1 Temperature and Batch Holding Time

Experiments were performed at different temperatures (240-350 °C) and batch holding times (0-300 min) to determine the effects of these variables on phytol conversion, product yields, and reaction kinetics. In general phytol conversion increased with increasing temperature and batch holding times. This section describes in detail the effect of these parameters on product yields and phytol conversion.

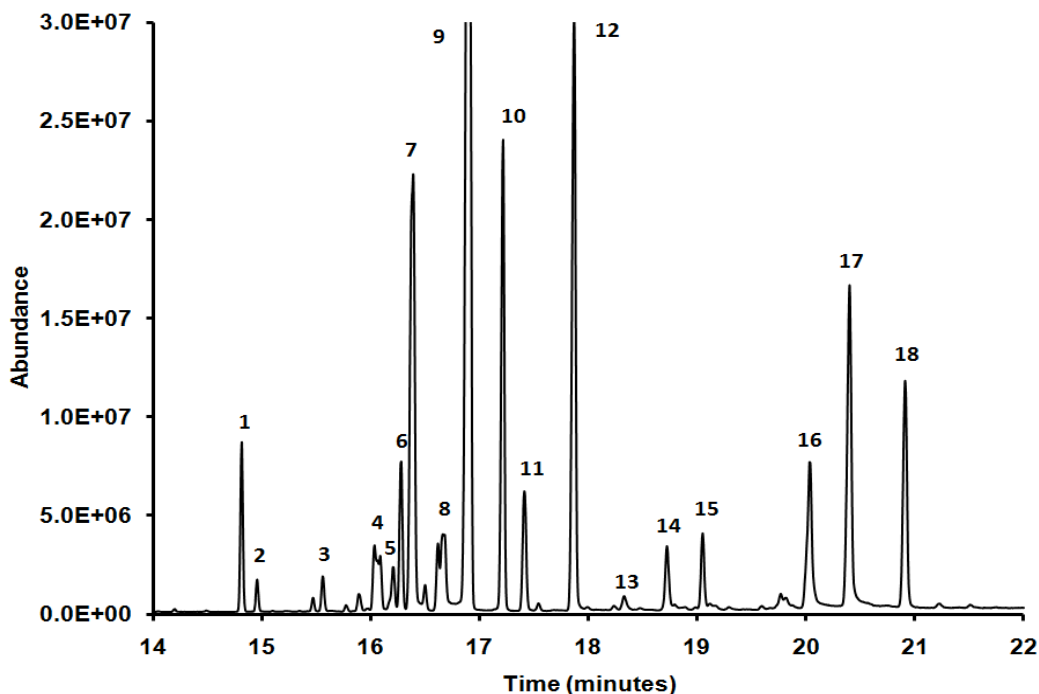


Figure 6.1 Total ion chromatogram for the product mixture obtained from the hydrothermal reaction of phytol at 300° C and 20 min

Table 6.1 Products from the hydrothermal processing of phytol

Peak ID Fig. 6.1	Common Name (IUPAC Name)	Chemical Structure
1,2	Pristene isomers (Pentadecene-2,6,10,14-tetramethyl-)	
3, 5	Phytene isomers (Hexadecene-3,7,11,15-tetramethyl-)	
4, 6, 8, 9, 10	Neophytadiene isomers (Hexadecene-7,11,15-trimethyl-3-methylene-)	
7	Phytone (2-Pentadecanone-6,10,14-trimethyl)	
11	Phytane (Hexadecane-2,6,10,14-tetramethyl-)	
12	Isophytol (1-Hexadecen-3-ol-3,7,11,15-tetramethyl-)	
13	Dihydrophytol (1-Hexadecanol-3,7,11,15-tetramethyl)	
14	C20 molecule	-----
15	C20 molecule	-----
16, 17	Phytol isomers (2-Hexadecen-1-ol-3,7,11,15-tetramethyl-)	
18	Impurity in phytol standard	-----

Figure 6.1 illustrates a total ion chromatogram of the product mixture obtained at 300° C and a batch holding time of 20 min. No peaks were detected before 14 min and after 21 min. Table 6.1 lists the chemical identity of each of the labeled peaks in Figure 6.1.

Inspection of the fragmentation patterns in the mass spectra and knowledge of the possible chemical reactions suggested that peaks 1 and 2 were isomeric forms of pristene. This product may exist as cis/trans isomers or as positional isomers (e.g., 1-pristene or 2-pristene).

The mass spectra of peaks 4, 6, 8, 9 and 10 were very similar to each other and were classified together as neophytadiene isomers. This group may include both configurational isomers (cis-trans) and positional isomers. The occurrence of multiple isomers of neophytadiene in the present study is consistent with Blumer and Thomas [2] reporting the isolation of four isomeric phytadienes from zooplankton and Hites [3] observing four major fractions from the pyrolysis of pheophytin *a* and identifying them as various isomers of phytadiene. All the peaks we identify as neophytadiene exhibited abundant ions at *m/z* 43, 57, 67, 82, 95 and 123 and a molecular ion at *m/z* 278. Figure 6.2 shows the mass spectrum for peak 10, one of the neophytadiene isomers. It is interesting to note that neophytadiene was a major constituent in the crude bio-oil recovered in a control experiment for hydrothermal liquefaction of the green microalga *Nannochloropsis* sp. at room temperature [4] and was detected in bio-oil produced from liquefaction at elevated temperatures as well [5]. Likewise, Bae *et al.* reported neophytadiene as a major component of the bio-oil produced during pyrolysis of macroalgae from 300-600° C [6].

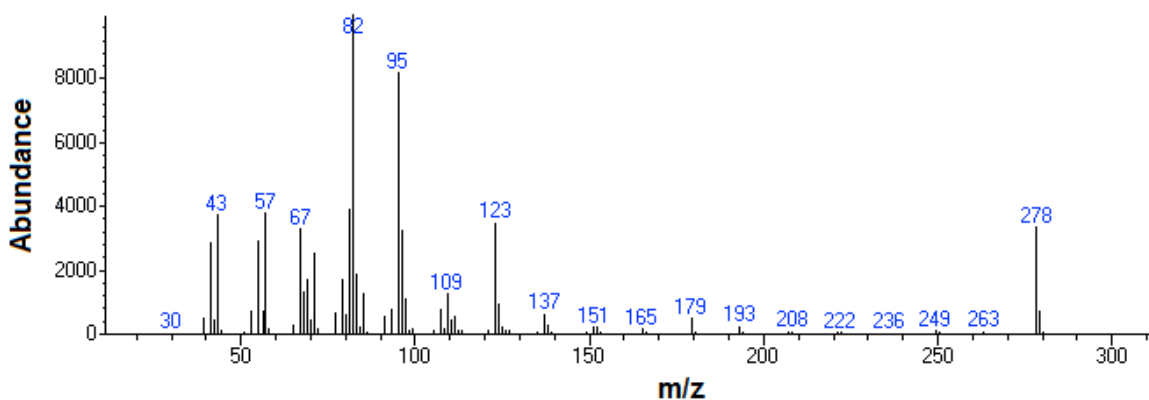


Figure 6.2 Representative MS fragmentation pattern of neophytadiene

Peaks 3 and 5 represent stereoisomers of phytene, which was also observed in crude bio-oil obtained from hydrothermal liquefaction of algae at 350° C [4,5,7]. Likewise, Zhou *et al.* reported phytene as one of the components of the bio-oil produced during liquefaction of macroalgae at 300° C [8]. Peaks 7, 11, 12 and 13 were identified as phytone, phytane, isophytol and dihydrophytol,

respectively. Phytane has also been identified as a component of crude algal bio-oil [4,5,7]. A phytol standard confirmed that peaks 16 and 17 represent stereoisomers of phytol.

The mass spectra of peaks 14 and 15 did not resemble any of those in the MS library, nor could we identify these compounds from their mass fragmentation patterns. Considering that these products have a retention time between dihydrophytol and phytol, we suspect that they are C₂₀ molecules and group them as such. Lastly, peak 18 was an impurity in the purchased phytol. We could not determine its identity via GC-MS. The amount of this impurity remained constant, within experimental errors, at nearly 3% of the phytol initially loaded, regardless of the reaction conditions. Hence, we conclude that the impurity did not react and did not lead to any of the major products reported herein.

Table 6.2 presents the product molar yields and phytol conversion for the hydrothermal reaction of phytol. The uncertainties reported are the standard deviation determined from triplicate runs conducted at one batch holding time for each temperature. The major products are neophytadiene, isophytol, and phytone. The minor products are pristene, phytene, phytane, and dihydrophytol. The yields for neophytadiene, pristene, and phytene are the sums for all isomers.

Neophytadiene was always the most abundant product, and the highest yield observed was about 0.30. Isophytol was the second most abundant product, with a yield ranging from about 0.02 to a maximum of 0.15. The yields for neophytadiene and isophytol are similar at 240 °C and 270 °C, whereas with an increase in temperature to 300 °C and for batch holding times below 40 min, the yield for neophytadiene becomes nearly twice that of isophytol. At 300 °C and 60 min and 350 °C and 5 min, the yield of neophytadiene is five times that of isophytol, whereas for the remaining batch holding times at 300 °C, the yield of neophytadiene is greater than 20 times that of isophytol. It is interesting to note that the yield of neophytadiene decreased at the longer batch holding times at 270 °C, 300 °C, and 350 °C, as does the yield of isophytol at 300 °C and 350 °C.

This behavior suggests decomposition of neophytadiene and isophytol to secondary products.

The yields of dihydrophytol were generally very low and relatively constant at about 0.0010 when the phytol conversion was less than about 0.50. At 300 °C and 350 °C, the yield of dihydrophytol decreased with time. The yields of phytone were < 0.01 at conversions < 0.20, but the yield increased sharply to about 0.06 as conversion increased. The highest yields of pristene, phytene, and phytane were about 0.01-0.02. The general trend in the yields of the aforementioned compounds was such that as both temperature and time increased, the yield also increased.

The conversion of phytol was below 0.15 at mild conditions of lower temperature and/or short times (e.g., 240 °C (60, 120, 180 min), 270 °C (15, 30 min) and 300 °C (5 min)). Nearly complete conversion was observed at 300 °C at a batch holding time of 60 min and 350 °C for batch holding times of greater than 5 min. In general, phytol conversion (X) increased with both temperature and time.

Table 6.2 shows that the carbon balance was 100% \pm 10% in most cases, and fell below 85% for the two experiments at 300 °C (40 and 60 min) and at 350 °C. The conversion of phytol was very high under these conditions. It is likely that the more severe conditions led to the formation of higher molecular weight products via oligomerization, as will be explained in the next section. The oxygen balance (% of O atoms in phytol initially loaded into the reactor that appear in the species quantified post-reaction) was 85% \pm 15% in most cases, but fell below 65% for 300 °C (> 10 min) and at 350 °C. The oxygen balance was lower at the more severe conditions because it does not include oxygen in lower molecular weight products such as CO₂, water, formic acid, and acetic acid. These products may be formed during the course of the reaction under the severe conditions, as will be explained in the next section.

Table 6.2 Conversion and molar yield of products for phytol in HTW

T(°C)	Time (mins)	Phytol (X)	Neophytadienes	Isophytol	Phytone	Pristene	Phytene	Phytane	Dihydrophytol	C-balance (%)	O-balance (%)
240	60	0.05	0.04	0.02	0.004	0.001	0.001	0.004	0.0010	101	97
	120	0.001	0.03	0.03	0.006	0.001	0.001	0.005	0.0011	108	104
	180	0.12 ± 0.08	0.08 ± 0.03	0.06 ± 0.02	0.006 ± 0.001	0.002 ± 0.0002	0.001 ± 0.0002	0.006 ± 0.0008	0.0010 ± 0.0001	104 ± 3	93 ± 6
	240	0.25	0.10	0.08	0.008	0.003	0.001	0.007	0.0010	94	83
	300	0.20	0.12	0.11	0.009	0.003	0.001	0.008	0.0008	105	92
270	15	0.09	0.09	0.06	0.006	0.001	0.001	0.007	0.0011	107	97
	30	0.14	0.07	0.06	0.007	0.002	0.002	0.007	0.0013	101	93
	45	0.22 ± 0.07	0.11 ± 0.04	0.08 ± 0.02	0.010 ± 0.002	0.003 ± 0.0001	0.002 ± 0.0003	0.008 ± 0.0012	0.0013 ± 0.0004	100 ± 5	87 ± 7
	60	0.08	0.07	0.08	0.011	0.005	0.003	0.008	0.0017	110	101
	90	0.30	0.13	0.12	0.017	0.008	0.004	0.009	0.0014	99	84
	120	0.29	0.10	0.10	0.017	0.009	0.004	0.008	0.0013	95	83
	150	0.37	0.12	0.13	0.021	0.012	0.004	0.008	0.0011	92	78
300	180	0.37	0.07	0.13	0.02	0.017	0.007	0.004	0.0011	97	78
	5	0.13	0.10	0.05	0.007	0.001	0.001	0.007	0.001	104	93
	10	0.49	0.28	0.12	0.015	0.003	0.002	0.011	0.0009	94	65
	15	0.54	0.26	0.12	0.02	0.005	0.003	0.011	0.0008	88	60
	20	0.58 ± 0.03	0.24 ± 0.03	0.15 ± 0.01	0.022 ± 0.001	0.006 ± 0.0001	0.004 ± 0.0007	0.011 ± 0.0005	0.0008 ± 0.0001	85 ± 1	59 ± 2
	40	0.83	0.30	0.12	0.042	0.013	0.006	0.012	0.0005	65	33
	60	0.98	0.25	0.06	0.058	0.017	0.008	0.012	0.0003	42	14
350	5	0.98	0.23	0.04	0.054	0.007	0.008	0.012	0.0008	36	11
	10	0.98 ± 0.005	0.13 ± 0.007	0.005 ± 0.006	0.056 ± 0.001	0.013 ± 0.003	0.017 ± 0.002	0.012 ± 0.0006	0.0008 ± 0.0001	24 ± 2	8 ± 1
	15	0.99	0.09	0.004	0.052	0.009	0.018	0.008	0.0005	18	6
	20	0.99	0.06	0.009	0.055	0.008	0.026	0.005	0.0003	18	9

6.2.2 Initial Concentration of Phytol

The above results have been reported for a base case loading of phytol of 50 μL . It was necessary to determine the effects of the initial concentration of phytol on the products before we develop a kinetics model for the reaction network. In this section, we explore the effect of two other initial loadings of phytol (25 and 75 μL) on the yields of the major products, neophytadiene and isophytol.

Table 6.3 Conversion and yield of major products for phytol in HTW at different initial concentrations of phytol

Initial Phytol Loaded (μL)	Time (min)	Phytol Conversion	Neophytadiene Yield	Isophytol Yield
25	10	0.48 ± 0.04	0.26 ± 0.15	0.13 ± 0.05
	20	0.61 ± 0.08	0.35 ± 0.02	0.14 ± 0.04
	40	0.84 ± 0.07	0.34 ± 0.05	0.09 ± 0.02
	60	0.98 ± 0.01	0.29 ± 0.02	0.03 ± 0.01
75	10	0.52 ± 0.03	0.22 ± 0.04	0.14 ± 0.03
	20	0.62 ± 0.03	0.29 ± 0.05	0.17 ± 0.02
	40	0.81 ± 0.03	0.27 ± 0.07	0.12 ± 0.08
	60	0.95 ± 0.05	0.22 ± 0.01	0.08 ± 0.05

Table 6.3 summarizes the phytol conversion and yield of neophytadiene and isophytol at 300 °C at different batch holding times. Comparing Tables 6.2 and 6.3, we can conclude that similar yields of neophytadiene and isophytol were obtained for different initial loadings of phytol, under similar conditions. These results indicate that the yields of these major products are independent of the initial phytol concentration, suggesting a first-order reaction for their formations.

6.3 Kinetics of Phytol Disappearance

The phytol conversion data shown in Table 6.2 were plotted as $-\ln(1-X)$ against the batch holding time as shown in Figure 6.3. The linear relationship observed indicates that the disappearance of phytol in HTW proceeds as a first order reaction.

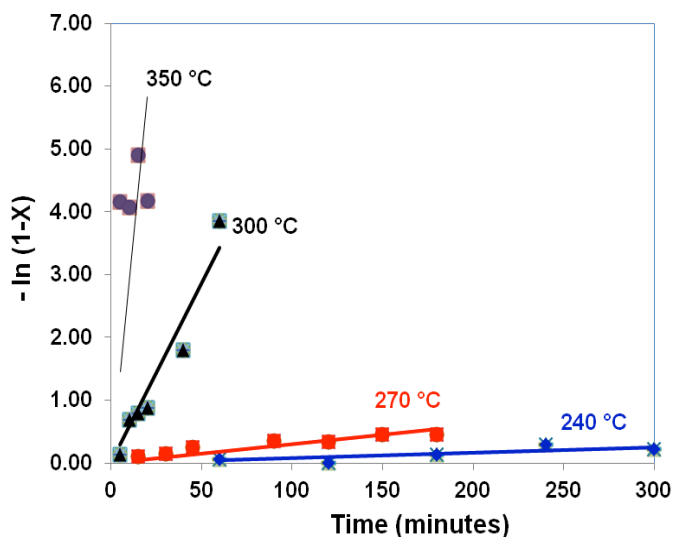


Figure 6.3 First-order plot for phytol conversion in HTW.

The slopes of the lines in Figure 6.3 provide the overall first-order rate constants, and Table 6.4 displays these values. An Arrhenius plot revealed the activation energy to be 145 ± 20 kJ/mol and the pre-exponential factor to be $10^{11.7 \pm 1.9} \text{ min}^{-1}$. This study is the first to report kinetics of phytol in HTW.

Table 6.4 First-order rate constants for phytol conversion in HTW

T (°C)	k (min ⁻¹)
240	8.03E-04
270	3.01E-03
300	5.71E-02
350	2.91E-01

6.4 Reaction Pathways

The previous section showed that the reactions of phytol in HTW produced a rich product spectrum. We desired to discover the reaction pathways that connected phytol and these various products. The first step in reaction pathway resolution is determining which of the products form directly from phytol (i.e., primary products) and which form indirectly (non-primary products). We conducted a first-rank Delplot analysis to deduce this discrimination. The first-rank Delplot is a plot of the selectivity of a product (ratio of yield to conversion) versus conversion. If extrapolation of the data on this plot to zero conversion

gives a positive y-intercept, then the product is primary for it has a non-zero initial selectivity. An intercept of zero indicates that the product is secondary, tertiary, etc. [9]. Figure 6.4 shows first-rank Delplots for all the products at 270 °C. All product yields were normalized by dividing by the carbon balance prior to making the Delplots because even small deviations of the carbon balance from 100% can lead to erroneous conclusions from the Delplots. It is clear in Figure 6.4 that neophytadiene and isophytol have positive intercepts and are primary products. The intercepts are both about 0.5, which indicates nearly equal initial selectivities to the two major products. The initial selectivities (i.e., y-intercepts on the Delplot) for phytone, pristene, phytene, and dihydrophytol are all low, and there is enough scatter in the data that, we cannot conclusively determine whether these are primary or non-primary products.

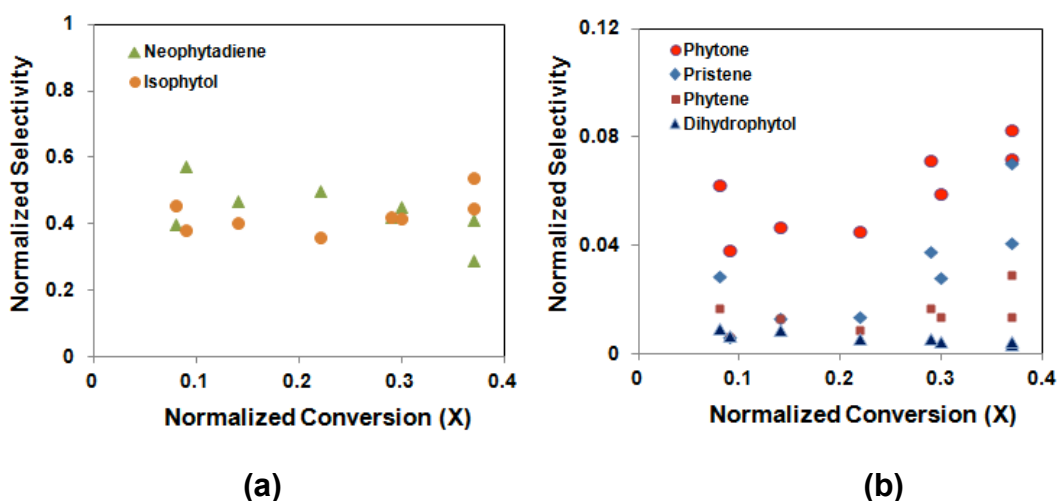


Figure 6.4 First-rank Delplot at 270 °C for different products. a) Neophytadiene and isophytol b) Phytone, pristene, phytene, and dihydrophytol

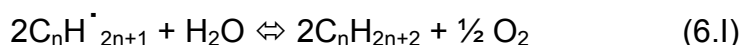
The Delplot analysis showed that the major products (neophytadiene and isophytol) form via parallel primary pathways as phytol reacts in and with HTW. Neophytadiene can be obtained via dehydration of phytol, and there is ample precedent for alcohol dehydration in HTW [1, 10-12]. Even though water is a product of dehydration, complete conversion of alcohols to alkenes can be achieved in HTW [1, 10]. Commonly established mechanisms for alcohol dehydration are E1cB, E1, and E2 [1]. These notations stand for elimination (“E”)

with a rate-limiting step that is either unimolecular (“1”) or bimolecular (“2”). Depending on the reaction conditions used, a given alcohol can undergo dehydration by any one of these mechanisms. E1cB is a special type of elimination reaction involving carbanions. Typically, the E1cB mechanism proceeds in the presence of a strong base and a weak acid, via a carbanion intermediate, which is formed when the base abstracts a proton from the β -carbon. The E1 mechanism occurs in the presence of a strong acid and a weak base, primarily via a carbocation intermediate formed by the loss of a protonated hydroxyl group ($-\text{OH}_2^+$). The E2 mechanism involves β -elimination in which the proton on the β -carbon and the hydroxyl group are eliminated in a concerted fashion [1, 13]. In pure water, E1cB is highly unlikely since no base is present that is strong enough to abstract a proton from the carbon backbone [1]. Therefore, with H_3O^+ from water being the catalyst, E1 and E2 mechanisms are the most likely candidates for phytol dehydration to neophytadiene in pure HTW.

Rotani *et al.* mention that isophytol can be obtained from biodegradation of phytol through an allylic rearrangement [14]. Brooks and Maxwell discuss a similar allylic rearrangement in their study on phytol during the acidic hydrolysis of sediments [15]. It is possible that allylic rearrangement also occurs in HTW to produce isophytol. Evidence of a similar allylic rearrangement exists for 2-methyl-3-buten-2-ol in supercritical water (SCW) and HTW, as confirmed through in situ IR measurements [16].

Though the Delplot analysis was inconclusive for dihydrophytol, a consideration of the likely formation pathways suggests that it is a primary product formed through the saturation of the double bond in phytol. The formation of phytone as a product from phytol is reasonable, since the literature [17-20] includes previous accounts of alcohols forming ketones in SCW. For instance, Moriya and Enomoto’s study related to cracking of polyethylene in SCW at 425 °C and 120 min showed that 2-propanol, 2-butanol, and 2-pentanol (products of SCW cracking of polyethylene) could oxidize to form 2-propanone, 2-butanone, and 2-pentanone, respectively [17]. Leif and Simoneit [19, 20] have

also shown aliphatic ketones to form via oxidation of alcohols under the hydrous pyrolysis conditions (350 °C and 72 hours). Lewan [21] mentions that water at high temperatures can furnish the oxygen required for oxidation of alcohols through different mechanisms. One source of oxygen could be the abundant OH⁻ ions present in the system due to the heterolytic dissociation of water into H⁺ and OH⁻ ions at high temperatures. A second source, molecular oxygen, could be produced by the reaction of water with an alkyl radical (generated in HTW), as shown in the reaction below [21]. This reaction is thermodynamically favorable and has been demonstrated experimentally by converting ethene to ethane in aqueous solutions at 325 °C and 35 MPa [22]. The molecular oxygen is highly reactive and can oxidize the alcohol to the corresponding aldehyde or ketone.



Previous work on phytol degradation, though done with reagents very different from the present study (marine bacteria [23] and natural sediments [14, 24-26]) and much lower temperature ranges, suggests a possible mechanism for the formation of phytone from phytol. Phytlenals (C_{20:1} aldehydes) can form by oxidation of phytol in the presence of water. Water can then add across the activated double bonds of these compounds through Michael addition. The resulting β-aldol can undergo a retro-aldolization reaction forming phytone, after the elimination of acetaldehyde.

The formation of pristene during phytol reaction in HTW could be via thermal or hydrothermal reactions. In their study of thermocatalytic and thermal degradation (without catalyst) of phytol at 60 °C over a period of 4 days, de Leeuw *et al.* explained the formation of pristene isomers as a two step process [27]. Initially, double bond isomerization occurs in the phytol molecule leading to an isomerized intermediate, which in a second step loses formaldehyde via intramolecular rearrangement to form pristene (see Figure 6.5). The hydrothermal path would be via decarboxylation of a phytenic acid intermediate. We did not observe phytenic acid, but organic acids can form in SCW, even from

hydrocarbons [17]. Moreover, previous studies of phytol degradation have reported phytanic acid as a product [14, 23, 25-27].

Phytene could form either through dehydration of dihydrophytol or the saturation of a double bond of neophytadiene. Akiya and Savage, Leif and Simoneit, and Lewan list a number of ways in which HTW could furnish the hydrogen required for saturation of the double bond [18, 20, 22]. There is abundant H^+ concentration from the heterolytic dissociation of water at elevated temperatures due to an increased ionic product of water at high temperatures [22]. Secondly, oxidation of alcohols to aldehyde intermediates and eventually to ketones will provide reducing power by liberating hydrogen [17, 18, 20]. Hydrogen can also be released during the decarboxylation of phytanic acid to pristene, as is seen during the decarboxylation of other acids [18]. Leif and Simoneit [20] demonstrated the formation of alkanes from corresponding alkenes during the hydrous pyrolysis of shale at 350 °C and attributed the hydrogen source to one of the aforementioned pathways. Based on this literature, there are numerous ways to furnish hydrogen and hydrogenated double bonds in the present reaction system. Phytene could undergo double-bond isomerization to form 1-phytene and 2-phytene isomers [27]. Double bond isomerization of alkenes is common in HTW as has been demonstrated by Leif and Simoneit [20]. Phytene can subsequently saturate its double bonds to form phytane.

As previously mentioned, the longer batch holding times resulted in a decrease in the yields of neophytadiene and isophytol. A pathway for isophytol disappearance is dehydration, to give an isomer of neophytadiene. As noted above, a pathway for neophytadiene disappearance is saturation, to form phytene and subsequently phytane. The yields of these products are low, however, so another pathway likely predominates. The diene could undergo oligomerization, perhaps via Diels-Alder reaction. We detected several dimers and trimers when we analyzed the samples from the more severe conditions using high-temperature GC. Evidence for oligomerization (dimers and trimers up to m/z of 860) has also been reported before [27].

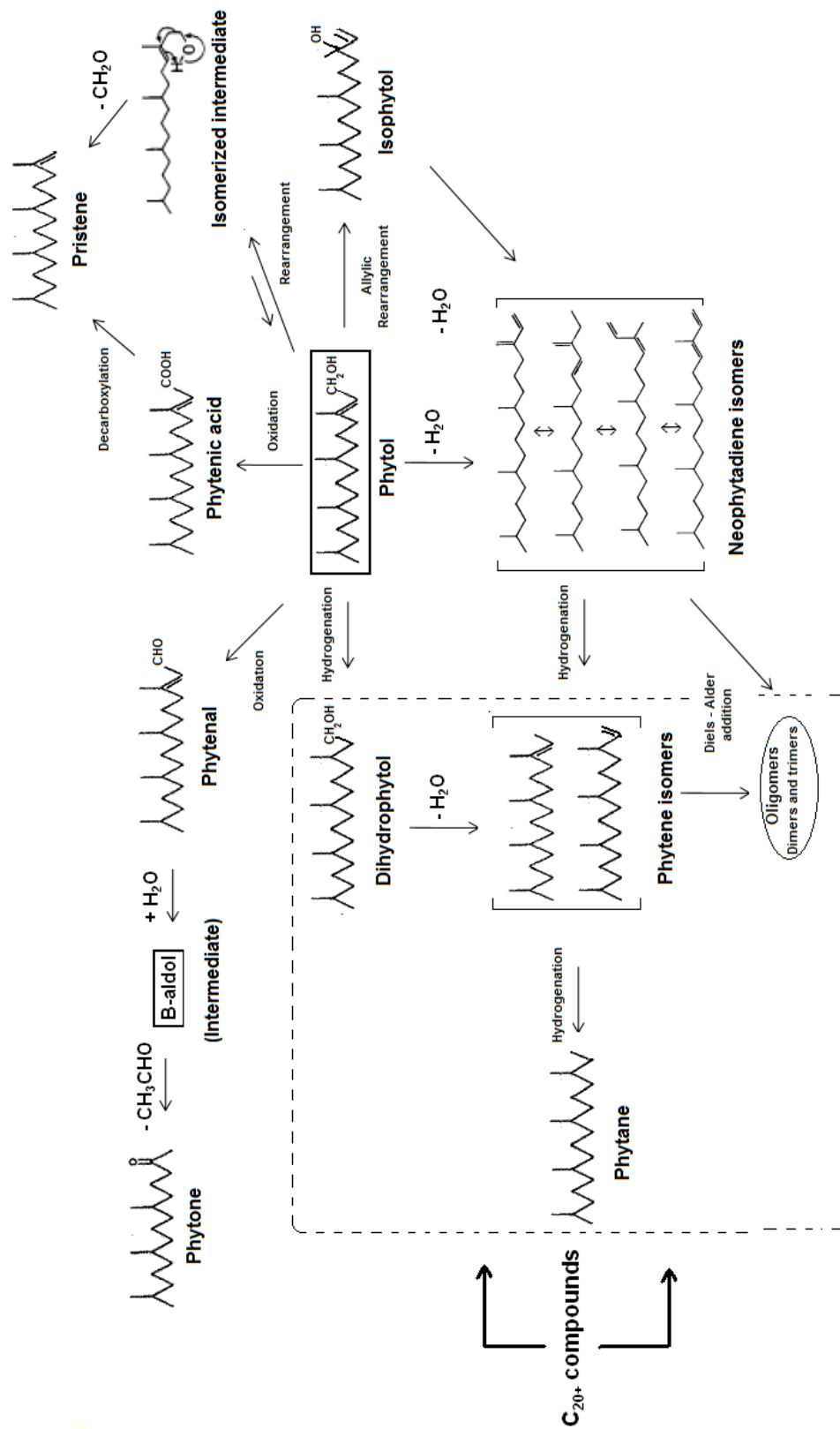


Figure 6.5 Reaction network for phytol in HTW

We propose the reaction network in Figure 6.5 to describe the reactions of phytol in HTW. The reaction chemistries include oxidation, hydrogenation, decarboxylation, isomerization, oligomerization, and allylic rearrangement, all of which have been previously documented in HTW.

6.5 Kinetic Model

The reaction network in Figure 6.5 provides details about the different pathways and likely intermediates. Our focus now turns to modeling the reaction network, and several simplifications can be made prior to construction of a quantitative kinetic model. We lump dihydrophytol, phytene, phytane, and oligomers together as C_{20+} products. We did not observe potential intermediates like phytenal, β -aldol, or phytenic acid in the experiments, so we do not include these in the simplified reaction network. The minor products, phytone and pristene, that we observed are assumed to form directly from phytol. Since we obtained almost complete conversion of phytol as seen in Table 6.2, we assume all reactions to be irreversible under the conditions investigated. Figure 6.6 shows the simplified reaction network considered for the purpose of modeling.

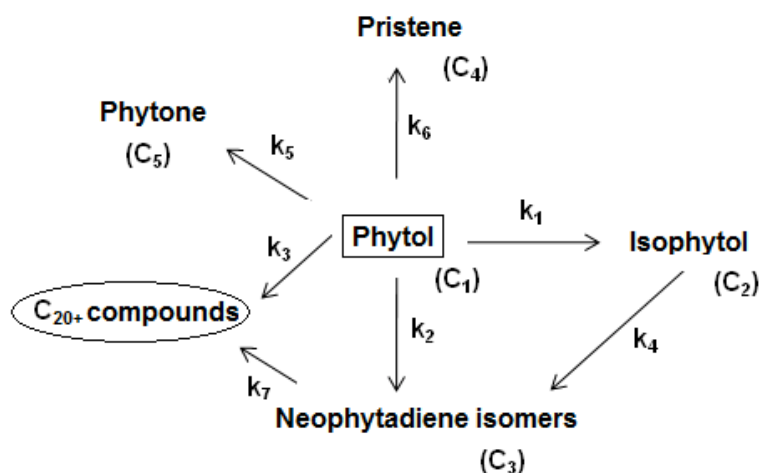


Figure 6.6 Simplified reaction network for kinetic modeling of phytol in HTW

Having proposed a simplified network for the reactions of phytol in HTW, we next constructed a chemical kinetics model based on this reaction network. All reactions in the network were assumed to proceed through first order kinetics. The model equations, which apply to reactions in a constant-volume batch reactor, are given in Eq. (6.1) – Eq. (6.5), where, C_1 – C_5 represent concentrations of phytol, isophytol, neophytadiene, pristene, and phytone respectively.

$$\frac{dC_1}{dt} = -(k_1 + k_2 + k_3 + k_5 + k_6)C_1 \quad (6.1)$$

$$\frac{dC_2}{dt} = k_1C_1 - k_4C_2 \quad (6.2)$$

$$\frac{dC_3}{dt} = k_2C_1 + k_4C_2 - k_7C_3 \quad (6.3)$$

$$\frac{dC_4}{dt} = k_6C_1 \quad (6.4)$$

$$\frac{dC_5}{dt} = k_5C_1 \quad (6.5)$$

We used the commercial modeling package MATLAB 2010 to solve simultaneously the set of ordinary differential equations and perform parameter estimation to obtain the values of the rate constants at each temperature. We used *fmincon* to perform the optimization using the *optimtool* GUI. The minimization algorithm uses a sequential quadratic programming active set optimization method [28]. The residual for minimization was calculated as the summation of squared relative errors (SSRE) between the calculated and experimental product concentrations. This quantity was calculated using Eq. (6.7) for data sets at each temperature shown in Table 6.2, where, j is the number of discrete reaction times at a particular temperature and i is the number of components.

$$SSRE = \sum_j \sum_{i=1}^5 \left[\frac{C_{j,i,model} - C_{j,i,exp}}{(C_{j,i,model} + C_{j,i,exp}) / 2} \right]^2 \quad (6.7)$$

Optimization was done at each temperature independently (240, 270, 300, and 350 °C) using the residual at that temperature (Eq.(6.7)) as the objective function. The rate constants at each temperature were then fit to the linearized form of the Arrhenius equation to get determine A_i and E_{a_i} and their associated standard errors for each rate constant.

Table 6.5 Arrhenius parameters for phytol reaction network

Index No.	A_o (min^{-1})	E_a (kJ/mol)	$k_{240 \text{ °C}}$ (min^{-1})
1	$10^{10.3 \pm 1.3}$	134 ± 13	4.62E-04
2	$10^{14.2 \pm 1.1}$	173 ± 11	3.56E-04
3	$10^{38.1 \pm 8.7}$	528 ± 93	1.75E-16
4	$10^{11.2 \pm 1.9}$	139 ± 20	1.14E-03
5	$10^{13.4 \pm 0.6}$	176 ± 6	3.06E-05
6	$10^{12.4 \pm 0.3}$	171 ± 4	8.66E-06
7	$10^{11.1 \pm 2.7}$	137 ± 29	1.21E-03

Table 6.5 displays the Arrhenius parameters that provided the best description of the experimental data. It also displays the values of the rate constants at 240 °C so that the relative rates of the different pathways can be easily discerned. The rate constants k_1 and k_2 are of comparable magnitude, indicating that dehydration of phytol to neophytadiene and its isomerization to isophytol occur with similar rates. The rate constant k_3 is negligible in all cases, i.e. the path to C_{20+} product formation from phytol has a very low rate. For all practical purposes, this pathway can be eliminated from the reaction network. The parameters were re-estimated without including k_3 . The optimization led to no significant changes in the values of the other parameters, indicating that the model is not sensitive to k_3 . The rate constants for the conversion of isophytol and neophytadiene to secondary products, i.e. k_4 and k_7 , are always the largest

and they exceed the rate constants for formation of these major products. The sum of rate constants k_1 , k_2 , k_3 , k_5 and k_6 at any temperature is of similar magnitude to the rate constant obtained from the slopes in Figure 6.3, assuming an overall pseudo-first order depletion of phytol at that temperature. This result shows that both sets of rate constants are consistent. For instance, the sum of these rate constants at 240 °C obtained from the model is $8.57 \times 10^{-4} \text{ min}^{-1}$, which is the same as that displayed in Table 6.4. The sum of the rate constants from the model at 350 °C is 0.64 min^{-1} , which is comparable to the value of 0.29 min^{-1} in Table 6.4. These values differ because different objective functions were used in their determination. The rate constants in Table 6.4 were obtained by considering solely the phytol conversion data, whereas the rate constants in Table 6.5 were obtained by considering the data for the yields of all of the reaction products, in addition to the phytol conversion data.

Figure 6.7 shows the calculated and experimental concentrations for phytol, isophytol, neophytadiene, pristene, and phytone. The parameters in Table 6.5 were used to calculate the concentrations of the reactant and products from the model. The model accurately describes the trends in the data and typically estimates the concentrations of the reactant and product within experimental errors.

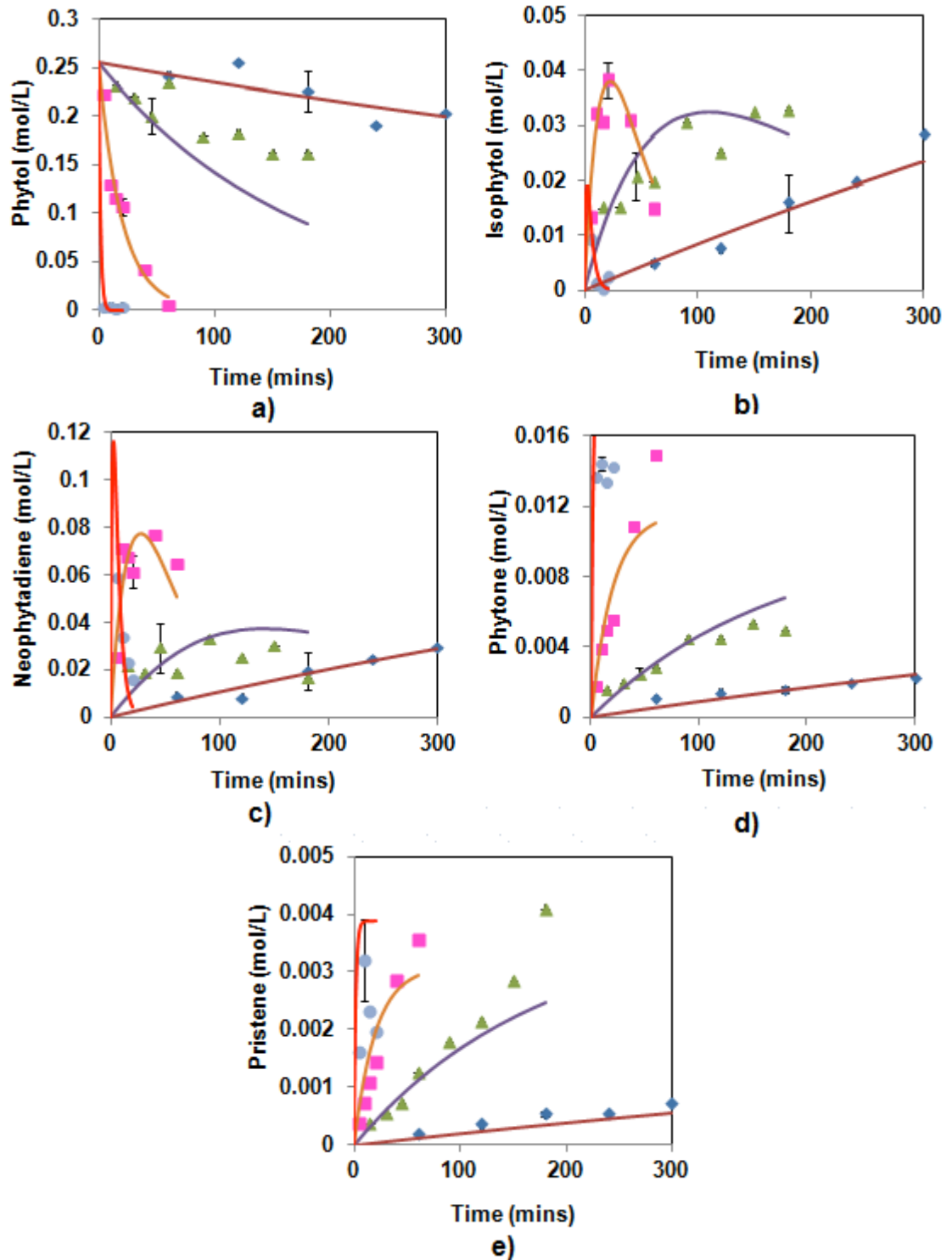


Figure 6.7 Comparison of experiment (discrete points) and model results (smooth curves) for reactant and product concentrations at different conditions. a) phytol, b) isophytol, c) neophytadiene, d) phytone, and e) pristene at \blacklozenge 240° C, \blacktriangle 270° C, \blacklozenge 300° C, and \bullet 350° C

Figure 6.8 shows a parity plot of the experimental and model-calculated concentrations for all species at all conditions. There is good agreement of the model with the data, given the experimental uncertainty. The data are scattered on both sides of the diagonal line, indicating the absence of systematic errors in the data fitting.

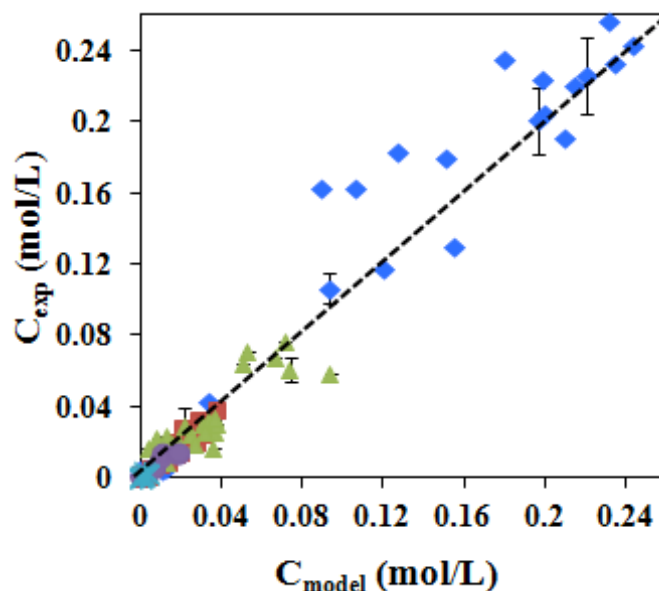


Figure 6.8 Parity plot between experimental and model concentration for reactant and products. Legends are ♦ phytol, ▲ isophytol, ■ neophytadiene, ● phytone, and * pristene at 240° C, 270° C, 300° C, and 350° C

6.6 Conclusions

Under the conditions studied, phytol readily underwent dehydration to form neophytadiene. In a parallel pathway, phytol underwent allylic rearrangement to form isophytol. A number of minor products were also formed which include phytone, pristene, phytene, phytane, and dihydrophytol. Neophytadiene, phytene, and phytane are also products identified in crude bio-oil obtained from hydrothermal liquefaction of algae.

Phytol disappearance in HTW followed first-order kinetics. Furthermore, the yields of products increased gradually with increasing time and temperature, except for neophytadiene, isophytol, and dihydrophytol, which showed a

decrease in yields at higher temperatures and longer batch holding times. This observation suggests that they could undergo further reactions to form secondary products. Furthermore, the carbon balances were low at the most severe conditions, indicating that most of the products formed under these conditions were most likely oligomers.

We propose a reaction network based on the above observations and a Delplot analysis. In this network, neophytadiene, isophytol, dihydrophytol, pristene, and phytone can be obtained through parallel reactions of phytol in HTW. Isophytol can undergo dehydration to form neophytadiene. Similarly, neophytadiene could possibly form phytene, phytane, and oligomers at higher temperatures, lumped together as C_{20+} molecules. A phenomenological kinetics model based on the proposed network accurately describes the trends in the data and typically estimates the concentrations of the reactant and product within reasonable experimental errors. The rates for isophytol and neophytadiene formation are similar. The rate constant for dihydrophytol formation is very low, and the rate constants for neophytadiene and isophytol secondary reactions are the highest at all experimental conditions. Thus, we broadly elucidate through the study of phytol that many different types of reactions (e.g., dehydration, reduction, oxidation, allylic rearrangement and decarboxylation) likely occur during hydrothermal liquefaction of algae. Each of these steps can be explored at a mechanistic level to better understand these reactions in HTW.

References

- [1] N. Akiya, P. E. Savage. Kinetics and mechanism of cyclohexanol dehydration in high-temperature water. *Ind. Eng. Chem. Res.* 40, 1822-1831, 2001
- [2] M. Blumer, D. W. Thomas. Phytadienes in zooplankton. *Science* 147, 1148, 1965
- [3] R. Hites. Phytadienes from the pyrolysis of Pheophytin a. *J. Org. Chem.* 39 (17), 2634-2635, 1974
- [4] T. M. Brown, P. Duan, P. E. Savage. Hydrothermal liquefaction and gasification of *Nannochloropsis* sp. *Energy Fuels* 24 (6), 3639-3646, 2010
- [5] P. Valdez, J. G. Dickinson, P. E. Savage. Characterization of product fractions from hydrothermal liquefaction of *Nannochloropsis* sp. and the influence of solvents. *Energy Fuels* 25, 3235-3243, 2011
- [6] Y. J. Bae, C. Ryu, J. Jong-Ki, J. Park, D. J. Suh, Y. W. Suh, D. Chang, P. Young-Kwon. The characteristics of bio-oil produced from the pyrolysis of three marine macroalgae. *Bioresour. Technol.* 102, 3512-3520, 2011
- [7] P. Duan, P. E. Savage. Hydrothermal liquefaction of a macroalga with heterogeneous catalysts. *Ind. Eng. Chem. Res.* 50(1), 52-61, 2011
- [8] D. Zhou, L. Zhang, S. Zhang, H. Fu, J. Chen. Hydrothermal liquefaction of macroalgae *Enteromorpha prolifera* to bio-oil. *Energy Fuels* 24, 4054-4061, 2010
- [9] N. Bhore, M. Klein. The Delplot technique: A new method for reaction pathways analysis. *Ind. Eng. Chem. Res.* 29, 313-316, 1990
- [10] X. Xu, M. J. Antal. Mechanism and temperature-dependent kinetics of the dehydration of *tert*-butyl alcohol in hot compressed liquid water. *Ind. Eng. Chem. Res.* 36 (1), 23-41, 1997

- [11] S. E. Hunter, C. E. Ehrenberger, P. E. Savage. Kinetics and mechanism of tetrahydrofuran synthesis via 1,4-butanediol dehydration in high-temperature water. *J. Org. Chem.* 71, 6229-6239, 2006
- [12] P. E. Savage. Organic chemical reactions in supercritical water. *Chem. Rev.* 99, 603-621, 1999
- [13] E. Uggerud, L. Bache-Andreassen. Theoretical models and experimental data for reactions between water and protonated alcohols: Substitution and elimination mechanisms. *Chemistry – A European Journal* 5, 1917-1930, 1999
- [14] J. F. Rotani, P. C. Bonin, J. K. Volkman. Biodegradation of free phytol by bacterial communities isolated from marine sediments under aerobic and denitrifying conditions. *Appl. Environ. Microbiol.* 65(12), 5484-5492, 1999
- [15] P. W. Brooks, J. R. Maxwell. Early stage fate of phytol in a recently-deposited lacustrine sediment, in: B. Tissot, F. Biennet (Eds.). *Advances in Organic Geochemistry* 1973, Technip, Paris, France, 977-991. 1974
- [16] M. Sato, Y. Ikushima, K. Hatakeda, R. Zhang. Applications of environmentally benign supercritical water to organic syntheses. *Anal. Sci.* 22, 1409-1416, 2006
- [17] T. Moriya, H. Enomoto. Characteristics of polyethylene cracking in supercritical water compared to thermal cracking. *Polym. Degrad. Stab.* 65, 373-386, 1999
- [18] N. Akiya, P. E. Savage. Roles of water for chemical reactions in high-temperature water. *Chem. Rev.* 102, 2725-2750, 2002
- [19] R. N. Leif, B. R. T. Simoneit. Ketones in hydrothermal petroleum and sediment extracts from Guaymas Basin, Gulf of California. *Org. Geochem.* 23 (10), 889-904, 1995
- [20] R. N. Leif, B. R. T. Simoneit. The role of alkenes produced during hydrous pyrolysis of a shale. *Org. Geochem.* 31, 1189-1208, 2000

- [21] M. D. Lewan. Experiments on the role of water in petroleum formation. *Geochim. Cosmochim. Acta* 61 (17), 3691-3723, 1997
- [22] J. S. Seewald. Evidence for metastable equilibrium between hydrocarbons under hydrothermal conditions. *Nature* 370, 285-287, 1994
- [23] F. T. Gillian, P. D. Nichols, R. B. Johns, H. Bavor. Phytol degradation by marine bacteria. *Appl. Environ. Microbiol.* 45 (5), 1423-1428, 1983
- [24] J. F. Rotani, M. Acquaviva. The aerobic bacterial metabolism of phytol in seawater: Temperature dependence of an abiotic intermediate step and its consequences. *Chemosphere* 26 (8), 1513-1525, 1993
- [25] J. F. Rotani, I. Combe, P. Giral. Abiotic degradation of free phytol in the water column: A new pathway for the production of acyclic isoprenoids in the marine environment. *Geochim. Cosmochim. Acta* 54, 1307-1313, 1990
- [26] J. F. Rotani, G. Bailet. Production of acyclic isprenoid compounds during the photodegradation of chlorophyll-a in seawater. *J. Photochem. Photobiol., A* 59, 369-377, 1991
- [27] J. W. De Leeuw, V. A. Correa, P. A. Schenck. On the decomposition of phytol under simulated geological conditions and in the top-layer of natural sediments, in: B. Tissot and F. Bienner (Eds.) *Advances in Organic Geochemistry*, Technip, Paris, France, 993-1004, 1974
- [28] <http://www.mathworks.com/help/toolbox/optim/ug/fmincon.html>. Date last accessed, 3rd September 2011

CHAPTER 7

Behavior of DOPC in HTW

In this chapter we explore the behavior of a model phospholipid (DOPC) in HTW. We first describe the preliminary work that was done to validate the experimental methods. We then report the effect of temperature, batch holding time, and initial addition of the products (oleic acid and phosphoric acid) on the conversion of DOPC. Next, we develop a quantitative phenomenological kinetics model to fit the experimental observations. We elaborate on the chemistry of the reaction of DOPC in HTW and propose a reaction network that is consistent with the experimental data.

7.1 Control Experiment

A control experiment (as mentioned in 3.3.4) was done to assess our ability to measure accurately the amount of DOPC in the reactor. This experiment, which was essentially a run performed at room temperature, gave a DOPC recovery of 98%, thereby verifying the suitability of the methods used for quantifying the amount of DOPC.

7.2 Effect of Reaction Conditions

7.2.1 Temperature and Batch Holding Time on DOPC Conversion

In this section, we present the results for the effects of temperature and batch holding time on the conversion of DOPC. Figure 7.1 shows the NMR spectrum of a sample from reaction of DOPC at 200 °C and 60 min along with the identities of several products. We have positive identification for peaks 1 – 4,

but we were not able to identify with certainty the compounds corresponding to peaks 5 – 7 due to lack of authentic compounds as standards. As will be discussed later in this section, using the yields of these products and knowledge of likely pathways from the literature, we tentatively identified peaks 5, 6, and 7.

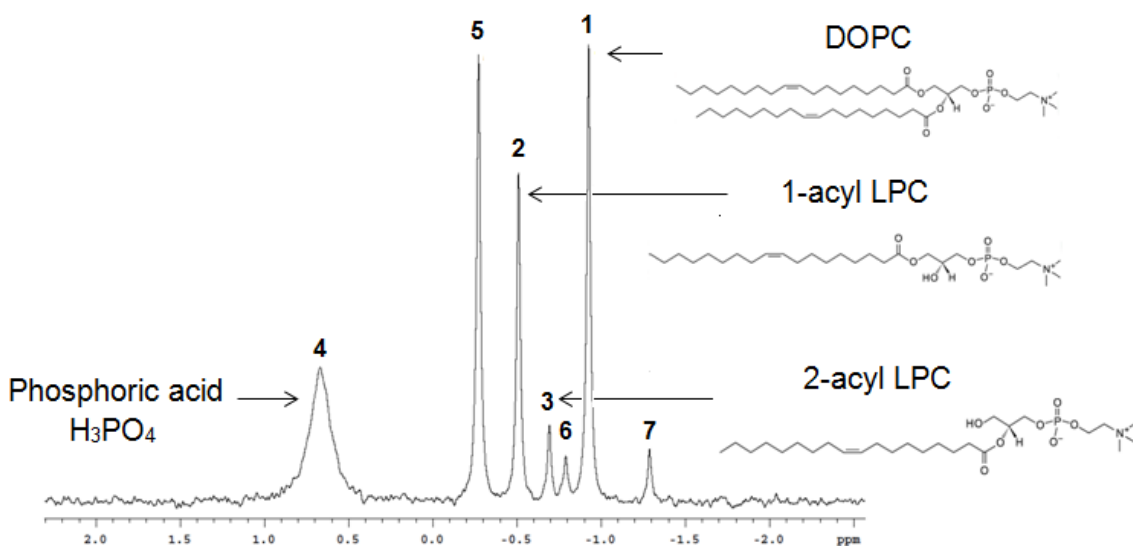


Figure 7.1 ^{31}P NMR spectrum of products from DOPC reaction at 200 °C and 60 min

Table 7.1 presents the product molar yields and DOPC conversion at different times and temperatures. The mean carbon balance was $90 \pm 15\%$. We expect the carbon balance to be below 100% since we have not quantified some of the carbon-containing products, such as glycerol and choline. The mean phosphorus balance was $95 \pm 15\%$, indicating that all of the phosphorus-containing compounds were identified and quantified.

Table 7.1 Conversion and molar yield of products for DOPC in HTW

Temp (°C)	Time (min)	DOPC C _{0,ini} (mol/L)	DOPC Conversion	1-acyl LPC Yield	2-acyl LPC Yield	H ₃ PO ₄ Yield	Peak 5 Yield	Peak 6 Yield	Peak 7 Yield	OA Yield	OPE Yield	C-Balance (%)	P-Balance (%)
175	30	0.071 ± 0.002	0.05 ± 0.04	0.08 ± 0.04	0.02 ± 0.007	0	0.01 ± 0.01	0	0	0.11 ± 0.05	0.01 ± 0.005	106 ± 4	106 ± 4
	60	0.067	0.14	0.16	0.03	0	0.03	0	0	0.3	0.04	112	109
	90	0.067	0.36	0.25	0.04	0	0.08	0	0.016	0.58	0.06	109	103
200	120	0.068	0.67	0.22	0.03	0.03	0.18	0.006	0.024	0.76	0.07	85	81
	150	0.067	0.85	0.13	0.02	0.13	0.30	0.023	0.014	1.08	0.12	78	78
	15	0.068	0.10	0.08	0.02	0	0	0	0	0.13	0.02	102	100
225	30	0.069	0.31	0.20	0.05	0	0.05	0	0.009	0.41	0.03	103	100
	45	0.067 ± 0.001	0.67 ± 0.03	0.18 ± 0.02	0.04 ± 0.004	0.13 ± 0.01	0.13 ± 0.002	0.014 ± 0.004	0.02 ± 0.001	0.56 ± 0.08	0.04 ± 0.004	73 ± 7	84 ± 4
	60	0.067	0.82	0.13	0.03	0.27	0.19	0.022	0.021	0.82	0.08	68	88
350	90	0.067	0.94	0.04	0.01	0.60	0.23	0.021	0.006	1.39	0.11	74	101
	15	0.068	0.36	0.19	0.04	0.15	0.06	0	0.019	0.48	0.04	99	109
	30	0.069	0.85	0.05	0.01	0.74	0.11	0.008	0.008	1.18	0.16	75	112
350	45	0.067 ± 0.001	0.97 ± 0.01	0.01 ± 0.003	0	0.94 ± 0.02	0.08 ± 0.005	0	0	1.39 ± 0.03	0.13 ± 0.02	67 ± 2	110 ± 2
	60	0.067	1	0	0	1.05	0.04	0	0	1.7	0.09	75	112
	90	0.069	1	0	0	1.18	0	0	0	1.91	0.03	80	110
350	15	0.069	1	0	0	0.94	0	0	0	2.00	0	82	94
	30	0.068	1	0	0	0.90	0	0	0	1.91	0	78	90
	45	0.068	1	0	0	0.92	0	0	0	2.00	0	82	92
	60	0.070	1	0	0	1.04	0	0	0	1.97	0	81	104

1-Acyl LPC was the major phosphorus-containing product at short batch holding times. Smaller amounts of 2-acyl LPC also formed. The yields of 1-acyl LPC at the two lower temperatures initially increased with increasing batch holding time, reached a maximum value, and then decreased. This behavior suggests that 1-acyl LPC decomposes to secondary products under the more severe reaction conditions. The yields of 2-acyl LPC were low (< 0.05) at all conditions, but they followed a trend similar to that of 1-acyl LPC. That is, the yield of 2-acyl LPC initially increased and then subsequently decreased at longer batch holding times and higher temperatures.

Phosphoric acid was not observed at the mildest reaction conditions, but once formed, its yield rapidly increased. It became the major phosphorus-containing product at higher temperature or longer batch holding time. Yields of essentially unity were obtained at the most severe conditions, indicating that phosphoric acid is the ultimate phosphorus-containing product from the hydrolysis of DOPC.

Oleic acid, the fatty acid obtained via the hydrolysis of DOPC, was always the product formed in highest yield. The yield of oleic acid increased steadily with time at all temperatures. The molar yields of oleic acid may exceed unity because one mole of DOPC can produce two moles of oleic acid. At 350 °C, this stoichiometric yield of oleic acid of two was obtained, indicating that this fatty acid was another end product of the hydrolysis of DOPC.

An ester of oleic acid and glycerol was another non-phosphorus-containing product that was quantified. The yield of the 9-octadecenoic-2,3-dihydroxypropyl ester (OPE) increased steadily with time at 175 and 200 °C. At 225 °C, however, the yield of OPE first increased from 0.04 at 15 min to 0.13 at 45 min and then decreased to 0.03 at 90 min, indicating secondary decomposition of OPE. No OPE was detected at 350 °C.

Of the three tentatively identified NMR peaks (peak 5, 6, and 7 in Figure 7.1), the molar yield of peak 5 is the highest at all conditions. The yields of the

products corresponding to peaks 5 and 6 responded to time and temperature very much like the yield of OPE. These yields increased with an increase in the batch holding time at 175 and 200 °C, but at 225 °C they reached a maximum and then decreased to zero. Furthermore, the yield of peak 5 at the shortest time at any temperature is similar to the yield of OPE formed under similar conditions. This observation of peak 5 being formed nearly in a molar equivalence to OPE and the formation of OPE requiring the co-formation of a P-containing co-product, suggests that peak 5 could possibly be this co-product. We speculate that peak 5 corresponds to phosphorylcholine, which is the P-containing compound that would be formed along with OPE, as will be described in the section 7.3. Phosphorylcholine has been observed previously during the acidic hydrolysis of DOPC [1]. The yield of peak 5 does not remain equal to that of OPE at higher temperatures or longer batch holding times. Rather, its yield exceeds that of OPE at the more severe conditions, even before the yield of OPE begins to decrease. This behavior indicates that if peak 5 is indeed phosphorylcholine, then as the batch holding time increases at 175 and 200 °C, there is also another pathway forming phosphorylcholine. As will be shown in the section 7.3, phosphorylcholine can indeed be formed through a parallel reaction involving hydrolysis of the LPC isomers. Furthermore, at a higher temperature of 225 °C, the yield of peak 5 is lower than OPE indicating that if this peak corresponds to phosphorylcholine, then the decomposition of phosphorylcholine is faster than that of OPE. Note that we could not obtain a pure standard of phosphorylcholine to confirm its identity.

The other phosphorus products that could appear as peak 6 and 7 could be cyclic glycerophosphates or α - and β - glycerophosphates, or glycerophosphoric acid, as has been suggested previously [1]. Once again these compounds were not available in their pure form, which prohibited their positive identification by NMR. For the unidentified peak 7, its yield increased and then decreased at all temperatures.

The conversion of DOPC was below 40% at mild conditions. Near complete conversion was observed at 225 °C (> 60 min) and at all batch holding times at 350 °C. Moreover, a plot of DOPC conversion against the batch holding time displays a sigmoidal behavior (Figure 7.2), i.e. the conversion increases slowly at shorter batch holding time and then rapidly increases. This behavior is associated with an autocatalytic system and is similar to the behavior observed previously for hydrolysis of ethyl oleate in HTW (chapter 4) and hydrolysis of triglycerides in sunflower oil [2].

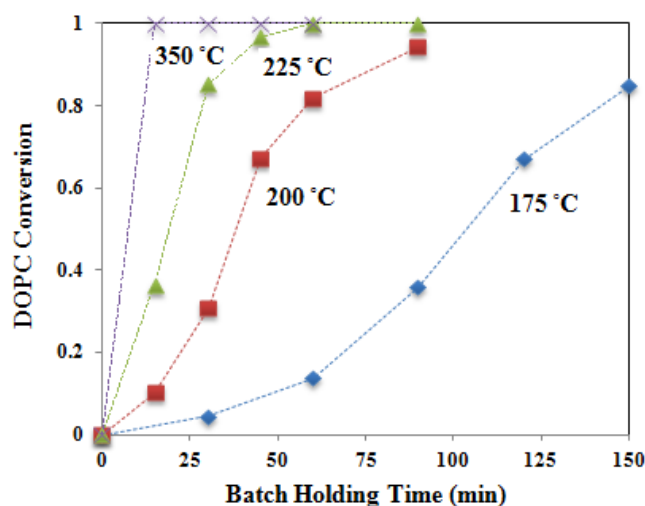


Figure 7.2 Temporal variation of DOPC conversion

7.2.2 Effect of Initial Addition of Oleic Acid and Phosphoric Acid

In the system under consideration, DOPC hydrolysis can likely be catalyzed by oleic acid and by phosphoric acid, as these compounds form during the course of the reaction. To test for catalysis by these acids, we carried out hydrolysis of DOPC at 200 °C and 15 min with different amounts of added oleic acid (equimolar) and phosphoric acid (one and a half times molar concentration of DOPC). Table 7.2 shows that both the conversion of DOPC and the yield of oleic acid increased in presence of added acids. Therefore, hydrolysis of DOPC is catalyzed by the oleic acid and phosphoric acid produced during the reaction.

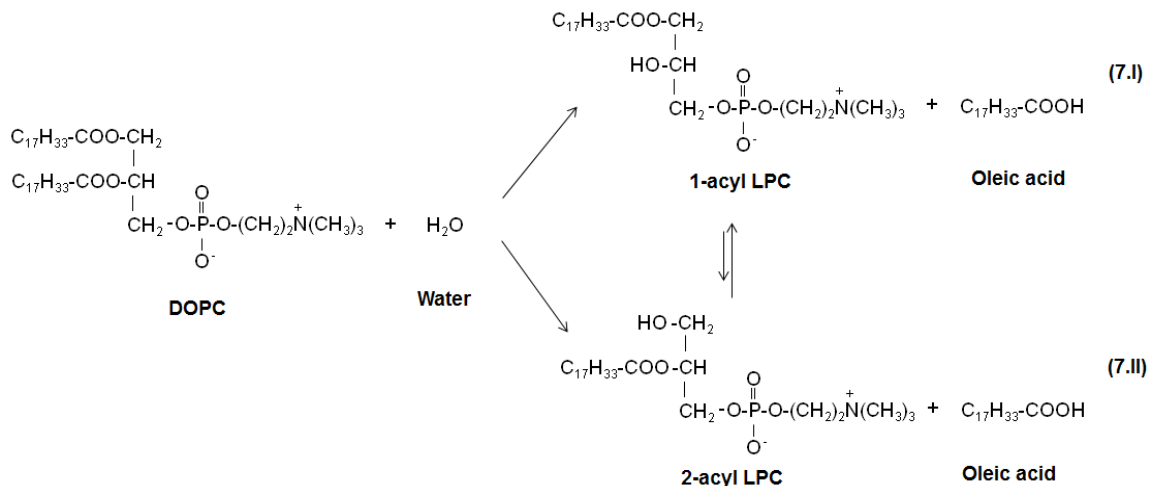
Table 7.2 Conversion of DOPC and yield of oleic acid with and without added acid at 200 °C and 15 min

Acid	DOPC Conversion	Oleic Acid Yield
None	0.10	0.13
Oleic	0.50	0.43
Phosphoric	1.00	1.31

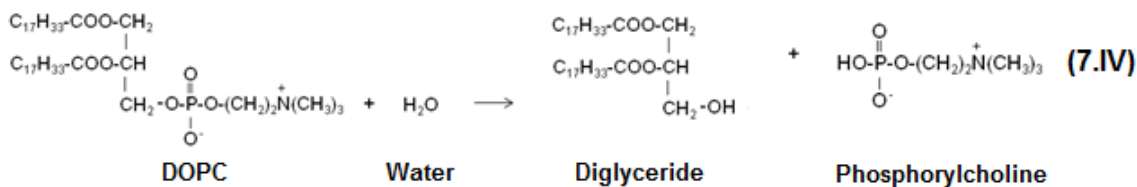
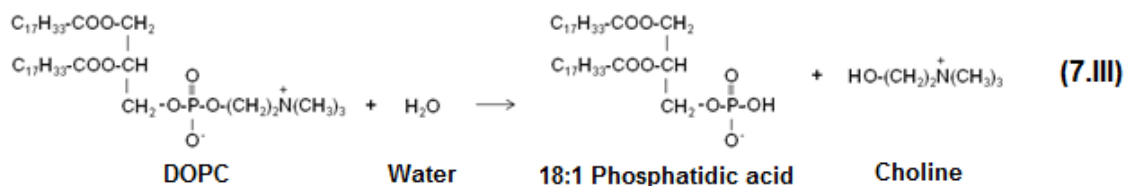
7.3 Reaction Pathways

Section 7.2.1 showed that hydrothermal treatment of DOPC produced a number of products. In this section, we elucidate more fully the reaction pathways for DOPC that lead to these products.

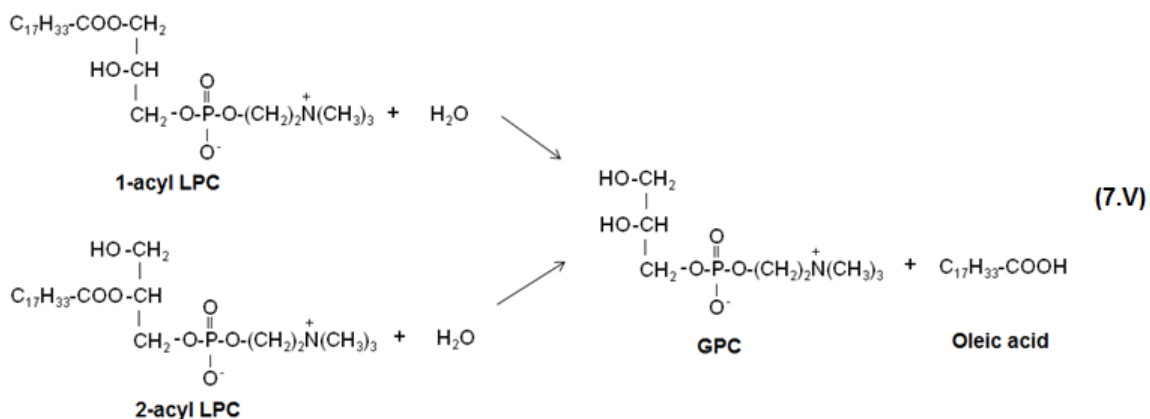
On the basis of the product yields discussed in the previous section, the main primary path for DOPC in HTW is hydrolytic cleavage of a fatty acid moiety linked to the glycerol backbone to form either 1- or 2-acyl LPC. This path has been mentioned previously in a number of studies on hydrolysis of phospholipids in liposomal dispersions at low temperature [1, 3-6]. 1-Acyl LPC is the major isomer observed in the present work, which is consistent with the results of Grit and coworkers [4-6]. Ester hydrolysis in HTW most commonly follows an Aac2 mechanism (mentioned in detail in chapter 4), wherein protonation of the ester is followed by a nucleophilic attack of water [7]. Formation of 1- and 2-acyl LPC by this mechanism would involve a secondary and primary carbocation, respectively. Since the secondary carbocation is more stable, 1-acyl LPC is expected to be the major product. Grit and Crommelin [6] also mention that 2-acyl LPC is rapidly converted to 1-acyl LPC via acyl migration. Hydrolysis of the ester linkages would release oleic acid, which could subsequently catalyze the further hydrolysis of DOPC. Shown below is the graphical representation of the primary paths for hydrolysis of DOPC.



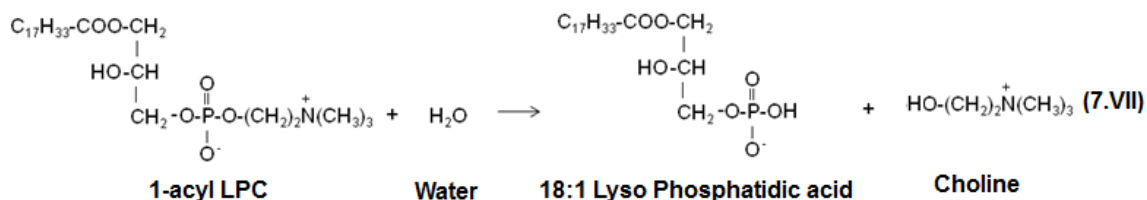
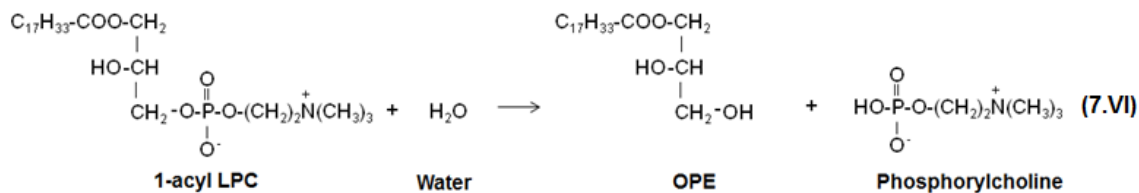
Note that no path is included for hydrolytic cleavage of the phosphorus-containing moiety. Two possible reactions could occur here depending on which phosphorus-oxygen bond was cleaved. Cleavage of the choline group would form a 18:1 phosphatidic acid (see reaction 7.III), but this product was not observed. The chemical shift of a pure 18:1 phosphatidic acid standard did not match any peak in the NMR spectrum shown in Figure 7.1. Another possibility is cleavage to form a diglyceride (see reaction 7.IV). We used high-temperature GC but did not detect the diglyceride that would necessarily form in such a path. The absence of the products shown in reactions 7.III and 7.IV indicates that these paths are negligible under the conditions of our investigation. Thus, we exclude these paths from further consideration.



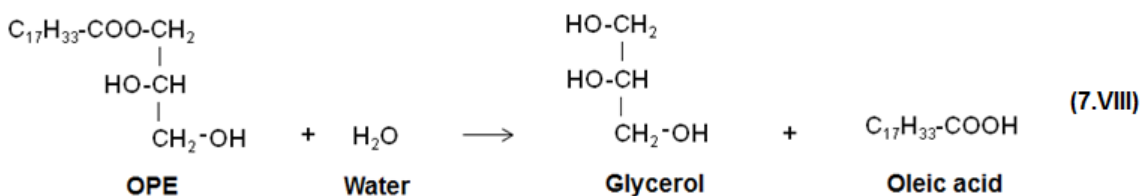
Following the formation of the LPC isomers in paths 7.I and 7.II, hydrolysis of the second fatty acid can take place to produce *sn*-glycerol-3-phosphorylcholine (GPC), as has been suggested in previous work at lower temperatures, see reaction 7.V [3, 6]. Since this step also involves hydrolysis of an ester bond, it could also be catalyzed by the fatty acid produced.



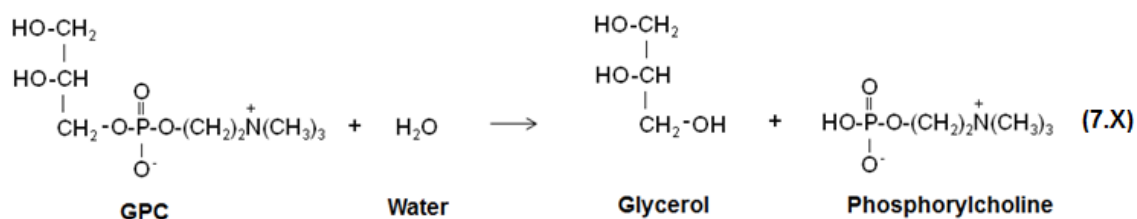
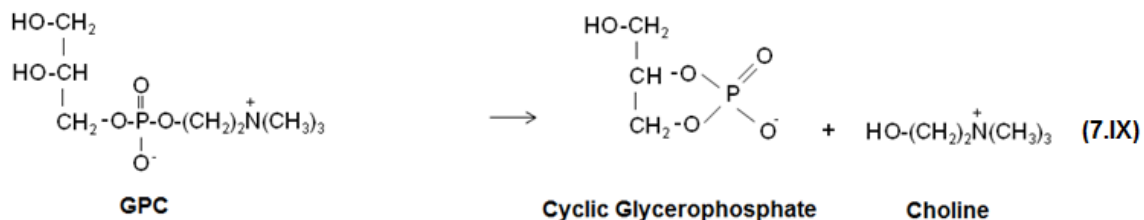
In parallel with the hydrolytic cleavage of the oleate moiety, LPC can also undergo hydrolysis at the phosphate bond in two different ways, similar to reactions 7.III and 7.IV. One possibility is that the 1-acyl LPC, being the major isomer, would form 9-octadecenoic-2,3-dihydroxypropyl ester (OPE) (reaction 7.VI), consistent with our observation of this compound as one of the reaction products. Phosphorylcholine would also be released as a co-product of this reaction. Alternatively, 1-acyl LPC could liberate choline and form 18:1 lyso-phosphatidic acid (see reaction 7.VII). However, none of the peaks in the NMR spectra corresponded to a pure standard of 18:1 lyso-phosphatidic acid. Therefore, reaction 7.VII seems unlikely under these conditions and has been excluded from further consideration.



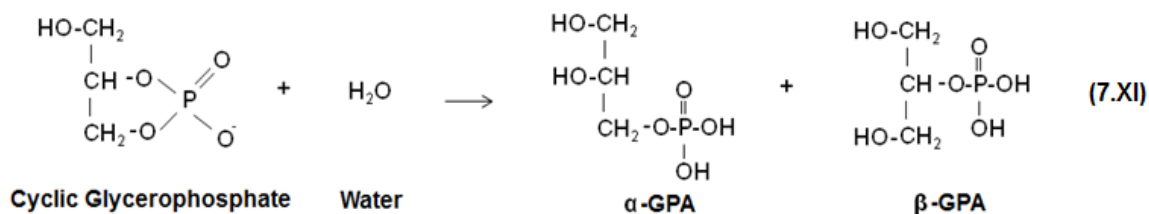
OPE, once formed in reaction 7.VI, can hydrolyze further to liberate glycerol and oleic acid as shown in reaction (7.VIII). Once again, OPE hydrolysis can be catalyzed by oleic acid and phosphoric acid.



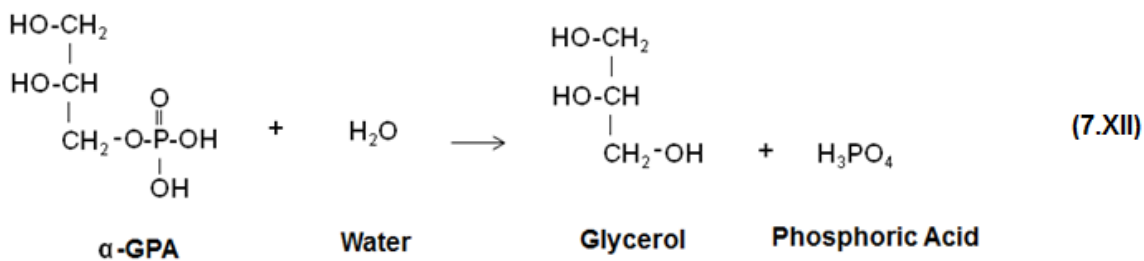
GPC, formed in path 7.V, could react at either of the two P-O bonds, giving rise to two parallel reactions [1, 8]. Protonation of the oxygen between the phosphorus atom and the choline moiety can occur via a cyclic ortho triester to form cyclic glycerophosphate and choline (reaction 7.IX). In a parallel reaction, protonation of oxygen between the glycerol carbon and phosphorus can occur to release glycerol and phosphorylcholine (reaction 7.X). Koning and McMullan mention that under acidic conditions, reaction 7.IX is favored over reaction 7.X, i.e. more cyclic glycerophosphate is formed than phosphorylcholine [1].



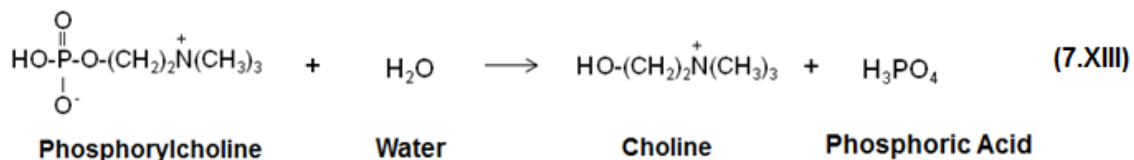
Cyclic glycerophosphate can be converted to an equilibrium mixture of α - and β -glycerophosphophate or glycerophosphoric acid (GPA), depending on the pH, as shown in reaction 7.XI. Usually the α -GPA is the major product [8, 9].



Glycerophosphate can further hydrolyze to release phosphoric acid and glycerol, both of which were observed as products in this investigation (reaction 7.XII).



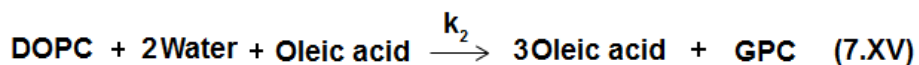
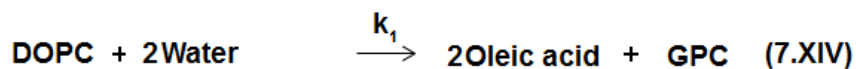
Lastly, phosphoric acid could also be formed via the hydrolysis of phosphorylcholine, see reaction 7.XIII. This reaction also liberates a choline molecule.



This section has summarized the different reaction pathways likely operative for the reaction of DOPC in HTW. We offer these pathways on the basis of the literature and the experimental results reported in the previous section. Other phospholipids could potentially undergo similar chemistry in HTW.

7.4 Phenomenological Autocatalytic Kinetics

In this section, we use the DOPC conversion data at 175, 200, and 225 °C as shown in Table 7.1 to develop a phenomenological model to explain the autocatalysis of DOPC disappearance. A simple model is proposed as shown below, in line with the previous autocatalytic model for ethyl oleate in HTW (chapter 4). Note that DOPC hydrolysis is treated as an overall reaction that produces GPC and oleic acid. Catalysis solely occurs by oleic acid.



Reaction 7.XIV is uncatalyzed hydrolysis of DOPC to produce fatty acid and GPC, while in reaction 7.XV, the fatty acid formed can catalyze the hydrolysis of DOPC to generate another two moles of the acid and GPC. We assumed the reaction orders are equal to the stoichiometric coefficients, and that the concentration of water, being in excess, does not change. The above set of reactions can be represented by a simple model comprising two differential equations (Eq.(7.1) and Eq.(7.2)).

$$\frac{dC_{DOPC}}{dt} = -k_1 C_{DOPC} - k_2 C_{DOPC} C_{OA} \quad (7.1)$$

$$\frac{dC_{OA}}{dt} = 2k_1 C_{DOPC} + 2k_2 C_{DOPC} C_{OA} \quad (7.2)$$

We used MATLAB 2010 to solve simultaneously the set of ordinary differential equations above and perform parameter estimation to obtain the values of the rate constants. We used *fmincon* to perform the optimization using the *optimtool* GUI. The minimization algorithm uses a sequential quadratic programming active set optimization method [10]. The objective function for minimization was the summation of squared error (SSE) between the calculated and experimental product concentrations at a given reaction temperature. This quantity was calculated using Eq. (7.3), where *j* is the number of discrete reaction times at a particular temperature.

$$SSE = \sum_j [C_{j,DOPC,model} - C_{j,DOPC,exp}]^2 \quad (7.3)$$

The rate constants at each temperature were then fit to the linearized form of the Arrhenius equation to get A_i and E_i along with the associated standard errors for each rate constant.

Table 7.3 Arrhenius parameters for phenomenological autocatalytic model (mol, L, min)

Index No.	A_i	E_i (kJ/mol)	$k_{200} \text{ } ^\circ\text{C}$
1	$10^{9.1 \pm 0.8}$	105 ± 7	1.25E-2
2	$10^{4.6 \pm 0.6}$	44 ± 5	9.64E-1

Table 7.3 displays the Arrhenius parameters that provided the best description of the experimental data. It also displays the values of the rate constants at 200 °C so that the relative rates of the non-catalyzed and catalyzed paths can be easily discerned. Initially, only the non-catalytic reaction 7.XIV would occur at time $t = 0$, leading to the formation of oleic acid. Once oleic acid is formed, reaction 7.XV begins to contribute. The pseudo first-order rate constant for the oleic acid catalyzed path, $k_2 C_{OA}$, will become larger than the first-order rate constant for the uncatalyzed step, k_1 , when the oleic acid concentration becomes greater than 0.013 mol/L (or molar yield of oleic acid is greater than 19 %). Although no one has reported on the autocatalytic behavior of phospholipids in HTW, Zuidam and Crommelin [11] report the rate constant for individual phospholipids at much lower temperatures and in liposomal

dispersions. We can compare the results of the latter study with the parameters obtained for reaction 7.XIV. Zuidam and Crommelin [11] have reported Arrhenius parameters for distearoylphosphatidylcholine (DSPC) (a C₁₈ saturated fatty acid containing PC) as A_i of 2.8E+03 min⁻¹ and E_i of 48 ± 4 kJ/mol. Their parameters give a rate constant for DSPC at 200 °C as 8.36E-03 min⁻¹, which is comparable to the value of k_1 reported in Table 7.3. The small discrepancy could arise due to extrapolating their parameters by 120 °C, differences in the fatty acid component attached to the glycerol backbone of the PC, and differences in pH and experimental conditions. Zuidam and Crommelin [11] carried out their experiments at pH 4.0 using liposomal dispersions, whereas we studied DOPC in HTW.

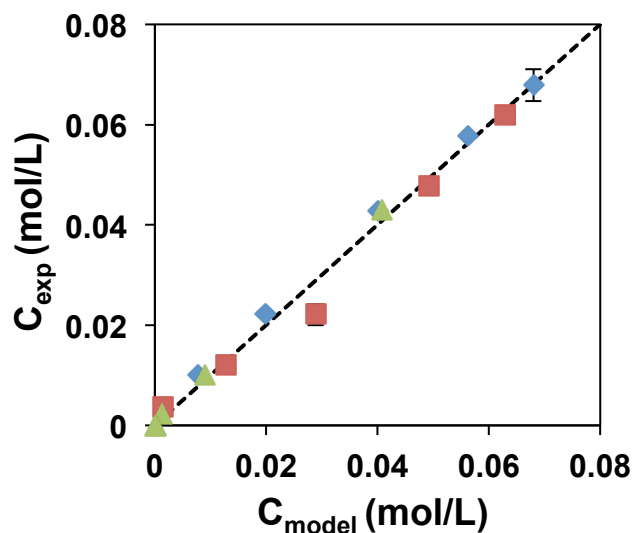


Figure 7.3 Parity plot for comparison of experimental and model concentration for DOPC. Legends are ◆ 175 °C, ■ 200 °C, and ▲ 225 °C

Figure 7.3 shows the parity plot for the experimental and model concentrations for DOPC. The model accurately describes the trends for experimentally obtained DOPC concentrations within experimental errors, consistent with the hypothesis of autocatalysis of DOPC by oleic acid.

Next, we use the Arrhenius parameters in Table 7.3 to predict the experimental concentrations of oleic acid. Figure 7.4 demonstrates that the model over-predicts oleic acid concentration at longer batch holding time, at all

temperatures. This discrepancy can be attributed to the fact that the model is only a simple phenomenological model assuming that DOPC only forms oleic acid. In reality one needs to account for different reaction pathways (mentioned in section 7.3) during the hydrolysis of DOPC. Thus, we are motivated to develop a detailed reaction network for DOPC in HTW.

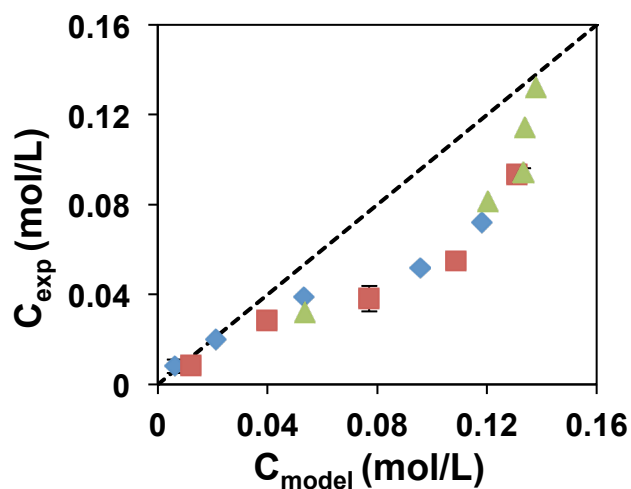


Figure 7.4 Parity plot for comparison of experimental and model concentration for oleic acid. Legends are \blacklozenge 175 °C, \blacksquare 200 °C, and \blacktriangle 225 °C

7.5 Kinetic Model

In this section, we use the reaction pathways just discussed as the basis for a more complete quantitative kinetic model. Figure 7.5, a simplified reaction network for DOPC in HTW, accounts for the reactions outlined in the previous section. We have streamlined the reaction network by lumping the 1- and 2-acyl LPC isomers together and denoting them as LPC. Additionally, we lumped together all of the phosphorus-containing products of LPC since we did not quantify all of these products and some of their identities are tentative.

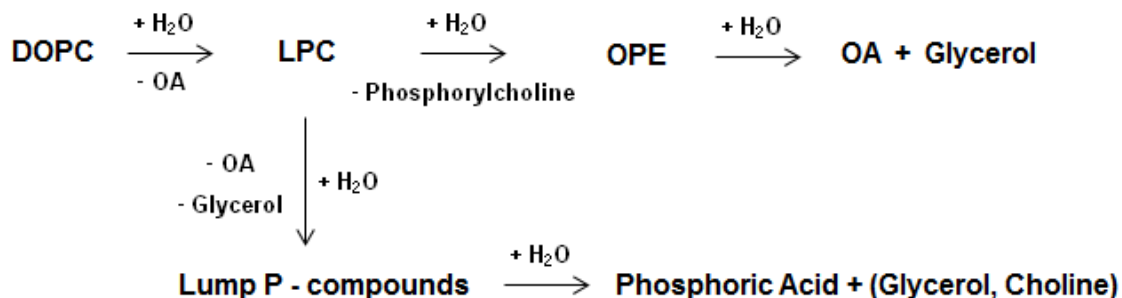
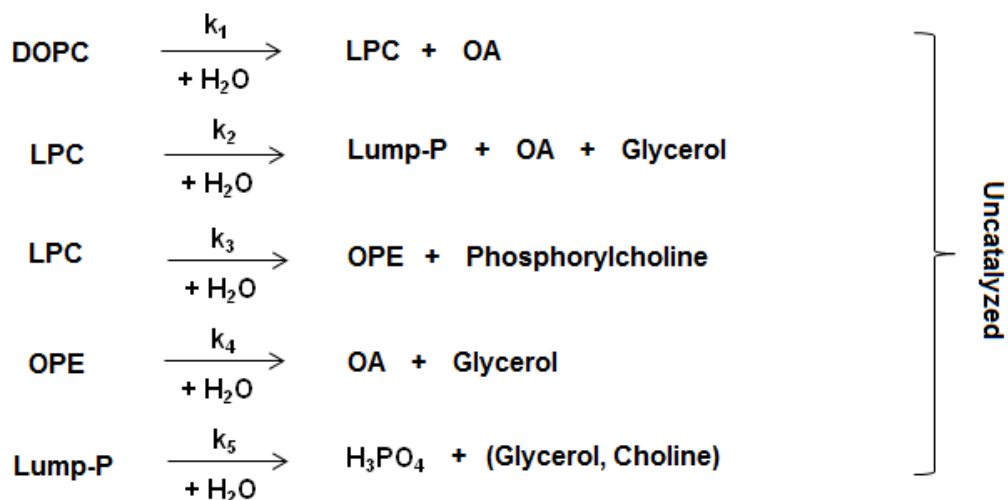
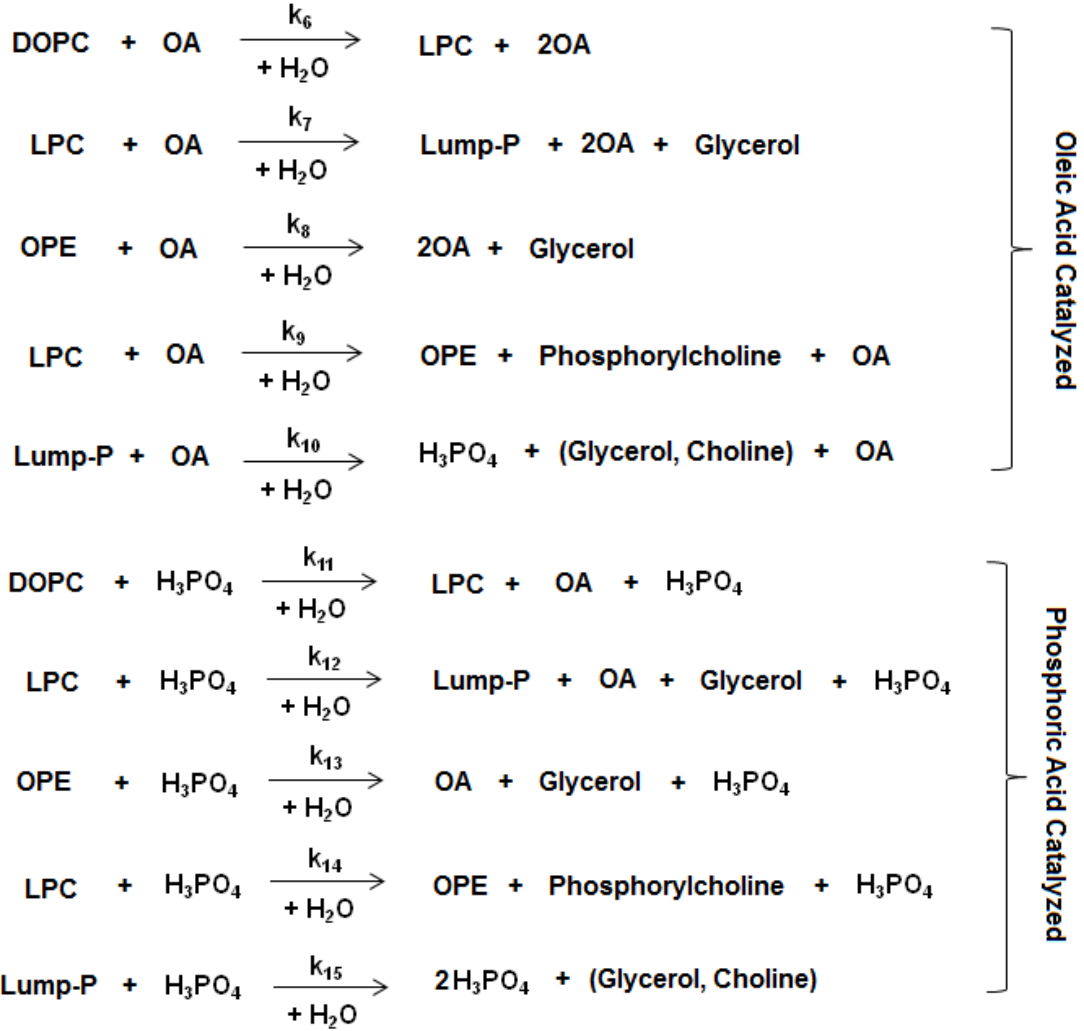


Figure 7.5 Streamlined reaction network for DOPC in HTW

This streamlined reaction network contains five different hydrolytic pathways. On the basis of our previous work with ethyl oleate hydrolysis (chapter 4), we allow each path that produces oleic acid to be catalyzed by both oleic acid and phosphoric acid. Thus, this network can be represented by a set of 15 individual reactions as shown below. The first group of five reactions in this set is uncatalyzed, the next set of five reactions is catalyzed by oleic acid, and the last set of five reactions is catalyzed by phosphoric acid.





We assume that all reactions are irreversible and first-order in each reactant. We do not include the concentration of water in the rate equations since it was present in large excess and did not change appreciably during the reaction. We obtain numerical values for the rate constants for the individual reaction paths by fitting the experimental product concentrations to the model equations (Eq. (7.4) – Eq. (7.9)), which apply to this reaction network and the constant-volume batch reactors used in the experiments.

$$\frac{dC_1}{dt} = -k_1 C_1 - k_6 C_1 C_4 - k_{11} C_1 C_6 \quad (7.4)$$

$$\begin{aligned} \frac{dC_2}{dt} = & k_1 C_1 - k_2 C_2 - k_3 C_2 + k_6 C_1 C_4 - k_7 C_2 C_4 - k_9 C_2 C_4 + k_{11} C_1 C_6 - k_{12} C_2 C_6 \\ & - k_{14} C_2 C_6 \end{aligned} \quad (7.5)$$

$$\frac{dC_3}{dt} = k_3C_2 - k_4C_3 - k_8C_3C_4 + k_9C_2C_4 - k_{13}C_3C_6 + k_{14}C_2C_6 \quad (7.6)$$

$$\begin{aligned} \frac{dC_4}{dt} = & k_1C_1 + k_2C_2 + k_4C_3 + k_6C_1C_4 + k_7C_2C_4 + k_8C_3C_4 + k_{11}C_1C_6 + k_{12}C_2C_6 \\ & + k_{13}C_3C_6 \end{aligned} \quad (7.7)$$

$$\begin{aligned} \frac{dC_5}{dt} = & k_2C_2 + k_3C_2 - k_5C_5 + k_7C_2C_4 + k_9C_2C_4 - k_{10}C_5C_4 + k_{12}C_2C_6 + k_{14}C_2C_6 \\ & - k_{15}C_5C_6 \end{aligned} \quad (7.8)$$

$$\frac{dC_6}{dt} = k_5C_5 + k_{10}C_5C_4 + k_{15}C_5C_6 \quad (7.9)$$

C is the concentration and the subscripts 1-6 represent DOPC, LPC, OPE, oleic acid, lumped P-containing compounds, and phosphoric acid, respectively. We used *fmincon* in MATLAB to solve simultaneously the set of ordinary differential equations above and perform parameter estimation to obtain the values of the rate constants at a given temperature. The objective function for minimization was the summation of squared relative error (SSRE) between the calculated and experimental product concentrations at a given reaction temperature. This quantity was calculated using Eq. (7.10), where *j* is the number of discrete reaction times at a particular temperature and *i* is the number of components.

$$SSRE = \sum_j \sum_{i=1}^6 \left[\frac{C_{j,i,model} - C_{j,i,exp}}{(C_{j,i,model} + C_{j,i,exp}) / 2} \right]^2 \quad (7.10)$$

The rate constants at each temperature were then fit to the linearized form of the Arrhenius equation to get A_i and E_{a_i} along with the associated standard errors for each rate constant.

Table 7.4 Arrhenius parameters for DOPC reaction network

Index No.	log A	E _a (kJ/mol)	Units of k _i	Rate 200 °C, 60min (mol/L/min)
1	6.4 ± 0.5	77 ± 5	min ⁻¹	1.84E-4
2	7.5 ± 0.7	119 ± 6	min ⁻¹	2.83E-8
3	5.9 ± 2.9	72 ± 27	min ⁻¹	1.24E-4
4	13.7 ± 4.4	192 ± 40	min ⁻¹	2.64E-10
5	11.9 ± 3.1	122 ± 28	min ⁻¹	5.45E-4
6	4.1 ± 1.7	42 ± 16	min ⁻¹ mol ⁻¹ L	4.75E-4
7	7.8 ± 0.4	71 ± 4	min ⁻¹ mol ⁻¹ L	8.33E-4
8	18.3 ± 4.6	182 ± 42	min ⁻¹ mol ⁻¹ L	2.31E-5
9	10.8 ± 4.8	111 ± 43	min ⁻¹ mol ⁻¹ L	3.45E-5
10	6.2 ± 1.1	64 ± 10	min ⁻¹ mol ⁻¹ L	1.92E-4
11	4.7 ± 1.5	47 ± 14	min ⁻¹ mol ⁻¹ L	1.15E-4
12	16.5 ± 3.9	151 ± 36	min ⁻¹ mol ⁻¹ L	1.10E-4
13	14.9 ± 7.2	162 ± 65	min ⁻¹ mol ⁻¹ L	1.37E-7
14	3.5 ± 0.4	37 ± 3	min ⁻¹ mol ⁻¹ L	4.75E-5
15	7.6 ± 0.3	72 ± 3	min ⁻¹ mol ⁻¹ L	1.29E-4

Table 7.4 gives the Arrhenius parameters for the DOPC reaction network and the rates for the different reaction steps at 200 °C and 60 minutes. Reactions 1, 6, and 11 all represent the same pathway (hydrolysis of DOPC), but steps 6 and 11 are catalyzed. The rate of the uncatalyzed path is nearly two and a half times less than that for the oleic acid catalyzed path and almost equal to that for the phosphoric acid catalyzed path. Reactions 2, 7, and 12 also represent the same pathway (hydrolysis of LPC), with steps 7 and 12 being catalyzed. For this path, the uncatalyzed step is orders of magnitude slower than the catalyzed paths. The same is found to be true when comparing the rates of reactions 4, 8, and 13, which describe OPE hydrolysis. Since the rates of uncatalyzed paths 2 and 4 are negligible at the conditions of Table 7.4 and more generally at all times at 200 °C, we removed these paths from the model and fit the data again using just thirteen rate constants. Removing these two parameters did not change the other rate constants.

Figure 7.6 shows the parity plot for the experimental and calculated concentrations of the different chemical species. The dotted diagonal line

represents a perfect fit of the model to the experimental data, and the dotted lines above and below represent $\pm 20\%$ error. Figure 7.6a shows that the model generally fits the experimental data to within $\pm 20\%$ and also predicts the concentrations of the major products at 350 °C well. Moreover, the data are scattered on both sides of the diagonal, indicating the absence of systematic error. Figure 7.6b shows that there is more scatter for the minor products, but even here the model often fits the data to within the experimental uncertainty.

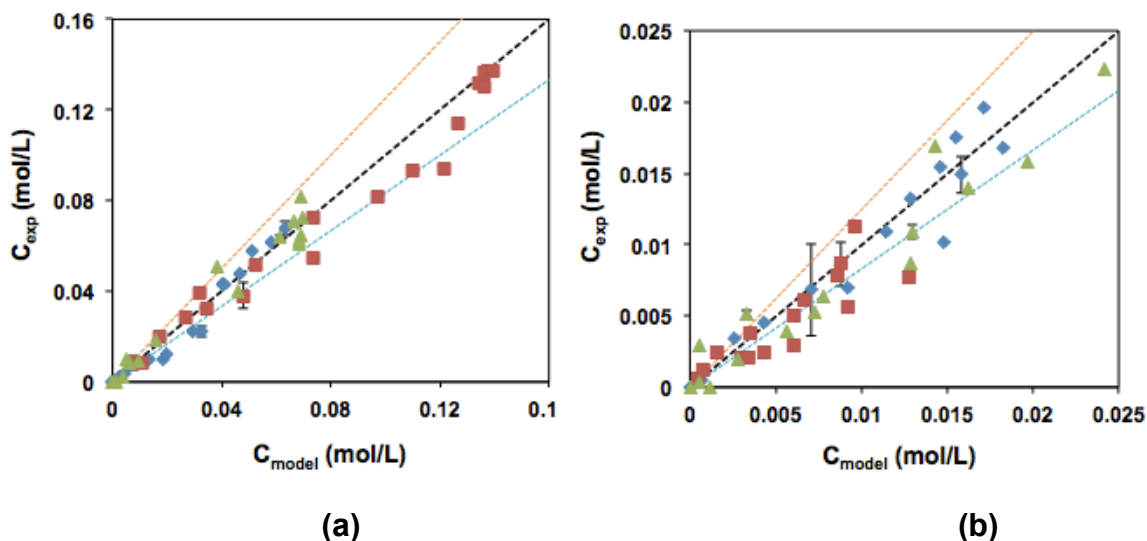


Figure 7.6 Comparison of experimental and calculated concentrations at 175 °C, 200 °C, 225 °C and 350 °C. Legends are a) \blacklozenge DOPC \blacksquare Oleic acid \blacktriangle Phosphoric acid and b) \blacklozenge LPC \blacksquare OPE \blacktriangle Lumped P-compounds

7.6 Conclusions

Under the conditions studied, DOPC hydrolyzed to form oleic acid, several phosphorus-containing compounds, glycerol, and choline. We also detected an ester of oleic acid and glycerol (OPE), which had not been documented previously. The conversion for DOPC showed a sigmoidal trend with increasing batch holding time, indicating catalysis by oleic and phosphoric acid, which was also confirmed experimentally.

The primary paths from DOPC form 1-acyl LPC and 2-acyl LPC, which subsequently hydrolyze via parallel reactions to form either OPE or α -GPA+ β -GPA+ phosphorylcholine, via GPC. Hydrolysis of both DOPC and LPC releases oleic acid. Phosphoric acid was the sole phosphorus-containing end product.

A phenomenological kinetic model based on these pathways accurately describes the trends in the data and typically estimates the species concentrations to within their experimental errors. The results from this study of DOPC in HTW have implications to algae processing, as will be discussed in detail in chapter 9.

References

- [1] A. J. De Koning, K. B. McMullan. Hydrolysis of phospholipids with hydrochloric acid. *Biochim. Biophys. Acta* 106, 519-526, 1965
- [2] R. Alenezi, G. A. Leeke, R. C. D. Santos, A. R. Khan. Hydrolysis kinetics of sunflower oil under subcritical water conditions. *Chem. Eng. Res. Des.* 87, 867-873, 2009
- [3] C. R. Kensil, E. A. Dennis. Alkaline hydrolysis of phospholipids in model membranes and the dependence on their state of aggregation *Biochemistry* 20, 6079-6085, 1981
- [4] M. Grit, J. H. de Smidt, A. Struijke, D. J. A. Crommelin. Hydrolysis of phosphatidylcholine in aqueous liposome dispersions. *Int. J. Pharm.* 50, 1-6, 1989
- [5] M. Grit, D. J. A. Crommelin. The effect of aging on the physical stability of liposome dispersions. *Chem. Phys. Lipids* 62, 113-122, 1992
- [6] M. Grit, D. J. A. Crommelin. Chemical stability of liposomes: implications for their physical stability. *Chem. Phys. Lipids* 64, 3-18, 1993
- [7] P. Krammer, H. Vogel. Hydrolysis of esters in subcritical and supercritical water. *J. Supercrit. Fluids* 16, 189-206, 2000
- [8] D. J. Hanahan. *Lipide Chemistry*. John Wiley & Sons, Inc., New York, 1960
- [9] B. Maruo, A. A. Benson. Cyclic glycerophosphate formation from the glycerolphosphatides. *J. Biol. Chem.* 234 (2), 254-256, 1959
- [10] <http://www.mathworks.com/help/toolbox/optim/ug/fmincon.html>. Date last accessed, 3rd September 2011
- [11] N. J. Zuidam, D. J. A. Crommelin. Chemical hydrolysis of phospholipids *J. Pharm. Sci.* 84 (9) 1113-1119, 1995

CHAPTER 8

Behavior of Binary Mixtures in HTW

Previous researchers have carried out hydrothermal liquefaction of algae and found that the yield of the bio-oil exceeded the starting lipid content of algae [1-3]. This observation implies that not only lipids but also other components of algae form constituents of bio-oil during HTL of algae. Proteins are important constituent in algae that can not only form several components of bio-oil (see Chapter 5) but also possibly interact with other biomacromolecules in algae. In order to understand this chemistry, we have studied phenylalanine with inorganic additives (salts and boric acid) and an organic compound (ethyl oleate) in HTW. In this chapter we first describe the preliminary work that was done to validate the experimental methods. We then report the effect of salts and boric acid on the conversion of phenylalanine and the yield of phenylethylamine. Next, we summarize the behavior of a binary mixture of phenylalanine and ethyl oleate in HTW. A quantitative phenomenological kinetics model is developed to describe experimental observations for the binary mixture of phenylalanine and ethyl oleate in HTW.

8.1 Control Experiments

Control experiments (as mentioned in 3.3.5) were done to assess our ability to measure accurately the amount of phenylalanine in the reactor. These experiments, which were essentially runs performed at room temperature, gave a phenylalanine recovery of 95%, with both K_2HPO_4 and ethyl oleate, and a recovery of 96% for ethyl oleate, thereby verifying the suitability of the methods used for quantifying the amounts of phenylalanine and ethyl oleate.

8.2 Binary Mixtures of Inorganics and Phenylalanine

In this section, we present the results of the effects of inorganics (NaCl, NaNO_3 , Na_2SO_4 , KCl, K_2HPO_4 , and H_3BO_3) on phenylalanine in HTW. Note that we have selected 250 °C and 30 minutes for this study because the conversion of phenylalanine without any additives under these conditions was 0.33. Furthermore at this condition, the yield of the main product, phenylethylamine, was 0.20. Since both the conversion of the reactant and the yield of the product were neither too high nor too low, one can observe any significant effects of the additives, if they exist. Table 8.1 gives the conversion of phenylalanine and the yield of the phenylethylamine in the presence of various additives. Note that the yields of styrene and phenylethanol are very low under these conditions for all cases and have been neglected.

Table 8.1 Conversion and yields of phenylalanine and phenylethylamine in presence of different additives at 250 °C and 30 min

Salt	C_{salt} (mol/L)	Ionic Strength (mol/L)	Phenylalanine Conversion	Phenylethylamine Yield	Carbon Balance (%)
None	-	-	0.33 ± 0.03	0.20 ± 0.04	88 ± 8
NaCl	0.069	0.069	0.46 ± 0.02	0.14 ± 0.01	66 ± 1
NaNO_3	0.047	0.047	0.55 ± 0.03	0.17 ± 0.01	60 ± 2
Na_2SO_4	0.028	0.085	0.46 ± 0.03	0.13 ± 0.02	65 ± 1
KCl	0.054	0.054	0.38 ± 0.06	0.11 ± 0.01	70 ± 4
K_2HPO_4	0.023	0.069	0.57 ± 0.04	0.11 ± 0.01	53 ± 4
H_3BO_3	0.065	0.387	0.46 ± 0.02	0.10 ± 0.01	62 ± 2

Figure 8.1a shows that addition of salts and boric acid generally increases the phenylalanine conversion. Comparing results from addition of the three sodium salts shows that NaNO_3 has the greatest influence on phenylalanine conversion (~ 66% increase). Based on this observation, we speculate that perhaps nitrate has a more favorable interaction with phenylalanine or stabilizes the transition state better than chloride or sulfate. KCl increases the phenylalanine conversion less than NaCl, though the uncertainty in the KCl result is higher. Mishima and Matsuyama [4] attributed the higher activity of sodium salts over potassium salts to the higher hydration enthalpy of Na^+ . The same

phenomenon might be at work in the present system as well. K_2HPO_4 shows the most pronounced effect on phenylalanine conversion (increase of about 71%), probably because of two divalent K^+ ions leading to greater interactions between the salt and phenylalanine. Lastly, H_3BO_3 increased the phenylalanine conversion only moderately (by around 40%).

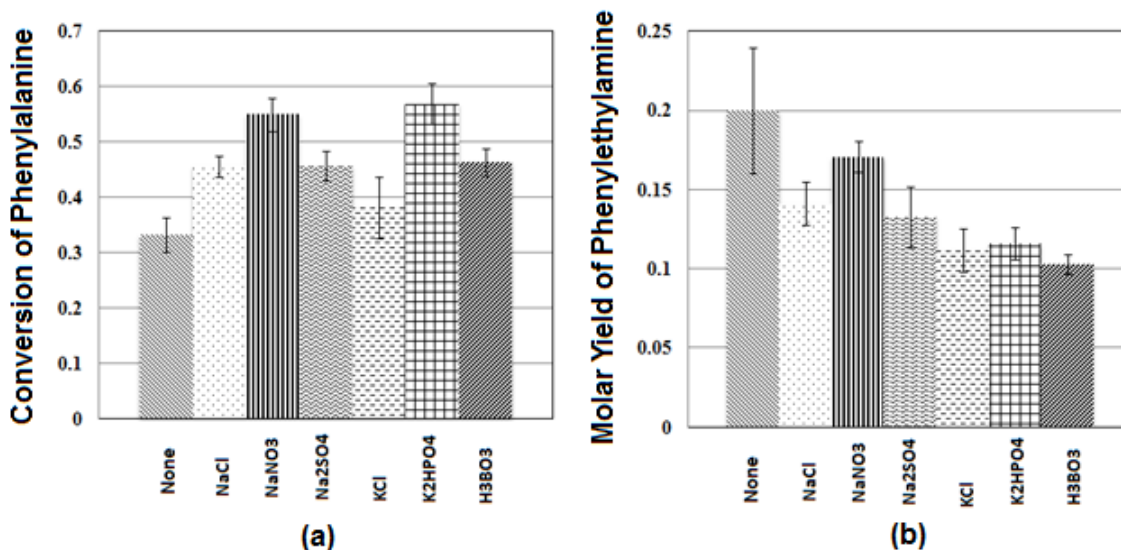


Figure 8.1 Effect of salts and boric acid on phenylalanine at 250 °C and 30 min in HTW. a) Phenylalanine conversion and b) Phenylethylamine yield

One might expect that an increase in phenylalanine conversion would lead to a corresponding increase in the rate of decarboxylation, the major reaction path for phenylalanine reacting alone, thus increasing the yield of phenylethylamine. Figure 8.1b, however, shows that the yield of phenylethylamine decreases in the presence of each of the additives. H_3BO_3 and KCl provide the greatest decreases (about 49% and 45% respectively) compared to the case with no additive. $NaNO_3$ induces the least decrease of about 15%. These observations are in accord with the addition of KCl reportedly reducing the decarboxylation rate for α -alanine [5]. Those authors proposed the decrease to be due to either, 1) formation of a transition state less polar than the starting zwitterion of α -alanine, or 2) formation of complexes of K^+ or Cl^- with ionic sites of α -alanine zwitterions, thereby reducing its ability to undergo decarboxylation.

The reaction network for phenylalanine alone in HTW, illustrated in chapter 5 (Figure 5.2), shows that phenylalanine can undergo two parallel primary reactions – decarboxylation or oligomerization. Since the rate of decarboxylation decreases in the presence of salts and boric acid, there must be an increase in the rate of the oligomer formation pathway. The carbon balances from the experiments with added salts were always lower than 70% (Table 8.1), whereas without salt the carbon balance was around 90% (see chapter 5, Table 5.1) under the same conditions. This result is consistent with an increase in the rate of formation of oligomers in presence of salts. LC-MS analysis of a sample from the reaction of phenylalanine in the presence of added NaNO_3 confirmed the presence of high molecular weight compounds (Figure 8.2).

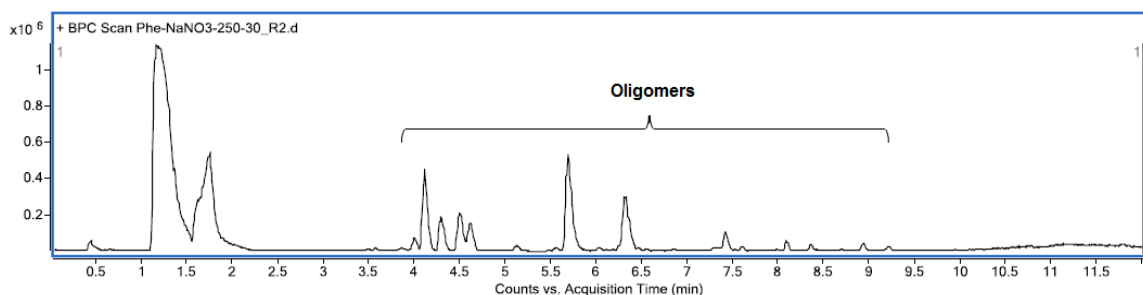


Figure 8.2 LC-MS chromatogram for phenylalanine and NaNO_3 reaction product in HTW at 250 °C and 30 min

From the results and discussion above, we conclude that the salts examined here and boric acid inhibit decarboxylation but lead to an increase in high molecular weight compound formation from phenylalanine, thereby increasing phenylalanine conversion. This work is the first to report this effect of salts (or boric acid) on oligomerization of amino acids in HTW. It also reveals that these inorganic compounds could influence the relative rates of different reaction paths during hydrothermal liquefaction of algae.

8.3 Binary Mixture of Ethyl Oleate and Phenylalanine

In chapter 5, we had characterized the products from phenylalanine alone in HTW, while in the previous section we saw the effect of added salts and boric acid on the behavior of phenylalanine. This section examines the effect of an

added organic molecule (ethyl oleate, which is a model compound for triglycerides in algae). The concentrations of ethyl oleate and phenylalanine were varied to mimic the broad range of triglyceride to protein ratios in different strains of algae. We carried out the reactions at 350 °C, since the yield of algal bio-oil is maximum at this temperature [1]. The conversion of phenylalanine was always complete at this temperature, however, so we focus this discussion on the influence of added ethyl oleate on the yields and identities of products from phenylalanine. The effect of phenylalanine on ethyl oleate conversion and oleic acid yield is also explored. It should be noted, as was mentioned in Chapter 5, that the yields of phenylethylamine and styrene are independent of the initial phenylalanine concentration. Therefore, any effects observed for mixtures involving phenylalanine solely arise from the addition of ethyl oleate alone.

We would like to remind the reader that we obtained similar yields of phenylethylamine (chapter 5, Tables 5.1 and 5.2) from the control experiments for phenylalanine alone in HTW (no ester added) at the different concentrations corresponding to those used in the mixtures (4000, 15000, and 22000 ppm). These results indicate that the yield of phenylethylamine is independent of the phenylalanine concentration (as expected for a first-order reaction) and that any effects observed in the mixtures arise solely from the addition of ethyl oleate.

8.3.1 Reaction Products and Distribution

Tables 8.2 and 8.3 provide the yields of the various products at different batch holding times and the different initial molar ratios of ethyl oleate and phenylalanine. We present just a representative subset of that data in Figure 8.3, Figure 8.5 and Figure 8.7, i.e. data at only 10 minutes is presented. We remind the reader that the yields of phenylethylamine, styrene, and phenylethanol (Figure 8.3) are based on initial moles of phenylalanine loaded into the reactor, the yields of oleic acid (Figure 8.5) are based on initial moles of ethyl oleate loaded, and the yields of oleamides (Figure 8.7) are based on the initial moles of the limiting reactant loaded (either phenylalanine or ethyl oleate).

Table 8.2 Effect of ethyl oleate on yield of products from phenylalanine at 350 °C and different batch holding times

Molar Ratio EO:Phe	Time (min)	Phenylethylamine Yield	Styrene Yield	Phenylethanol Yield	Phenylacet-aldehyde Yield	Overall Carbon Balance (%)
0.2	10	0.51 ± 0.02	0.14 ± 0.02	0.012 ± 0.003	0.0006 ± 0.0003	74 ± 5
	20	0.35 ± 0.01	0.30 ± 0.03	0.030 ± 0.005	0.0013 ± 0.0009	75 ± 1
	30	0.28 ± 0.05	0.35 ± 0.06	0.037 ± 0.009	0.0013 ± 0.0005	71 ± 1
	40	0.18	0.43	0.047	0.0015	68
	60	0.07	0.47	0.055	0.0024	60
1.0	10	0.36 ± 0.02	0.19 ± 0.04	0.026 ± 0.002	0.0014 ± 0.0004	81 ± 3
	20	0.24 ± 0.02	0.31 ± 0.02	0.039 ± 0.001	0.0017 ± 0.0007	78 ± 2
	30	0.16 ± 0.02	0.34 ± 0.03	0.044 ± 0.001	0.0016 ± 0.001	73 ± 7
	40	0.16	0.41	0.054	0.0017	52
	60	0.07	0.39	0.060	0.0031	74
5.0	10	0.30 ± 0.04	0.18 ± 0.03	0.027 ± 0.002	0.014 ± 0.0006	82 ± 5
	20	0.16 ± 0.01	0.33 ± 0.02	0.044 ± 0.004	0.013 ± 0.013	79 ± 1
	30	0.13 ± 0.01	0.37 ± 0.01	0.051 ± 0.003	0.016 ± 0.014	77 ± 5
	40	0.08	0.38	0.054	0.024	81
	60	0.05	0.41	0.068	0.037	77

Table 8.3 Effect of phenylalanine on yields of oleic acid, oleamides, and conversion of ethyl oleate at 350 °C and different batch holding times

Molar Ratio Phe:EO	Time (min)	ODM Yield	EODM Yield	PEODM Yield	Oleic Acid Yield	Ethyl Oleate Conversion
0.2	10	0.021 ± 0.002	0.007 ± 0.002	0.164 ± 0.054	0.67 ± 0.03	0.81 ± 0.05
	20	0.022 ± 0.003	0.023 ± 0.002	0.161 ± 0.012	0.83 ± 0.01	0.99 ± 0.003
	30	0.024 ± 0.002	0.026 ± 0.002	0.142 ± 0.024	0.82 ± 0.05	0.99 ± 0.005
	40	0.030	0.032	0.122	0.89	1.00
	60	0.032	0.032	0.071	0.84	1.00
1.0	10	0.008 ± 0.002	0.007 ± 0.003	0.149 ± 0.011	0.76 ± 0.02	0.96 ± 0.02
	20	0.013 ± 0.001	0.015 ± 0.003	0.156 ± 0.010	0.73 ± 0.01	0.99 ± 0.003
	30	0.019 ± 0.002	0.014 ± 0.003	0.117 ± 0.017	0.72 ± 0.06	0.99 ± 0.003
	40	0.026	0.021	0.139	0.86	0.99
	60	0.031	0.014	0.055	0.82	1.00
5.0	10	0.011 ± 0.003	0.026 ± 0.002	0.142 ± 0.033	0.78 ± 0.13	0.96 ± 0.003
	20	0.020 ± 0.002	0.024 ± 0.007	0.235 ± 0.018	0.67 ± 0.02	0.99 ± 0.004
	30	0.020 ± 0.006	0.021 ± 0.004	0.224 ± 0.031	0.62 ± 0.04	0.99 ± 0.006
	40	0.031	0.019	0.152	0.62	0.98
	60	0.032	0.024	0.087	0.63	1.00

First we report and discuss the effect of added ethyl oleate on the products obtained from phenylalanine. Figure 8.3a shows that the molar yield of phenylethylamine decreases from 0.62 without added ester to 0.30 as the initial ratio of ethyl oleate in the binary mixture increases from 0.0 to 5.0. This behavior suggests faster reaction of phenylethylamine to form secondary products in the presence of ethyl oleate. To test the hypothesis of accelerated disappearance of phenylethylamine, we did an experiment with 20 μL of phenylethylamine (0.10 mol/L), with and without 40 μL (0.075 mol/L) of ethyl oleate, in water at 350 $^{\circ}\text{C}$ for 10, 20, and 30 min. This amount corresponds to a molar ratio of ethyl oleate to phenylethylamine equal to 0.7.

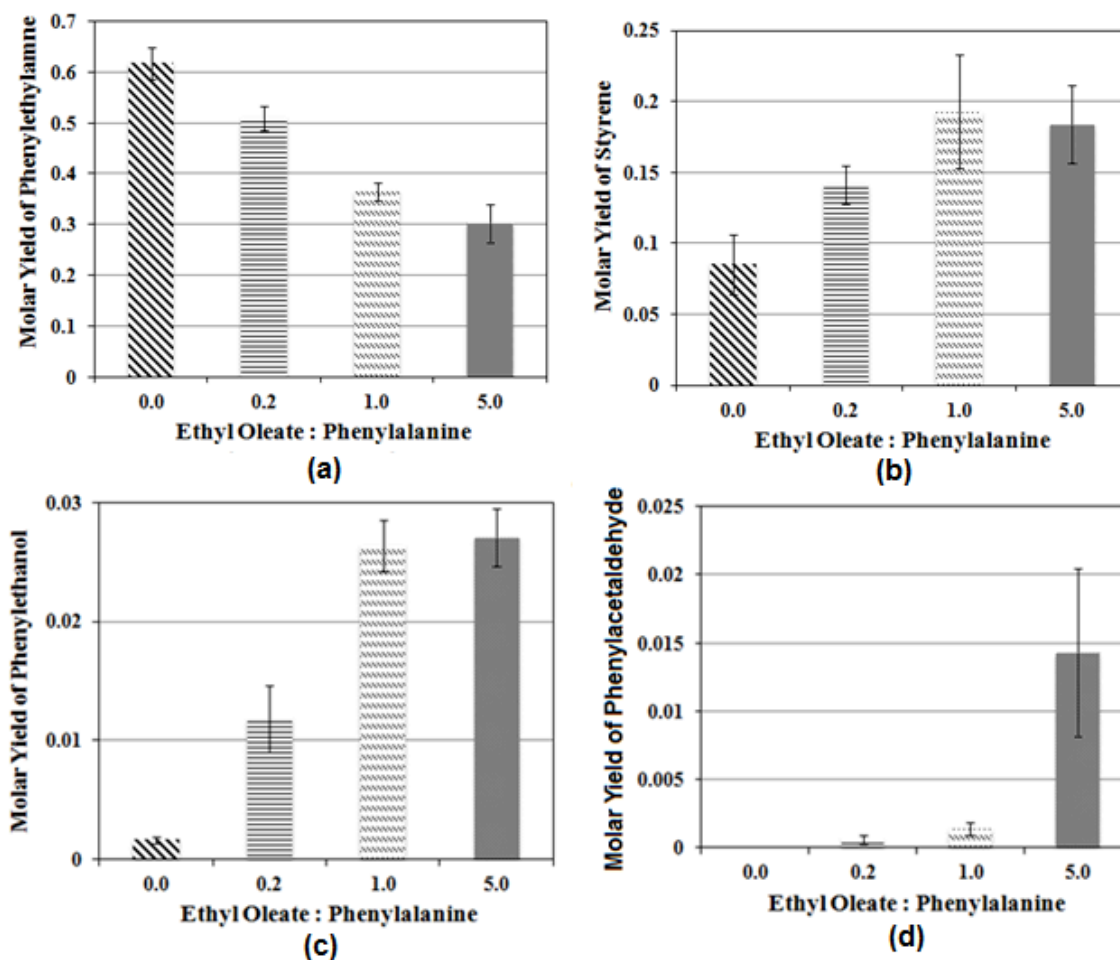


Figure 8.3 Effect of ethyl oleate on molar yields of different products at 350 $^{\circ}\text{C}$ and 10 min. a) phenylethylamine, b) styrene, c) phenylethanol, d) phenylacetaldehyde

Figure 8.4 shows that the conversion of phenylethylamine was always higher in the presence of ethyl oleate, thereby confirming that the disappearance of phenylethylamine is enhanced in the presence of ethyl oleate. For example, phenylethylamine conversion increased from 0.28 (without added ester) to 0.37 (in the presence of ester), at 10 min, which is a net increase of 32%. This increase in the conversion of phenylethylamine with added ester implies a corresponding decrease in its molar yield (~30%) when it is formed from phenylalanine with and without ethyl oleate (0.0 and 0.7 molar ratio). Interpolation of the data in Figure 8.3a leads to an estimated molar yield of phenylethylamine of about 0.4 at an initial molar ratio of 0.7. This value (0.4) is about 30% lower than the yield obtained without added ester, a relative decrease that is consistent with the results in Figure 8.4.

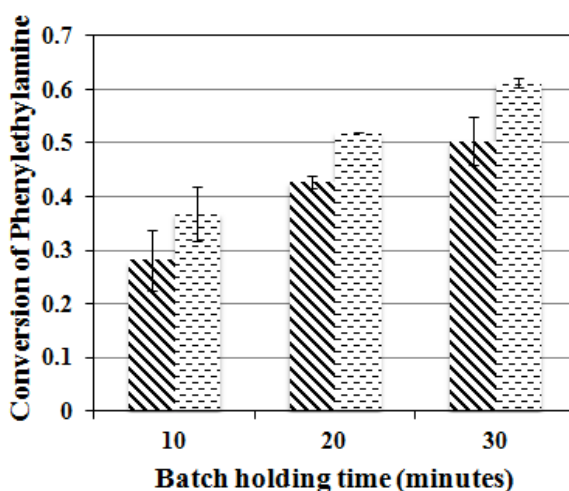




Figure 8.4 Conversion of phenylethylamine at 350 °C and different batch holding times. Legends are  without,  with 40 µl ethyl oleate (0.7 : 1 molar ratio)

The increased conversion of phenylethylamine in the presence of ethyl oleate suggests an accompanying increase in the molar yield of styrene on increasing the amount of ester. Figure 8.3b confirms this expectation. The molar yield of styrene at 10 min is 0.09 without any ester and around 0.18 when the molar ratio of ethyl oleate to phenylalanine is 5.0. Similarly, Figure 8.3c shows that the molar yield of phenylethanol increases from 0.002 to 0.027 as the ethyl

oleate ratio increases from 0.0 to 5.0. Thus, the addition of ethyl oleate enhances both deamination of phenylethylamine to styrene and hydration of styrene to phenylethanol.

These paths are accelerated upon addition of ethyl oleate, because both deamination of organic compounds and hydration of styrene and other alkenes in an aqueous medium are acid catalyzed reactions [6-9]. The addition of ethyl oleate reduces the pH of the system due to the production of oleic acid from its hydrolysis [10, 11], thereby catalyzing both the deamination and hydration reactions in the binary mixture.

In addition to altering the yields of products identified from reaction of phenylalanine alone, addition of ethyl oleate also permitted quantification of a new product, phenylacetaldehyde. Figure 8.3d shows that the molar yield of phenylacetaldehyde increases with an increase in the molar ratio of ethyl oleate to phenylalanine. The yield of phenylacetaldehyde also increases with an increase in the batch holding time at a given concentration ratio (see Table 8.2). Klinger *et al.* [10] have previously reported the formation of acetaldehyde from alanine via a lactic acid intermediate. A similar pathway could be at work here, wherein phenylalanine first forms phenyllactic acid via deamination, which then decarboxylates to form phenylacetaldehyde. The highest yield of phenylacetaldehyde was 0.04, obtained from the reaction at the longest time (60 min) and most added ester (molar ratio of 5.0). Once again, it is likely that ethyl oleate catalyzes deamination of phenylalanine to form phenyllactic acid, subsequently forming phenylacetaldehyde under these conditions.

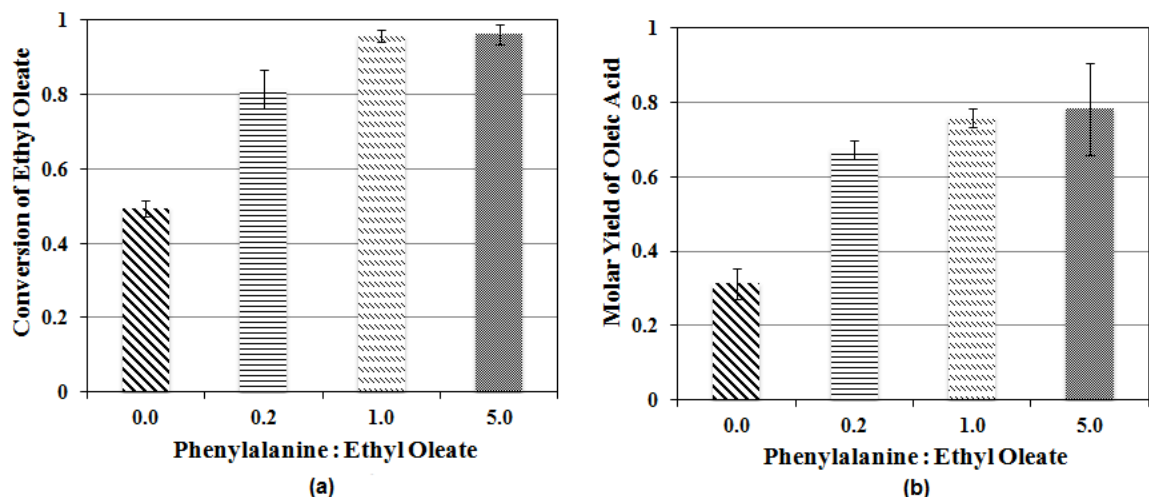


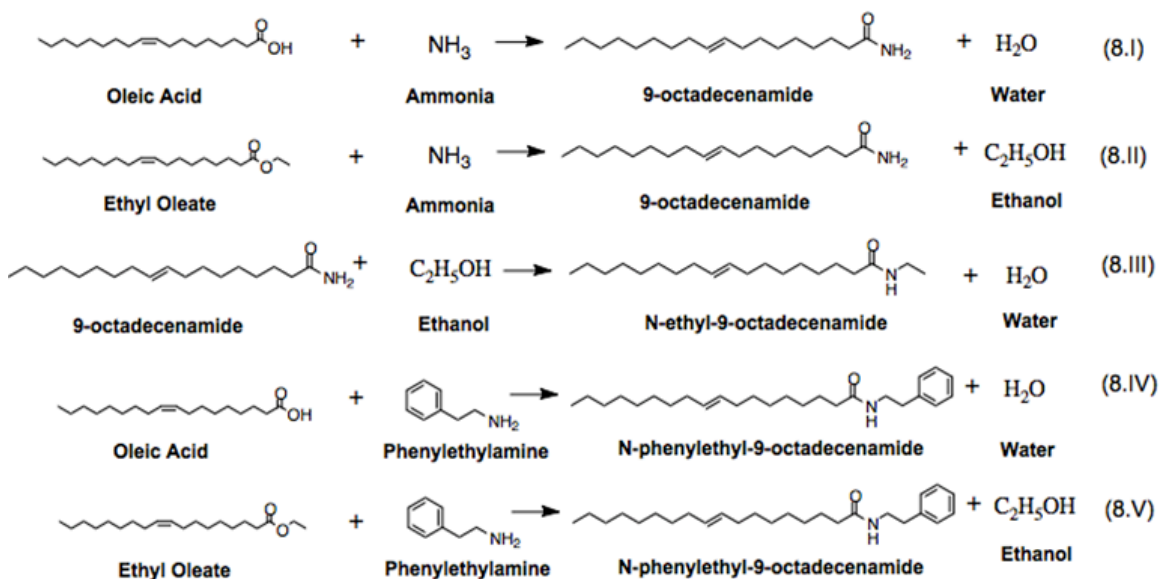
Figure 8.5 Effect of phenylalanine on ethyl oleate and oleic acid at 350 °C and 10 min. a) Conversion of ethyl oleate and b) Yield of oleic acid

Having discussed the results from these binary mixture experiments in terms of the influence of added ester on phenylalanine, we now examine the other side of the coin and discuss the influence of added phenylalanine on ethyl oleate. Figure 8.5a shows that the ethyl oleate conversion at 10 min is 0.49 without phenylalanine and 0.96 at a phenylalanine to ethyl oleate molar ratio of 5.0. The general trend is that higher the amount of phenylalanine more is the conversion of ethyl oleate. This behavior is expected because ethyl oleate conversion is acid catalyzed [10, 11] and the presence of phenylalanine would reduce the initial pH of the solution (isoelectric point of phenylalanine is 5.3 at room temperature [12] and an aqueous solution of phenylalanine (15000 ppm) has a pH of 5.9 at room temperature).

Higher conversion of ethyl oleate implies a corresponding increase in the yields of oleic acid, the major reaction product, which arises from hydrolysis. Figure 8.5b offers confirmation, as the yield of oleic acid at 10 min increases from 0.31 without phenylalanine to 0.78 at a phenylalanine to ethyl oleate molar ratio of 5.0. At batch holding times greater than 10 min, however, the molar yields of oleic acid show the opposite trend at a molar ratio of phenylalanine to ethyl oleate of 5.0 (see Table 8.3 and Appendix, Table A.2). That is, at 60 min the oleic acid yield decreases from 0.73 without phenylalanine to 0.63 at a molar ratio of

phenylalanine to ethyl oleate of 5.0. As we show below, this observation is consistent with oleic acid undergoing secondary reactions in the presence of phenylalanine to form additional products.

Figure 8.6, which shows the total ion chromatogram for a reaction at 350 °C and 30 min with phenylalanine to ethyl oleate molar ratio of 1.0, indicates the presence of three oleamides (9-octadecenamide (ODM), N-ethyl-9-octadecenamide (EODM), and N-phenylethyl-9-octadecenamide (PEODM)). Roe [13] mentioned previously that ODM can be formed in HTW by the reaction of oleic acid or ethyl oleate with ammonia. For the binary system of phenylalanine and ethyl oleate, ammonia is generated in situ during deamination of phenylethylamine to styrene. It is also possible in this environment for ODM to undergo condensation with ethanol (formed in small quantity during formation of ODM from ethyl oleate) and form EODM [14]. Lastly, phenylethylamine could also react with oleic acid or ethyl oleate in a similar fashion to form PEODM. The reactions of amide formations are shown below (8.I-8.V). These reactions would lead to a decrease in the yield of oleic acid, and this decrease would be expected to be most significant at longer times and in mixtures with more phenylalanine. Both of these expectations are consistent with the experimental results.



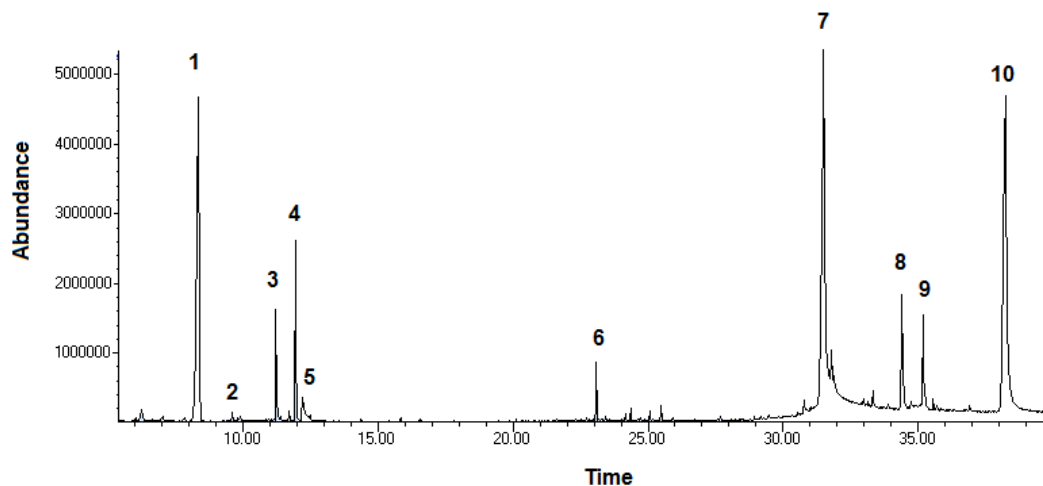


Figure 8.6 GC-MS chromatogram for binary mixture of phenylalanine and ethyl oleate (1.0 : 1.0) at 350 °C and 30 min

Table 8.4 Chemical names and structure of labels for GC-MS chromatogram for phenylalanine and ethyl oleate binary mixture (1.0 : 1.0) at 350 °C and 30 min

Peak No.	Chemical Name	Structure
1	Styrene	
2	Phenylacetaldehyde	
3	1-phenylethanol	
4	Phenylethylamine	
5	2-phenylethanol	
6	1,3-diphenylbutane	
7	Oleic Acid	
8	9-octadecenamide	
9	N-ethyl-9-octadecenamide	
10	N-phenylethyl-9-octadecenamide	

Figure 8.7a shows that the total yield of amides at 10 min is always about 16-20% of the theoretical maximum yield. The yield is not affected by different initial molar ratios of phenylalanine to ethyl oleate, considering the experimental uncertainty. Similar results were obtained at other batch holding times (see Table 8.3).

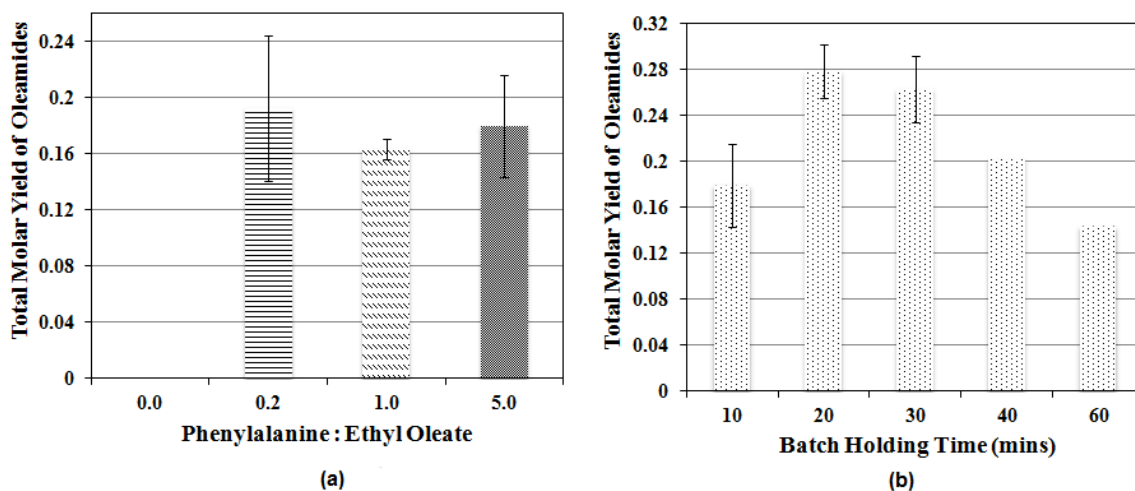
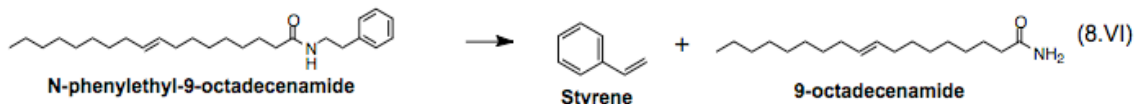


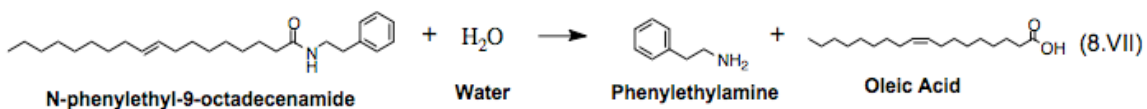
Figure 8.7 a) Total yield of amides at 350 °C and 10 min for different initial molar ratios of phenylalanine to ethyl oleate and b) Total yield of amide at various batch holding times and phenylalanine to ethyl oleate molar ratio of 5.0

Figure 8.7b shows that at a particular initial ratio of phenylalanine to ethyl oleate, the total yield of amides first increases and then decreases as the batch holding time is increased. Results obtained at the other molar ratios showed this same trend. Table 8.3 shows that the yield of PEODM is always higher than the yields of ODM or EODM, and that the yield of PEODM first increases with time and then decreases, whereas the yields of ODM or EODM continually increase with time. These trends suggest that PEODM undergoes secondary decomposition. One possibility to account for these observations is deamidation of PEODM to styrene, as shown below. The oleamide group on PEODM ($C_{17}H_{33}-CO-NH-$) is a better leaving group than the amino substituent ($-NH_2$) in phenylethylamine because the former anion is stabilized via conjugation with the carbonyl group. Therefore, PEODM can undergo deamidation to form styrene similar to the deamination of phenylethylamine (8.VI), the latter path having being

demonstrated in our work. Deamidation could be another reason why the yield of styrene (Table 8.2) and ODM (Table 8.2) increase at longer batch holding times for the binary mixture.



Along with deamidation, hydrolysis is another potential pathway for PEODM degradation. Duan *et al.* [15] reported that N-substituted amides hydrolyze to give the corresponding amine and carboxylic acid. This reaction is reversible and follows first-order kinetics. Thus, there exists a possibility of hydrolysis of PEODM to form phenylethylamine and oleic acid under our conditions (8.VII). Hydrolysis of PEODM would be favored as more PEODM is formed at higher batch holding times, thus, accounting for a net decrease in total yield of amides.



Brown *et al.* [1] and Valdez *et al.* [16] have characterized and quantified fatty acid amides as products from the hydrothermal liquefaction of algae. Valdez *et al.* [16] reported that the yields of palmitic acid amide varied from 0.5 to 3 (mg/g of dry algae) depending on whether hexane or hexadecane was used, respectively, for recovery of bio-oil. However, these authors have only proposed the reaction of fatty acids with ammonia to account for the amide formation, neglecting the possibilities of amines reacting with fatty acids. The present work offers this new possibility.

Based on the above discussions and results, we propose a reaction network in Figure 8.8 to account for the reactions that occur in a binary mixture of phenylalanine and ethyl oleate.

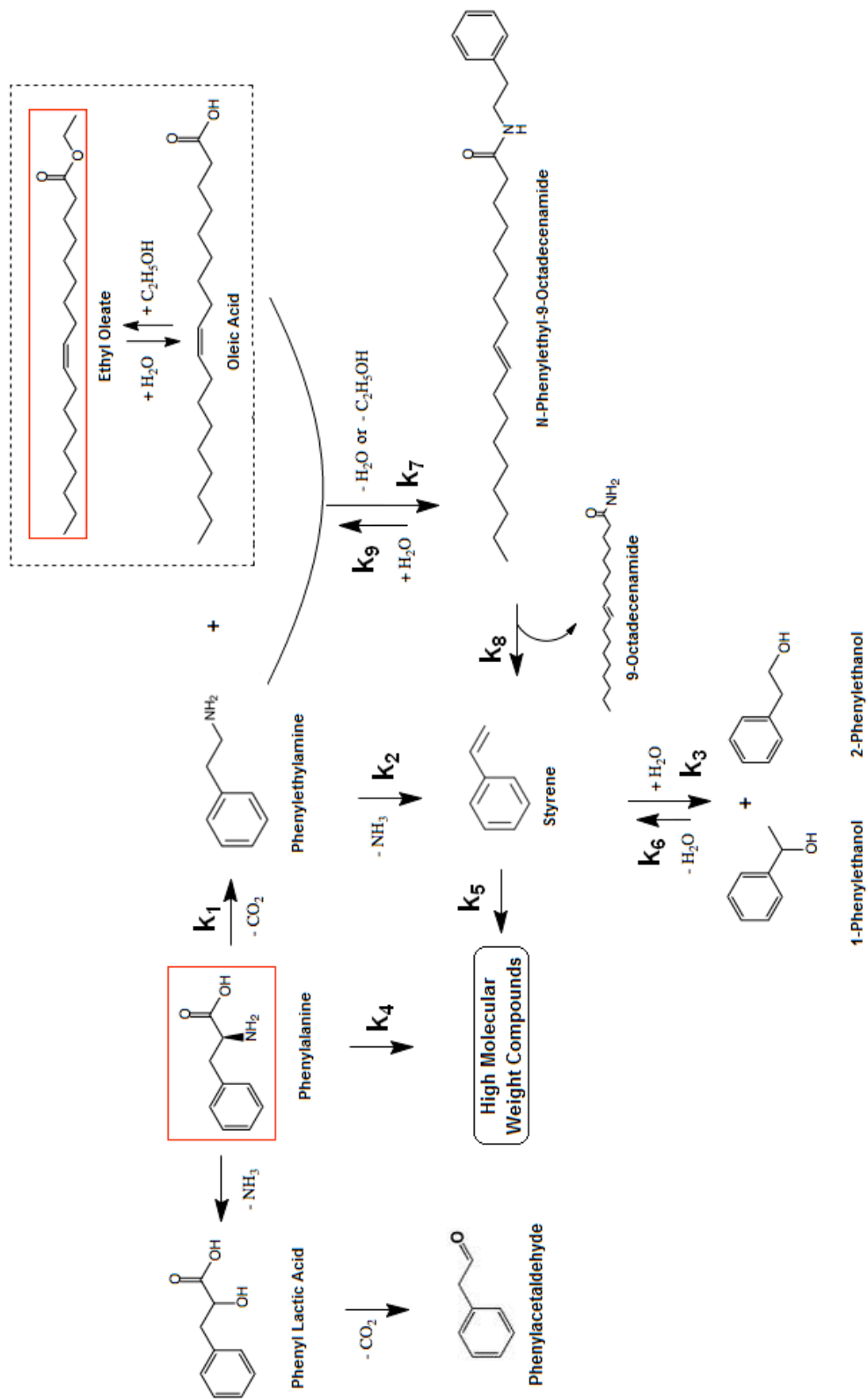


Figure 8.8 Reaction network for binary mixture of ethyl oleate and phenylalanine in HTW

8.3.2 Kinetics Model for Phenylalanine and Ethyl Oleate

Having developed a combined reaction network for phenylalanine and ethyl oleate in Figure 8.8, our next objective was to verify that this network could quantitatively account for the effect of addition of ethyl oleate on phenylalanine. Thus, we used the system of differential equations implied by this network (Eq.(8.1) – Eq.(8.5)), which is derived by modifying the system of differential equations (Eq.(5.3) – Eq.(5.6)) for phenylalanine alone in HTW (see section 5.5).

$$\frac{dC_{PA}}{dt} = -k_1C_{PA} - k_4C_{PA}^2 \quad (8.1)$$

$$\frac{dC_{PEA}}{dt} = k_1C_{PA} - k_2C_{PEA} - k_7C_{PEA} + k_9C_{PEODM} \quad (8.2)$$

$$\frac{dC_{STY}}{dt} = k_2C_{PEA} - k_3C_{STY} - k_5C_{STY} + k_6C_{PEOH} + k_8C_{PEODM} \quad (8.3)$$

$$\frac{dC_{PEOH}}{dt} = k_3C_{STY} - k_6C_{PEOH} \quad (8.4)$$

$$\frac{dC_{PEODM}}{dt} = k_7C_{PEA} - k_8C_{PEODM} - k_9C_{PEODM} \quad (8.5)$$

where, C is the concentration and the subscripts PA , PEA , STY , $PEOH$, and $PEODM$ represent phenylalanine, phenylethylamine, styrene, phenylethanol, and N-phenylethyl-9-octadecenamide, respectively.

We used MATLAB 2010 to solve simultaneously the set of ordinary differential equations above and perform parameter estimation to obtain the values of the rate constants at each temperature. We used *fmincon* to perform the optimization using the *optimtool* GUI. The minimization algorithm uses a sequential quadratic programming active set optimization method [17]. The objective function for minimization was the summation of squared relative error (SSRE) between the calculated and experimental product concentrations at a given reaction temperature. This quantity was calculated using Eq. (8.6), where, j

is the number of discrete reaction times at a particular temperature and i is the number of components.

$$SSRE = \sum_j \sum_{i=1}^5 \left[\frac{C_{j,i,model} - C_{j,i,exp}}{(C_{j,i,model} + C_{j,i,exp}) / 2} \right]^2 \quad (8.6)$$

The rate constants at each temperature were then fit to the linearized form of the Arrhenius equation to get A_i and E_{a_i} along with the associated standard errors for each rate constant.

Table 8.5 compares the values of the rate constants obtained for the different pathways in the reaction network for different ratios of ester to phenylalanine. Note that the rate for formation of PEODM (k_7) is taken to be first order in phenylethylamine, but zero order with respect to oleic acid. This approximation simplified the modeling and allowed us to maintain focus on the pathways for phenylalanine.

Table 8.5 Rate constants at 350 °C for different initial ratios of ester to phenylalanine

Rate Constant (k_i) in Figure 8.8	Units	Initial Ratio of Ethyl Oleate to Phenylalanine			
		0	0.2	1.0	5.0
1	min ⁻¹	1.65	1.91	2.02	2.22
2	min ⁻¹	0.018	0.029	0.035	0.043
3	min ⁻¹	0.004	0.013	0.018	0.023
4	L mol ⁻¹ min ⁻¹	11.62	12.07	11.25	12.75
5	min ⁻¹	0.0002	0.0016	0.0131	0.0217
6	min ⁻¹	0.0006	0.0920	0.1024	0.1316
7	min ⁻¹	-	0.0084	0.0379	0.0501
8	min ⁻¹	-	0.0375	0.0340	0.0361
9	min ⁻¹	-	0.0431	0.0413	0.0391

Table 8.5 shows that the decarboxylation rate constant k_1 increases by 35% at the highest molar ratio. Li and Brill [12] reported that the rate constant for decarboxylation of phenylalanine nearly doubled as the pH decreased from 5.3 to 2.5 (at 330 °C). A similar effect of pH could be at work in this binary system, as

more oleic acid would be generated at the higher ester concentrations, thereby lowering the pH of the solution.

The addition of ester has an even more marked effect on the rate constants k_2 and k_3 (increasing by 140 and 530%, respectively, at the highest molar ratio of 5.0), as deamination of phenylethylamine to styrene and hydration of styrene to phenylethanol is enhanced upon adding ester. The rate constant for oligomerization of phenylalanine (k_4) is independent of added ester, suggesting that the rate of this path is not pH dependent. However, the rate constant for styrene conversion to high molecular weight compounds (k_5) increases by two orders of magnitude as more ester is added, probably because of enhanced acid catalysis at the higher ethyl oleate concentrations. Dimers of styrene (1,3-diphenylbutane) were identified in the GC analysis but not quantified (see Figure 8.6). Lastly, the dehydration of phenylethanol is increased nearly 230-times in the presence of ethyl oleate at a molar ratio of 5.0. Once again, the acidic environment (in presence of fatty acid from ester hydrolysis) would be favorable for dehydration of alcohols as has been previously reported [18-20]. The rate constant for formation of PEODM (k_7) increases by an order of magnitude as the ethyl oleate to phenylalanine molar ratio increases from 0.2 to 5.0, but this increase can probably be attributed to the model not explicitly accounting for the higher oleic acid concentrations present at the higher ratios. The rate constant for formation of styrene from PEODM (k_8) and that for hydrolysis of PEODM (k_9) does not change significantly with change in ester concentration, suggesting that they are not affected by change in the pH. For instance, Duan *et al.* [15] have shown that the rate of hydrolysis of N-methylacetamide is increased at a low pH (< 2) but remains constant otherwise, at near-neutral pH.

The model fits the temporal variation of the experimental product concentrations very well at all of the molar ratios explored for the binary mixture of phenylalanine and ethyl oleate as is seen in the parity plot in Figure 8.9.

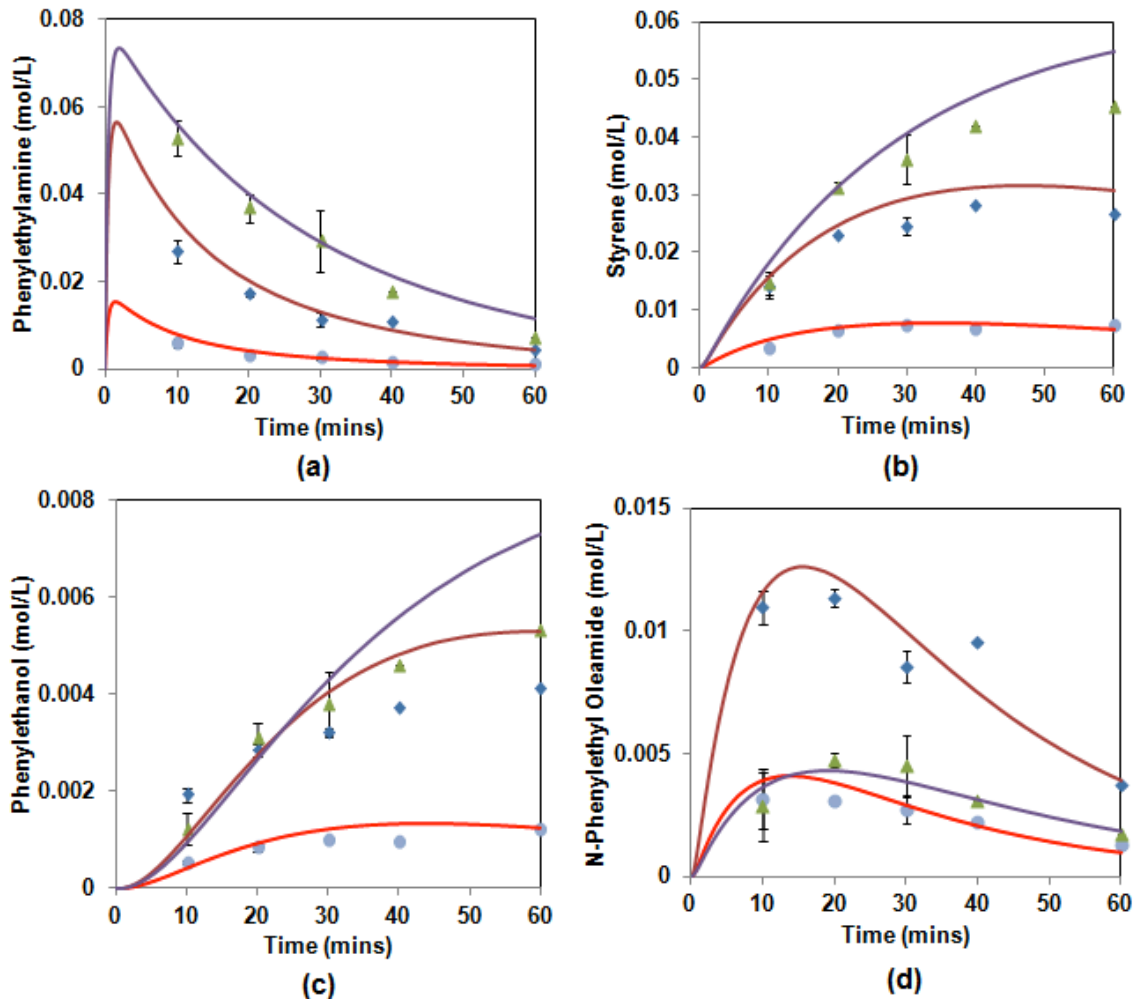


Figure 8.9 Comparison of experiment (discrete points) and model (smooth curves) results for different products for binary mixture of ethyl oleate with phenylalanine at 350 °C and different batch holding times. a) Phenylethylamine, b) Styrene, c) Phenylethanol, and d) N-phenylethyl-9-Octadecenamide. Legends are ethyl oleate to phenylalanine molar ratios of ● 0.2 : 1.0, ◆ 1.0 : 1.0, and ▲ 5.0 : 1.0

Figure 8.10 shows a parity plot of the experimental and model calculated concentrations for all species at all conditions. There is good agreement of the model with the data, given the experimental uncertainty. The data are scattered on both sides of the diagonal line, indicating the absence of systematic errors in the data fitting.

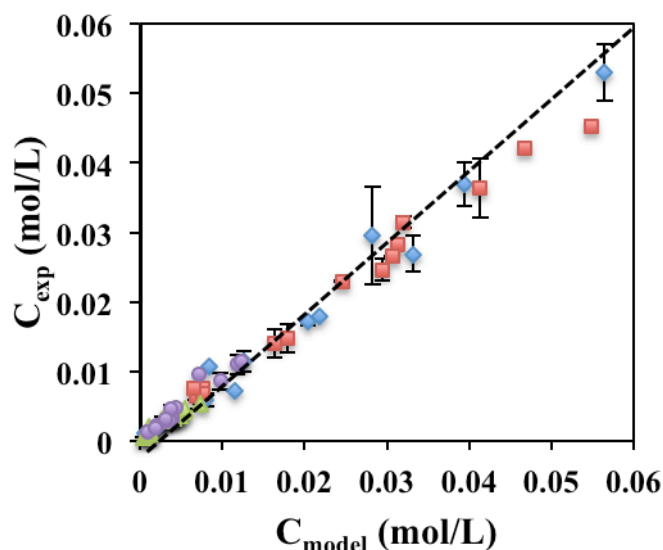


Figure 8.10 Parity plot of experimental and model concentrations at 350 °C and different batch holding times. Legends are ◆ phenylethylamine, ■ styrene, ▲ phenylethanol, and ● N-phenylethyl-9-octadecenamide

8.4 Conclusions

A study of binary mixtures involving inorganic and organic additives has been accomplished in this work. Experiments that explored the effects of salts and boric acid on the rate of decarboxylation of phenylalanine revealed that NaNO_3 and K_2HPO_4 have the most influence on phenylalanine conversion. However, the phenylethylamine yield and the carbon balance both decrease, indicating that oligomerization is probably favored in presence of salts.

Mixtures of ethyl oleate and phenylalanine showed several interesting results. As the concentration of ethyl oleate increases, deamination of phenylethylamine and hydration of styrene are increasingly favored. Thus, the yield of phenylethylamine decreases and those of styrene and phenylethanol increase with increasing ester amount. As the amount of ester increases, phenylalanine also undergoes deamination, as a parallel reaction, to form phenylacetaldehyde, possibly being favored due to lowering of the pH. On the other hand, as the relative amount of phenylalanine is increased, the conversion of ethyl oleate and yield of oleic acid increased. New reaction products (9-

octadecenamide, N-ethyl-9-octadecenamide, and N-phenylethyl-9-octadecenamide) are also formed in the binary mixture due to the interaction of phenylethylamine/ammonia with ethyl oleate/oleic acid. The total yield of the amides remains similar with changing molar ratios of the binary components. Due to the formation of these amides, the yields of oleic acid and phenylethylamine decreased at longer times.

A modified reaction network is proposed for the binary mixture, and the rate constants for this network were compared at different ratios of ethyl oleate to phenylalanine. Increasing the relative amount of ester led to higher rate constants for decarboxylation of phenylalanine, deamination of phenylethylamine, and hydration of styrene. The rate constant for dehydration of phenylethanol also increases by two orders of magnitude as compared to its value with no ester added. The proposed network for the binary mixture accurately describes the trends in the data and typically estimates the concentrations of different products within their experimental errors.

This chapter concludes the results and discussions related to all the model compounds and their binary mixtures considered in this study. The next chapter summarizes the implications of this study to algae liquefaction in HTW.

References

- [1] T. M. Brown, P. Duan, P. E. Savage. Hydrothermal liquefaction and gasification of *Nannochloropsis* sp. *Energy Fuels* 24 (6), 3639-3646, 2010
- [2] T. Minowa, S. Yokoyama, M. Kishimoto, T. Okakura. Oil production from algal cells of *Dunaliella tertiolecta* by direct thermochemical liquefaction. *Fuel* 74 (12), 1735-1738, 1995
- [3] Y. Dote, S. Sawayama, S. Inoue, T. Minowa, S. Yokoyama. Recovery of liquid fuel from hydrocarbon-rich microalgae by thermochemical liquefaction. *Fuel* 73 (12), 1994
- [4] K. Mishima, K. Matsuyama. Effects of salts on the decomposition behavior of cellulose in subcritical water. *14th International Conference on the Properties of Water and Steam in Kyoto* 350-353, 2003
- [5] J. Li, X. Wang, M. T. Klein, T. B. Brill. Spectroscopy of hydrothermal reactions, 19: pH and salt dependence of decarboxylation of α -alanine at 280-330 °C in an FT-IR spectroscopy flow reactor. *Int. J. Chem. Kinet.* 34 (4), 271-277, 2002
- [6] S. Slae, R. Shapiro. Kinetics and mechanism of the deamination of 1-methyl-5,6-dihydrocytosine. *J. Org. Chem.* 43 (9), 1721-1726, 1978
- [7] H. Zhen, F. Meng. Theoretical study of water-assisted hydrolytic deamination mechanism of adenine. *Struct. Chem.* 20, 943-949, 2009
- [8] V. J. Nowlan, T. T. Tidwell. Structural effects on the acid-catalyzed hydration of alkenes. *Acc. Chem. Res.* 10, 252-258, 1977
- [9] W. M. Schubert, J. R. Keeffe. The acid-catalyzed hydration of styrenes. *J. Am. Chem. Soc.* 94 (2), 559-566, 1972
- [10] S. Changi, T. Pinnarat, P. E. Savage. Modeling hydrolysis and esterification kinetics for biofuel processes. *Ind. Eng. Chem. Res.* 50, 3206-3211, 2011

- [11] S. Changi, T. Pinnarat, P. E. Savage. Mechanistic modeling hydrolysis and esterification kinetics for biofuel processes. *Ind. Eng. Chem. Res.* 50, 12471-12478, 2011
- [12] J. Li, T. B. Brill. Spectroscopy of hydrothermal reactions 25: Kinetics of the decarboxylation of protein amino acids and the effect of side chains on hydrothermal stability. *J. Phys. Chem. A.* 107, 5987-5992, 2003
- [13] T. E. Roe, J. T. Scanlan, D. Swern. Fatty acid amides. IV. Reaction of fats with ammonia and amines. *J. Am. Chem. Soc.* 71 (6), 2215-2218, 1949
- [14] M. C. Cesa, S. L. Denman. Synthesis of N-disubstituted amides by reaction of amides with certain organic hydroxyl compounds. *U.S. Patent No. 5,041,659*, August 20, 1991
- [15] P. Duan, L. Dai, P. E. Savage. Kinetics and mechanism of N-substituted amide hydrolysis in high-temperature water. *J. Supercrit. Fluids* 51, 362-368, 2010
- [16] P. Valdez, J. G. Dickinson, P. E. Savage. Characterization of product fractions from hydrothermal liquefaction of *Nannochloropsis* sp. and the influence of solvents. *Energy Fuels* 25, 3235-3243, 2011
- [17] <http://www.mathworks.com/help/toolbox/optim/ug/fmincon.html>. Date last accessed, 3rd September 2011
- [18] X. Xu, M. J. Antal. Mechanism and temperature-dependent kinetics of the dehydration of *tert*-butyl alcohol in hot compressed liquid water. *Ind. Eng. Chem. Res.* 36 (1), 23-41, 1997
- [19] S. E. Hunter, C. E. Ehrenberger, P. E. Savage. Kinetics and mechanism of tetrahydrofuran synthesis via 1,4-butanediol dehydration in high-temperature water. *J. Org. Chem.* 71, 6229-6239, 2006
- [20] N. Akiya, P. E. Savage. Roles of water for chemical reactions in high-temperature water. *Chem. Rev.* 102, 2725-2750, 2002

CHAPTER 9

Implications, Conclusions, and Future Work

In chapters 4-8, we discussed the behavior of different model compounds and their binary mixtures in HTW. We explored the product distribution, reaction pathways, mechanisms, and kinetics for these systems. We conclude the thesis by identifying the major implications of our findings to better understand the HTL of algae, in line with the overall objective. We also suggest some future work on the foundations laid herein.

One of the major implications of this project was finding autocatalysis for hydrolysis of esters (ethyl oleate) and phospholipids (DOPC). Autocatalysis has implications for process design and optimization for the hydrothermal biofuel production process. Autocatalytic reactions exhibit a maximum in their rate at some intermediate conversion, and for strongly autocatalytic reactions this maximum is at $X = 0.5$. Thus, one could minimize the total reactor volume required for hydrolysis by using a reactor sequence (continuous stirred tank reactor followed by a plug flow reactor) rather than a single reactor, thereby reducing the capital cost for reactors. The first reactor should be designed to operate at the intermediate conversion that maximizes the reaction rate. A second process implication is that recycling a portion of the hydrolysis product stream could serve to reduce the reactor volume. This product stream would contain a high concentration of fatty acids, which would accelerate the hydrolysis rate. Of course, the advantage gained in reaction rate would need to be balanced against the disadvantage of processing a larger volume of fluid through the reactor. The advantages for economical design can be tied to one of the elements of sustainability.

We also elucidated the common mechanism for fatty acid ester hydrolysis and fatty acid esterification without added acid or base catalysts. Ethyl oleate hydrolysis is both specific acid catalyzed and general acid catalyzed by oleic acid. In the presence of other biomacromolecules present in algae that either have or generate products with acidic functional groups (amino acids), the hydrolysis rate of triglycerides would increase. This hypothesis is consistent with the results obtained in our study for the binary mixture of phenylalanine and ethyl oleate, where the conversion of ethyl oleate is increased with an increase in phenylalanine concentration.

A mechanistic model was developed for the hydrolysis of ethyl oleate that provided reliable quantitative predictions both within the experimental conditions used to determine its parameters and outside this parameter space (including different pH values) and for a multicomponent system of fatty acid, ester, water and alcohol. The conversion predicted by the mechanistic model is very sensitive to the dissociation constant K_a , for oleic acid. Accurate determination of dissociation constants of fatty acids in ethanol, water, and ethanol-water systems at high temperatures would enable more accurate mechanistic kinetics models. Although we estimated K_a as a parameter in our model, one can use a different methodology to obtain K_a of oleic acid in ethanol-water system at HTW and compare it with our estimated values. Rahman *et al.* [1] have reported the dissociation constant of saturated fatty acids (stearic, palmitic, myristic, and lauric acid) in ethanol-water mixture, however, at room temperatures. One can use their procedure to obtain estimation of pK_a for oleic acid at room temperature. One can then develop a K_a and temperature correlation, as reported previously [2, 3] for carboxylic acids to extrapolate the K_a obtained at room temperatures to that at high temperatures.

We conducted pH experiments for ester hydrolysis and found base catalysis at high pH (pH >10). The current mechanistic model does not account for specific base catalysis by hydroxide ion and is unable to quantitatively predict conversion of ester at such conditions. A compensation term containing $[OH]^-$

and/or $[C_{17}H_{33}COO]^-$ can be added to the model to capture the trends in conversion at high pH, as was done previously by Comisar *et al.* [4] during their study of hydrolysis of methyl benzoate. Oleate ion chemistry can also play an important role for not only ethyl oleate but also binary mixture system of ethyl oleate and phenylalanine. One needs to account for additional corrections in reaction mechanism and kinetics accordingly.

The results from the study of phenylalanine and phytol reactions in HTW also have implications for hydrothermal liquefaction of algae. Several products identified in bio-oil from algae could have originated from amino acids within the proteins and chlorophyll in algae cells. E.g.: crude bio-oil obtained during algae liquefaction contains amines, which can be formed via decarboxylation of amino acids. Phytol reactions in HTW revealed the formation of some products (e.g., neophytadiene, phytene, phytane) that had been previously identified in crude bio-oils from HTL of algae. It seems reasonable to conclude that those products in the bio-oils arose from the decomposition of chlorophyll, and in particular, its phytol side chain.

Brown *et al.* [5] reported that 350 °C and a processing time of 60 min gave the highest yield of crude bio-oil from the liquefaction of *Nannochloropsis* sp. At these conditions, bio-oil contains high molecular weight compounds, which could possibly arise due to oligomerization during the reaction of amino acids and chlorophyll in HTW. The phenylalanine pathway to oligomerized products following second order kinetics implies that oligomerization will become more significant at higher concentrations (higher biomass loadings). Oligomerization products can also arise from styrene, which contains a vinyl group permitting it to undergo addition reactions to form dimers and trimers. Phytol results also indicate that experiments at 350 °C gave the lowest carbon balances. Reactions were run only up to 20 min, where the carbon balance was only 18%. We suspect this number would be even lower for an experiment run for 60 min. This result supports the fact that the primary products formed from phytol undergo secondary reactions at 350 °C to form primarily higher molecular weight material

(oligomers), which would be undesirable in a bio-oil. We speculate that these oligomerization products form because the double bonds present in the major primary products (neophytadiene, phytene) admit the possibility of addition reactions.

Oligomerization occurring with phenylalanine or other amino acids is difficult to control. Some strategies that can be used to reduce oligomerization are to use a chain-terminating molecule that can reduce the possibility of this kind of step-polymerization or perform liquefaction at lower temperatures or lower biomass loadings. For reducing the rate of oligomerization of primary products, one strategy would be hydrogenation of their double bonds. Thus, one might anticipate that algae liquefaction in the presence of a known hydrogenation catalyst and H₂ might produce a bio-oil with less of a high-molecular-weight component. Duan and Savage [6] report results that are consistent with this expectation. They showed that the presence of H₂ and a Pt/C catalyst in the reactor reduced the viscosity of the bio-oil produced from hydrothermal liquefaction. The bio-oil from catalytic liquefaction was a freely flowing liquid, whereas the product from uncatalyzed liquefaction was more tar-like.

The kinetic modeling work reported for phytol has implications for effective conversion of microalgae to bio-oils via hydrothermal liquefaction. We note that the activation energy for the step that produces neophytadiene (E_{a2}) is higher than that for the oligomerization of neophytadiene to high-molecular weight products (E_{a7}) (see chapter 6). This feature in the reaction network means that increasing the reaction temperature would increase the rate of neophytadiene formation more than it would increase the rate of oligomer formation. This behavior is apparent in Figure 6.7 of chapter 6, which shows that the highest calculated concentration of neophytadiene was achieved at the highest temperature examined (350 °C), but at a short reaction time. Therefore, performing liquefaction at higher temperatures, but for shorter times, might be a pathway toward reducing the amount of heavy material in bio-oils from microalgae liquefaction.

Hydrolysis of DOPC produces several phosphorus containing compounds that give valuable insights for the behavior of phospholipids in HTW. In an ideal process, all of the phosphorus atoms would reside in compounds that partition into the aqueous, rather than organic, phase after hydrothermal processing. This outcome would provide a phosphorus-free fuel product and a phosphorus-rich aqueous stream that can be used to grow more algal biomass. Many of the phosphorus-containing compounds reported here (α -, β -GPA, phosphorylcholine) would likely distribute themselves into the organic phase, whereas phosphoric acid would go into the aqueous phase. Thus, phosphorus recycling after hydrothermal processing of algae would be facilitated by processing at conditions that produce phosphoric acid as the sole phosphorus-containing product. This study provides a reaction network and kinetics of different pathways that can be useful for identifying these conditions.

In a more complex system, such as algae, additional interactions could possibly exist amongst biomacromolecules and their products. We studied binary mixtures to affirm this hypothesis. We have discovered that inorganic additives (salts and boric acid) that are present in media to cultivate algae accelerate phenylalanine conversion but decrease the yield of phenylethylamine and increase the yield of oligomers. Salts are present in 5-15 wt% in dry algae. It seems that their presence in algae can lead to undesirable oligomer formation from proteins and reduce the quality of bio-oil obtained from algae. A study of the binary mixture of ethyl oleate and phenylalanine gives valuable insights for the reactions of complex systems such as triglycerides and proteins. The rate of deamination of phenylethylamine to styrene increases in the presence of ester. Deamination liberates ammonia, which can react with fatty acid/ester to form amide. Similarly, phenylethylamine can react with the fatty acid/ester to form the corresponding amide, which could potentially give additional styrene at higher temperatures or longer batch holding times. The amide formation is undesirable as it adds to the nitrogen content in the bio-oil and decreases the fatty acid yields. Phospholipids could also interact in similar to fatty acid esters in a mixture. Additionally, one of the main products of phospholipid hydrolysis, phosphoric acid,

could form phosphate salts at higher temperatures, provided the reaction media is alkaline. This can have implications for upgrading of bio-oil to reduce its P-content. Furthermore, phosphate salts with metal cations could increase the conversion of amino acids and lead to an increased rate of formation of undesirable high molecular weight compounds in crude bio-oil. One can design experiments to test this hypothesis for a binary mixture of DOPC and phenylalanine in HTW.

To summarize the research, we have comprehensively used experiments and modeling to elucidate the chemistry, reaction network, pathways, and kinetics for model compounds (ethyl oleate, phenylalanine, phytol, and DOPC) and binary mixtures (phenylalanine with salts and ethyl oleate) in high temperature water. Several products were qualitatively and quantitatively identified using the model compounds. The study helps us differentiate the products that are desirable and undesirable for crude bio-oil production during HTL of algae. One can use the kinetics to optimize the production of desirable components of the crude bio-oil. The findings of this study have several direct and indirect implications to the hydrothermal liquefaction of algae. We believe that the results presented herein provide the foundations that can be built upon to the study of more complex systems (ternary or quaternary model compounds or even algae) to attain our quest of better understanding the hydrothermal liquefaction of algae.

References

- [1] M. Rahman, A. Ghosh, R. Bose. Dissociation constants of long chain fatty acids in methanol-water and ethanol-water mixtures. *J.Chem.Tech.Biotechnol.* 29, 158-162, 1979
- [2] P. Krammer, H. Vogel. Hydrolysis of esters in subcritical and supercritical water. *J. Supercrit. Fluids* 16, 189-206, 2000
- [3] J. L. Oscarson, S. E. Gillespie, J. J. Christensen, R. M. Izatt, P. R. Brown. Thermodynamic quantities for the interaction of H^+ and Na^+ with $C_2H_3O_2^-$ and Cl^- in aqueous solution from 270 to 320 °C. *J. Solution Chem.* 17 (9), 865-885, 1988
- [4] C. Comisar, S. Hunter, A. Walton, P. E. Savage. Effect of pH on ether, ester, and carbonate hydrolysis in high-temperature water. *Ind. Eng. Chem. Res.* 47, 577-584, 2008
- [5] T. M. Brown, P. Duan, P. E. Savage. Hydrothermal liquefaction and gasification of *Nannochloropsis* sp. *Energy Fuels* 24 (6), 3639-3646, 2010
- [6] P. Duan, P. E. Savage. Hydrothermal liquefaction of a microalga with heterogeneous catalysts. *Ind. Eng. Chem. Res.* 50 (1) 52-61, 2011

Appendices

Table A.1 Pressure and density of saturated liquid water at different temperatures

T (°C)	Pressure (MPa)	Density (g/mL)
175	0.9	0.892
200	1.6	0.862
210	1.9	0.85
220	2.3	0.838
230	2.8	0.825
240	3.3	0.812
250	4.0	0.799
260	4.7	0.786
270	5.5	0.77
280	6.4	0.755
290	7.4	0.74
300	8.6	0.726
310	9.9	0.709
320	11.3	0.692
330	12.9	0.675
340	14.6	0.658
350	17.0	0.642

Table A.2 Conversion of ethyl oleate and yield of oleic acid at different temperatures and batch holding times

T (°C)	R _w	Time (mins)	X _{EO}	Y _{OA}	X _{avg}
240	569	30	0.13	0.00	0.07
		45	0.03	0.05	0.04
		75	0.17	0.16	0.17
		90	0.31	0.30	0.31
		105	0.62	0.70	0.66
		120	0.69	0.74	0.72
		150	0.75	0.77	0.76
260	554	30	0.01	0.06	0.03
		45	0.16	0.18	0.17
		75	0.65	0.68	0.67
		90	0.81	0.83	0.82
		105	0.91	0.90	0.90
		120	0.94	0.86	0.90
		150	0.96	0.88	0.92
280	530	15	0.28	0.12	0.20
		30	0.38	0.30	0.34
		40	0.51	0.47	0.49
		50	0.76	0.78	0.77
		75	0.89	0.85	0.87
300	510	15	0.20	0.22	0.21
		30	0.59	0.56	0.57
		40	0.92	0.96	0.94
		50	0.95	0.87	0.91
		75	1.00	0.99	1.00
350	478	10	0.50	0.31	0.40
		20	0.98	0.78	0.88
		30	0.99	0.79	0.89
		40	1.00	0.80	0.90
		60	1.00	0.73	0.86